APPLICATION OF PLASTIC THEORIES

ANALYSIS OF FRACTURE CRITICAL STEEL TWIN-TUB GIRDER BRIDGES

A Thesis

by

AMREEN FATIMA

Submitted to the Office of Graduate and Professional Studies of
Texas A&M University
in partial fulfillment of the requirements for the degree of

MASTER OF SCIENCE

Chair of Committee,	John B. Mander
Co-Chair of Committee,	Stefan Hurlebaus
Committee Member,	Mohammed E. Haque
Head of Department,	Robin Autenrieth

December 2018

Major Subject: Civil Engineering

ABSTRACT

Plastic theories of limit analyses are effective tools to estimate the true collapse load of a structure since the load carrying capacity is not underestimated as in case of the elastic analysis. This research aims to implement the plastic theories for the evaluation of capacity of Steel Twin-Tub Girder (STTG) bridges since a declassification of these bridges from their current fracture critical status will prevent the transportation authority from allocating funds on unwarranted maintenance and inspections. In this research, the limit theories are studied to understand the application of plastic analysis to bridge structures by validation of results from yield line analysis using experimental data. Further analysis is conducted to postulate a mechanism to analyze the bridge under specified traffic loads. The analysis guidelines are formulated to incorporate the theories as per the geometrical, loading and boundary conditions of the three major groups of bridges being analyzed: simply supported single-span bridges, exterior spans of two-span and three-span bridges and interior spans of three-span bridges. These guidelines are implemented for all the 15 bridges selected using the recommendations of the Texas Department of Transportation. The applications and ramifications of the results are discussed and the concluding remarks are drawn to assess whether the bridge remains as fracture critical or further advanced investigation is needed for a conclusive declassification.

DEDICATION

To the Almighty, for all the miracles. My family, Mr. Azeem Osman, Mrs. Qadeerunnisa Begum and Mr. Aleem Osman. My mentors, Dr. John B. Mander and Dr. Stefan Hurlebaus.

ACKNOWLEDGEMENTS

I wish to thank my mentors for what I can only describe as a *"new lease of life,"* by giving me the opportunity to work with them on this project. Their teaching, guidance, advice and leadership have transformed my professional style and brought a marked improvement in me. I thank Dr. Mander for showing me that engineering is the art of achieving *"elegant simplicity"* through scientific accuracy. I thank Dr Hurlebaus for teaching me the importance of perseverance and punctuality in research to pursue courageous innovations with immaculate precision. This project is a result of their combined vision, intellect, leadership and inspiring work ethic. I shall forever be deeply indebted to both my mentors for their help, recommendations, encouragement and patience. I thank Dr. Haque for his helpful recommendations, encouragement and for his time and support in being a part of this committee. His inputs have enhanced the orientation of this research and the timely accomplishment of the research work. I thank the Texas Department of Transportation, the Zachry Department of Civil Engineering and the Texas A&M Transportation Institute under the supervision of Dr. Stefan Hurlebaus for funding me through the research.

I thank Dr. Tevfik Terzioglu for his tireless effort and help without which this research would not have been possible. I am grateful to Ms. Natasha Boger for her constant support, both personally and professionally. The research team of TxDOT 0-6937 Project shall always be my academic family and I am thankful for this sense of belonging. I am grateful to all the faculty members at Texas A&M University for their academic guidance. I thank all my friends at Texas A&M for their help and support, particularly Mr. Venu Pokuri Subbaramiah.

I thank Ms. Amina and her family, Mr. Shakeel Ayjaz, Mr. Waheed Siddiqui, Mrs. Mahmuda and Mrs. Tahira for treating a complete stranger as one of their own. I am grateful to Ms. Hanisha Kaja for her generosity. I thank Ms. Sneha Akkineni for her unconditional support. I owe Mr. Pranav Pradeep Kumar for being the epitome of selfless helpfulness, kindness and friendship. I thank my brother for having the vision, faith and courage for dreaming that I pursue masters from the best possible university. I thank my parents for never caging my dreams, no matter how improbable, by the shackles of any hardship; this is a result of all your prayers and sacrifices.

CONTRIBUTORS AND FUNDING SOURCES

This work was supervised by a thesis committee consisting of Professor John B. Mander and Professor Stefan Hurlebaus of the Zachry Department of Civil Engineering and Professor Mohammed E. Haque of the Department of Construction Science.

All work for the thesis was completed by the student, under the advisement of Professor John B. Mander and Professor Stefan Hurlebaus of the Zachry Department of Civil Engineering. The selection of the 15 STTG bridges and the Finite Element Analysis of these bridges was done by Dr. Tevfik Terzioglu, postdoctoral research associate at Texas A&M Transportation Institute. The specification data management and the grillage analysis for the bridges was conducted by Ms. Natasha Boger, doctoral candidate at Texas A&M University, in collaboration with Dr. Tevfik Terzioglu. The plotting of cumulative distribution curves for the data was accomplished with the assistance of Mr. Pranav Pradeep Kumar, doctoral candidate at Texas A&M University, under the guidance of Professor John B. Mander.

Graduate study was supported by a scholarship from Texas A&M University and a research assistantship from Texas A&M Transportation Institute, funded by the Texas Department of Transportation and by Zachry Department of Civil Engineering under the supervision of Professor Stefan Hurlebaus.

TABLE OF CONTENTS

Page

LIST OF FIGURES

Page

LIST OF TABLES

Page

CHAPTER I

INTRODUCTION

1.1. Background

The plastic theory for slabs is becoming an increasingly popular choice for analysis and design due to the ease of these methods once the designer has gained experience in the behavior of collapse. The designs submitted using these methods of the upper bound and lower bound theories are quite economical in terms of the time and monetary resources consumed. These solutions can provide a quick method to check the load carrying capacity of slabs and therefore assess whether a structure can sustain the design load.

Although the plastic method such as the yield line theory has been used for the analysis and design of bridges, there is still a huge untapped potential of this method yet to be utilized, particularly on a large scale. Recently, Steel Twin Tub Girder (STTG) bridges are noted to be an architecturally pleasing solution when a large span bridge of a tighter radius is required. However, the current norms of classification of bridges in the industry have grouped STTG bridges as a class of bridges susceptible to sudden collapse in the event of a single member failure. Therefore, the Federal Highway Administration (FHWA) stipulates that these bridges undergo strict and intense biannual inspection. While such rigorous practice for prevention of failure is necessary, STTG bridges may not be vulnerable to the extent to which they are feared to be. The Texas Department of Transportation (TxDOT) may be investing an enormous proportion of funds on examination and subsequent traffic control measures that are probably not required due to the inherent capacity of the bridge that would make the system redundant and avoid failure even if one of the members of such a system fail.

In order to check whether the STTG bridges are truly in the requirement of the hands-on inspection, analyses studies shall be conducted to estimate the design capacity of the bridge system. Since there are a large number of STTG bridges in Texas, it is essential that the methods developed to analyze these bridges are convenient for use, in terms of time and technology. The yield line method of the plastic analyses can serve as a *"litmus test"* to indicate if further advanced studies using computational resources are required to be undertaken for a particular bridge or if the bridge should continue to have its status of requiring elaborate inspections.

The development of yield line solutions for bridges can lead to expedited analysis and design for bridges. It can also aid in verifying the results of the advanced computer-generated programs for structural analyses and for nonlinear finite element analyses. Since the plastic methods are based on actual crack patterns formed when the collapse occurs at ultimate load, the mechanism postulated shall attempt to simulate the exact conditions taking place. Thus, this independent check of the capacity has several benefits. The results of this analyses can lead to the formulation of certain standard specifications for the bridges in terms of the span length, radius of curvature, width, and the boundary conditions in order to ensure that the system shall possess sufficient internal capacity.

1.2. Significance

The STTG bridges serve to be an aesthetic solution to bridge problems with long spans and tight radii. However, the current classification of these bridges as fracture critical has caused TxDOT to invest huge sums of money —approximately $2 million — on the hands-on inspections and maintenance procedures (inclusive of the traffic controlling costs) prescribed by National Bridge Inspection Standards (NBIS) once in two years. These inspections are elaborate and require the

allocation of large amounts of resources of time, skills and money. Since the aftermath of the Silver Point bridge collapse tragedy, all the STTG bridges are supposed to be examined regularly as per the aforementioned policy based on the present classification of fracture critical systems. However, the STTG bridges may be removed from this status of fracture critical if the bridges are proven to safely have a load carrying capacity higher than the load that it is likely to undergo throughout its lifetime.

An informed decision can only be made if there is sufficient data that shows that the STTG bridges have the redundancy to bear the service loading. TxDOT has launched a research study to investigate the capacity of selected STTG bridges. The research project, TxDOT 0-6937, proposed to evaluate 15 selected STTG bridges from the National Bridge Inventory (NBI) by three mutually independent methods (Hurlebaus et al. 2018). The nonlinear finite element analysis, the grillage method, and the plastic methods are utilized to find the load carrying capacity of the bridge and the results are compared to assess if all the three methods consistently suggest that declassification from fracture critical status is advisable. The three methods are of varying computational effort, time and accuracy, and an agreement between all the three methods may lead to the use of the more convenient method to be favored over the more tedious methods to ease the bridge engineers if and when they evaluate the other STTG bridges by following the guidelines of the project.

This research is a part of the third methodology undertaken in the TxDOT 0-6937 research project. The plastic theories are implemented to develop a procedure that evaluates the load carrying capacity of the bridges resulting in a range formed by the lower bound (strip method) and the upper bound (yield line theory). This method is a manual technique of computation that can reduce the two methods to simple formulae and can be expedited using any spreadsheet program,

once the mechanism for a typical STTG bridge is established. Moreover, this band of upper bound and the lower bound solution can serve as a quick check for the two other methods that are carried out in advanced finite element and structural analyses programs. Since the plastic theories are completely diverse in nature of the analysis method, it gives a different perspective of solving the problem and a consistency between the methods proves to be a thorough check of the three methods. Once the initial failure mechanism is established and validated, the formula generated from this method can serve as a very helpful tool to analyze the similar STTG bridges. The procedure is simple and can be easily repeated to bridges of similar geometry and loading conditions with appropriate modifications that will be explained in detail in this thesis. Although the upper bound and lower bound plastic methods are a popular choice for slab designing these days, there is still a need for the evaluation of the potential of these methods for the bridge industry on a large scale.

1.3. Objective

The objective of this research is to investigate the application of plastic theories for the analysis of STTG bridges by deriving suitable admissible mechanism that can accurately predict the failure load. The upper bound and lower bound methods are used to assess the load carrying capacity of the bridges. The experimental test bridge of the TxDOT 9-5498 project shall be analyzed to derive a suitable mechanism and validate with the experimental results. The capacity shall be analyzed under standard American Association of State Highway and Transportation Officials (AASHTO 2017) loading for the 15 preselected bridges from all the STTG bridges in Texas based on key parameters such as the span length, radius of curvature and the continuity or support conditions. The results of these evaluations shall present the upper bound and lower bound range of the

overstrength capacity of the bridges that will indicate that either the bridge may be investigated further using more advanced computational analysis or may continue to remain fracture critical.

1.4. Outline of Thesis

This thesis consists of 8 major chapters that constitute the research procedures and outcomes of the application of the plastic theory to the analysis of STTG bridges. It starts with the introductory Chapter I which also serves as the overall roadmap for the proposed work. Chapter II outlines the previous work conducted on the subject that is cited on the open literature. It concludes with the research questions arising from the present body of knowledge. Chapter III describes the verification of the plastic methods of analysis applied to experimental Steel Twin-Tub Girder (STTG) bridge. Chapter IV proposes a general theory to develop a solution that is applicable to HL-93 loading for selected 15 STTG bridges. The solutions thus developed are explained in a detailed manner and are provided with supplementary analysis guidelines and examples for the application of the theories to two selected bridges in Chapter V. Chapter VI documents the application of the methodology explained in the previous chapter to the 15 selected bridges in brief. This chapter also highlights the ramifications and further application of these methods. Chapter VII discusses the results of the research with the results in comparison with the other methods of analysis such as the Finite Element Method and the Grillage Analysis. The recommendations that are formulated as a consequence of this comparison are also documented in this chapter. The final Chapter VIII gives the concluding remarks on the research conducted.

CHAPTER II

LITERATURE REVIEW AND PREVIOUS WORK

2.1. Chapter Summary

The primary objective of this research is the applicability of the outcomes and developments of plastic analysis on a sample of STTG bridges. Therefore, this first task of the research ensures the comprehensive understanding of the general issues that are needed to be addressed and whether or not the methodology can be implemented according to the prevalent norms and practices.

The next stage of this research process is to review all the existing work on the plastic theories. The previous applications of these theories are studied and reviewed. This task will help in the collection and assimilation of the existing knowledge, technical know-how and case studies which will enable in the development of an astute understanding of the plastic theories and the fracture critical bridge case-studies. An in-depth knowledge of the current problems and conditions will help in the necessary acquaintance of the application of plastic methods to bridges which constitutes the final task of the literature review. Since this task deals with acquiring information needed for addressing the problems, it has a continuing nature, it means that although the task is scheduled for the initial phase of the project, it will be conducted throughout the course of the project to gather vital information.

2.2. Introduction

The chapter deals with the literature available on the plastic upper bound and lower bound theories, the application of these theories on bridges and on the fracture critical bridges obtained through sources ranging from research papers, textbooks, and material available for commercial and academic use through electronic media. The relevant works are presented in a sequential order to

establish the existing information from various resources, describing the different theories, advancements and modifications and the differing opinions currently existing regarding the topics central to this research. The chapter concludes with the technical needs for further research that have emerged from this research.

2.3. Fracture Critical Members

The present NBIS of the Federal Highway Administration (FHWA) defines fracture critical members (FCM) as *"a steel member in tension, or with a tension element, whose failure would probably cause a portion of or the entire bridge to collapse,"* (Lwin 2012). These fracture critical members are, therefore, significant for the inspection of bridges to avoid failure. In the past there have been tragic occurrences of the collapse of bridges with FCMs. There was a massive loss of life and property recorded in the aftermath of such collapses that were caused due to negligent maintenance and inspections. Two of such cases are discussed in this section (Herald-Dispatch December 15, 1967; Hogarty July 17, 1983). The sudden collapse of the Silver Bridge across the Ohio River in 1967 claimed 46 lives, injured 9 people, and 84% vehicles fell off the bridge as per the National Transportation Safety Board (NTSB) data. NTSB (1970) reported a cleavage fracture located in the north suspension chain (at the Ohio end of the bridge) in the eye of the eyebar 330. It was also stated that one of the possible reasons for the collapse was the stress and fatigue caused due to corrosion that was not anticipated for the material used the under conditions to which the bridge was exposed. This disastrous event led to the reforms of the NBIS policy under the Federal Aid Highway Act (Barker and Puckett 1987). According to this policy change, a regular hands-on inspection is required every 2 years for bridges cataloged over 600,000 bridges of the National Bridge Inventory (NBI) with spans longer than 6.1 m.

The Mianus River Bridge collapse in Greenwich, Connecticut in 1983 caused 3 deaths and 3 critical injuries according to NTSB (1984) data. The Mianus River Bridge, crossing over the Mianus River in the Cos Cob section of Greenwich Connecticut, is an example of the need for better maintenance methodology and stipulations. This incident highlighted the rampant negligence that was prevailing despite the shocking calamity of the Silver Bridge collapse. The National Transportation Safety Board investigated the collapse and concluded that two pin and hangar assemblies that secured the deck in place on the exterior part of the bridge had failed, leading to the collapse. It was pointed out that there existed sheer negligence toward channeling adequate funds for the inspection of bridges since the State had assigned 12 engineers to work in pairs to inspect around 3,425 bridges, at the time of the accident as reported by the State Transportation Department Chief Engineer, Robert W. Gubala to New York Times (Schmalz June 24, 1984). As a consequence of which the lateral hanger displacement of the pin and hanger suspension assembly in the southeastern end of the bridge was caused due to stresses from corrosion that led to the collapse.

The new reforms insist on the intense inspection and maintenance that incurs huge expenditure. The current standards impose that the same elaborate and expensive measures be implemented for all the STTG bridges in the NBI. Recent studies have shown that some of the bridges classified as FCM may not, truly, be so due to their structural redundancy. This implies that the structure may possess more strength than what is expected from an elastic assessment. FCMs of bridges are characterized by the non-redundancy of the system. Load and Resistance Factor Design (LRFD) defines redundancy as *"the quality of a bridge that enables it to perform its design function in a damaged state"* and redundant member as *"a member whose failure does*

not cause failure of the bridge," (Lwin 2012) in an FHWA memorandum in 2012. These redundancies may be divided into three types: load path redundancy, structural redundancy, and internal member redundancy. There is a concern that some of the bridges may be wrongly classified as FCM since the redundancy of the bridge system has not been evaluated. This conservative classification may be depleting the funds due to the expensive bridge examinations of the systems which are not as much at risk of failure as an FCM system would be.

TxDOT funded a research project 9-5498 to evaluate if STTG bridges are truly fracture critical. One of the methods of evaluation undertaken was the yield line theory method. Barnard et al. (2010) tested a decommissioned typical fracture critical STTG bridge under sand loading to analyze the capacity of the bridge. The shear studs were evaluated by Mouras et al. (2008) to assess all the possible load-path redundancy that was associated with the bridge system. The results of the yield line analysis were then compared with the experimental method. The sand load that was experimentally observed to cause the collapse of the bridge system was 1618 kN while that calculated through yield line analysis was 1254 kN, which is less than the actual load by 22.5%. This difference could possibly be since the loading of the yield line analysis was modeled as point load of an equivalent HS-20 truck and not exactly as the sand loading (uniformly distributed load) applied during the experiment (Barnard et al. 2010). There is a need for evaluating the accuracy of the yield line theory by conducting the analysis under the influence of a loading that can be modeled as close to the actual experimental sand loading as possible. It is to be noted that the sand loading may not have been as uniformly distributed as a water load stored in a temporary tank. Although the exact capacity of the bridge was not calculated using the yield line mechanism proposed by (Barnard et al. 2010), it showed that yield line theory possessed the quality of a

possible tool to analyze bridges with further modifications. This paves way for further research to develop more accurate yield line mechanism that can incorporate all the components such as the twin-tub girders and shear studs to simulate the redundancy of the system.

2.4. Plastic Analysis Methods

Plastic methods are known to be effective in estimating the true capacity of a structural system (Park 1968). While elastic methods remain to be a simple approach to deal with structural design and analysis, the underlying prediction of stress being proportionate to strain (Hooke's Law) makes this method conservative. When yielding of material at a certain load occurs, the property of redistribution of the load is not captured by the elastic methods (Milošević et al. 2010). Thus, the evaluation of such structures using plastic method is advised. When a gradually increasing load is applied to a structure, a point of plastic failure is reached such that the deflections go on increasing plastically at a constant load. Determination of the critical load for a perfectly elasto-plastic member is the key aspect of limit analysis (Drucker et al. 1952; Park 1968).

2.4.1. Limit Theorems in Plastic Analysis

The limit analysis is based on the theorems of plastic failure of an idealized elasto-plastic member. Gvozdev (1938) first formulated the theorems that form the basis of limit analyses. The theorems are discussed in this section.

Upper Bound or Kinematic Theorem:

This theorem considers the formation of a failure mechanism occurring due to the plastic hinges that make the member kinematically unstable (Neal 1977). The limit load is found by equating the work done by the external actions with the work absorbed during the hinge formation, for the critical among all possible failure mechanisms. The upper bound theorem states that the limit load

thus found based on the assumed failure mechanism will be greater than or equal to the actual failure load when the internal actions are in equilibrium.

Lower Bound or Static Theorem:

This theorem considers the body to be in static equilibrium. Drucker et al. (1952) explained that a large distribution of moments, which is assumed to be in equilibrium due to a given externally applied load, is a *"statically admissible distribution."* The lower bound theorem states that an external load that ensures that the system has a stable and statically admissible distribution of internal actions, will be less than or equal to the limit load, such that the actions are within the range of limit values and are in equilibrium.

Uniqueness or Singularity Theorem:

This theorem is formulated from the upper and lower bound theorems. It states that there exists only one load calculated from the assumed failure mechanism that ensures a stable and statically admissible distribution of the internal actions, wherein the internal actions are in equilibrium and are within the range of limit values (Nielsen and Hoang 2016).

2.4.2. Beams and Frames

While the elastic methods based on the Euler-Bernoulli and Timoshenko beam modes are quite popular for solving the problems of beams and frames, the additional capacity or the reserve capacity due to the redistribution of the load is better calculated using the plastic limit load of these structures. The collapse mechanism or the plastic hinge formation is the basis of this analysis. A statically determinate beam fails on the formation of one hinge while statically indeterminate beam fails after the formation of 2 or more hinges depending on the boundary conditions. The hinge formation occurs when the entire cross-section of the beam reaches yield stress. Once a mechanism

is formed in a structure, it will not be able to resist any load. The aforementioned theorems of limit analyses are applied to find the reserve capacity of beam and frame elements. Horne (1971) and Neal (1977) have explained the examples of these applications.

2.4.3. Slabs

The limit analysis of the yield line and strip methods have traditionally been applied to reinforced concrete slabs provided the ductility of the member is maintained by conservatively defining the material properties of concrete and with a cautious design of the reinforcement so as to ensure that the yielding of the steel reinforcement is the governing criterion of failure of the slab (Meyboom 2002).The upper bound and the lower bound theorems are applied to the rigid-plastic slab members for the plastic analysis. The two subsequent sections of the chapter give a brief introduction of the background and a review of the previous work done in the origin and evolution of the two theories. Prager and Hodge (1951) paved the way for the use of limit analysis of slab based on the classical plastic theories for plates. It is proposed that the ultimate collapse load of slabs falls in the range of the upper bound and lower bound solutions. Both of these methods are explained in detail by (Park and Gamble 2000). These methods shall be discussed in detail in the remainder of this chapter.

Upper Bound Limit Analysis Theory for Slabs

The upper bound theory is based on the yield line theory. Ingerslev (1923) proposed that limit analysis method of yield line theory can be used to study reinforced concrete slabs. Johansen (1962) contributed towards the advancement and expansion of its scope as an upper bound solution. The method essentially predicts the ultimate load capacity of the slab system through various collapse mechanisms that are postulated such that the boundary conditions are satisfied

(Johansen 1962; Johansen 1972). Park and Gamble (2000) stated that, *"The moments at the plastic hinge lines are the ultimate moments of resistance of the sections, and the ultimate load is determined using the principle of virtual work or the equations of equilibrium."* The solution can either be exact or upper bound.

It is to be noted that the slab regions between yield lines (plastic hinge lines) are not considered so that the ultimate moments of resistance of the sections are not exceeded by the moments in the intermediate areas. If the collapse mechanism is inadmissible, however, an exceedance of the ultimate moment capacities may occur in those regions. It is therefore necessary that all the possible collapse mechanisms are assessed thoroughly. Most of the correct collapse mechanisms for standard cases are known to the designers due to the experimental evidence of crack formations along the yield lines defined by (Park and Gamble 2000) as, *"the lines of intense cracking across which the tension steel has yielded."* Various proven results that can be found in the literature of yield line also serve as an adequate guide for most of the typical failure analyses and design of reinforced concrete slabs.

Initially, the yield line theory assumes that collapse occurs in the flexure alone, with ample shear resistance to avoid failure due to shear mode. Hognestad (1953) first summarized the literature on yield line theory that was originally in Danish in 1953. The works done by Wood (1961), Jones (1962), Shukla (1973), Wood and Jones (1967), Kemp (1965), European Concrete Committee (ECC 1962; ECC 1972) and the Dutch Committee for Concrete Research (DCCR 1962; DCCR 1963), (Park et al. 1975), and Park and Gamble (2000) throw light on the mathematical background and design applications of the yield line theory for slabs. Park and Gamble (2000) explain the conditions for the application of this upper bound method to analyze

uniformly reinforced slabs for each constant area of steel reinforcement of unit wide sections across the slab. The reinforcement may, however, differ in two directions and at the top and bottom levels of the slab, with a constant ultimate moment of resistance per unit width, along a linear path in the plane of the slab. There are more complicated solutions to deal with the problem of non-uniform distribution of reinforcement.

Ductility in slab sections is essential for the plastic rotation at critical sections when the slab undergoes plastic hinging. Bending moment redistribution occurs for the development of the collapse mechanism. It is explained in Park and Gamble (2000) that the formation of collapse mechanism occurs at ultimate load. As reinforced concrete slab undergoes progressive loading until failure takes place, the elastic distribution of bending moment is followed by a plastic redistribution after cracking of concrete due to a decreasing flexural rigidity that takes place at cracked sections. The moment tends to be constant at the ultimate moment of resistance when the tension steel yields (at the section where the bending moment reaches peak values) on further loading. As the loading increases, the yield lines spread from the location of the yield origin (that is at the maximum bending moment section derived using the elastic theory). The yield line pattern is formed by the network of yield lines dividing the slab into segments that form the collapse mechanism. The type of loading, the boundary conditions and the reinforcement arrangement influence this pattern. The slab cannot be loaded after it forms a mechanism.

Certain properties are suggested by Park and Gamble (2000) for postulating the yield line patterns which state that the yield lines are linear since these serve as the axes of rotation for the segments of the collapse mechanisms formed after the plastic hinge formation occurs. The axes of rotation intersect the location of supports (columns) and the fixed edges of the slab also serve as

yield lines. It is also stated that the yield lines are supposed to pass through points where the axes of rotation of adjoining slab segments intersect. However, Quintas (2003) has conducted research to further to examine curved yield lines and the comparison of these results with the straight yield line analysis. He has also discussed additional equilibrium conditions that were not considered in the classical yield line method. He revisited the *"normal moment method"* and *"skew moment method"* and investigated these methods. The analysis can be carried out in 2 ways, namely the principle of virtual work and the equations of equilibrium:

a) Principle of virtual work: This method assumes the slab segments to be rigid plates that undergo deformation under collapse mechanism. These segments are under equilibrium in terms of the applied load as well as the internal actions of flexure, torsion, and shears along the yield lines. A deformation δ is assumed at a convenient point of maximum deflection. The other deformations throughout the slab are expressed as fractions of δ. The internal actions are equated to the externally applied ultimate load to analyze the slab and are represented by the following equation

$$\sum W_u \Delta = \sum m_{un} \theta_n l_\theta \tag{2.1}$$

where W_u = externally applied load on each segment; Δ = downward deflection of the centroid of segments, respectively; m_{un} = ultimate moment resistance per unit width; l_θ = the length of the yield line under consideration; and θ_n = the relative rotation between the 2 segments along the yield line under consideration.

b) Equations of Equilibrium: In this method, every segment of the slab that is formed as a result of the yield line pattern occurring due to the collapse mechanism is analyzed individually

under the influence of the flexural and torsional moments and shear forces as well as the applied loading. These equations are formed by considering moments about the appropriate axes. The unknown dimensions needed to compute the ultimate load are computed by solving the set of simultaneous equations generated by considering the equilibrium condition. This method is considered to be simpler than the virtual work method since it eliminates the need for calculus or of complex algebraic rearrangement. However, the shear forces and the torque actions that are neglected in the virtual work method since the summation over the whole system balances and nullifies the effects of these entities (for a small deflection of the yield line system), can no longer be ignored because individual segments are considered.

The torsional moments are found using Johansen's yield line criterion and the shear actions are found using Johansen's theorem for computation of shear forces at yield lines. Jones (1962) explained the method to find the nodal forces between 2 yield lines, which is an extension of Johansen's method (Johansen 1962; Johansen 1972). There are, however, limitations on the cases where this method of computation of nodal forces is not allowed (Jones 1965; Kemp 1965; Kemp et al. 1965; Morley 1965; Nielsen 1965; Wood 1965; Wood and Jones 1967). For such restricted cases, the nodal forces can be found by comparing the virtual work method solution with the equation of equilibrium method since it is recently perceived that the two methods are alternate representations of one another (Wood and Jones 1967). Kemp (1962), Kemp et al. (1965) and Morley (1988) have also explained that nodal forces are equivalent to the total twisting moments acting along the yield lines and not are equivalent to the shear forces, especially in case of isotropic slabs.

The aforementioned upper bound theory has been experimentally validated. Johansen (1962) proved the relevance of the theory by comparing the theoretical results with the experimental data acquired from the tests conducted by German Reinforced Concrete Board (GRCB) at Stuttgart Materials Testing Establishment (Bach et al. 1911-1925). The experiments conducted by Sawczuk and Jaeger (1963) at the Technical University of Berlin show promising results due to the good agreement between experimental and theoretical results. Jaeger stated that serious cracking may occur at service load conditions if the arrangement of the reinforcement bar varies largely from the arrangement obtained via elastic theories. Promising results have also been achieved by the experiments conducted at the TNO Institute of Building Materials and Structures in Holland reported by the Dutch Committee for Concrete Research (DCCR 1963) and those conducted by Taylor et al. (1966) in University of Manchester. Kennedy and Goodchild (2004) have explained in detail about the yield line theory, its importance, feasibility and various real-time applications of this upper bound solution as an economic method of design. Reinforced concrete slabs are known to behave plastically, as opposed to the misconception that such slabs exhibit elastic behavior. Yield line theory deals with the limit state without explicitly addressing the serviceability aspects such as deflection (Kennedy and Goodchild 2004).

It is, however, possible to derive a formula for the deflections using the yielding moment capacity. Kennedy and Goodchild (2004) have explained in detail about the usage and principles of yield line theory, as a complementary material for experienced engineers as well as an initiation for those who are new to this design practice. At the design level, yield line theory results in quite economic results. In the *"Practical Yield Line Design,"* a comparison is drawn between the

quantity scheduling and estimation of the reinforcement bars obtained via an elastic design and the yield line design. For a given case study of yield line theory application at Cardington, yield line method showed a design requirement of 14.5 tons of reinforcement while elastic design predicted 16.9 tons (Kennedy and Goodchild 2004). The study also advocates the diversity in the usage of yield line design for addressing a wide variety of problems ranging from flat slabs (of different shapes and support conditions), bridges (with a combined slab beam action) to foundations. Kennedy and Goodchild (2004) have prescribed some rules for the formation of the yield line patterns: (i) The plates divided by the yield lines rotate about the lines of support and about the axes passing alongside any piers or columns; yield lines are linear and should terminate at slab boundary; and yield lines tend to move toward the simple supports and tend to move away from continuous supports.

The upper bound theories based on kinematics may be correct or unsafe, whereas the strip and lower bound solutions based on the static methods may by conservative or correct. The study explained in the "*Practical Yield Line Design*" by (Kennedy and Goodchild 2004) dispels the misconceptions against yield line theory as not being a good choice of design by allowing for adequate safety factors to account for the predicted likelihood of the overestimation of the capacity. The content of the study also explains the yield line theory in detail, mentioning the collapse mechanism formation through supporting worked out examples. The affine transformation for orthotropic reinforcement in slabs based on the Affinity Theorem (Park and Gamble 2000) is also explained in this report by Kennedy and Goodchild (2004).

This section presents the application of yield line theory in refurbishment that was also highlighted in the report by Kennedy and Goodchild (2004). The document shows the application

of yield line theory for designing slab and foundation of works such as One Washington Gardens (London W9) and 43-47 St. John's Wood Road (London NW8). The yield line theory was used to analyze the load capacity of the refurbished structure of the Onslow House (Saffron Hill, London EC1). The Nokia Headquarters (Stanhope Road, Camberley) is an example of yield line theory for designing the reinforcement at support location by using local failure patterns. The East India Dock Redevelopment is a case study showing how the simplicity of Yield Line Design solutions can expedite the construction because of repetition in reinforcement bar pattern. The yield line theory proved to be a handy solution to the challenges posed by the construction of 66 Buckingham Gate (London SW1). The elimination of downstands from the thin solid concrete slab because of the yield design was convenient for the architectural compliance of the standards set by Planning Authorities on building heights. Prefabricated reinforcement mats accelerated the construction in the rather confined site. The simple reinforcement design solution obtained through yield line analysis was implemented using the Bamtec systems for rapid construction of 80 Oxford Road (High Wycombe) commercial complex.

Lindsay (2004) and Lindsay et al. (2004) conducted research to evaluate whether precast concrete building frames with precast concrete hollow-core floor slabs developed in New Zealand are sufficient in terms of seating support details under earthquake loading. Figure 2.1 presents a folded plate mechanism that was observed from the crack patterns developed in an infill slab around the central column of a building frame. In her thesis of related work, Lindsay (2004) explained how yield line theory was employed to find the extent to which the moment capacity of this mechanism contributes to the capacity of hinges of the central column.

Lindsay's (2004) results were a part of a forensic analysis of full-scale experimental observations. The evaluation of the moment contribution of the folded plate mechanism thus observed from the crack pattern is conducted using the principle of virtual work done by equating of internal and external work done. The calculation was based on the angle of crack of the observed pattern. The moment interaction diagram indicates that the moment originated at the lower part of the tension quadrant of that diagram. Soon after the yield of the super-assemblage, the mechanism changed from being predominantly flexural to a tensile membrane phenomenon because of the tension introduced in floor system due to a *"bowstring effect."* There was a loss in the moment capacity at the interface and a reduction in the base shear capacity was observed. It was observed that as the vanishing of the moment capacity of along the yield line H,I,J,K,L,M takes place as shown in Figure 2.1 (b), the folded plate mechanism contribution at the central column drops to approximately 1% of the overall resistance and was thus ignored in the analysis of overstrength. However, this mechanism has shown how the crack patterns will develop in slabs subjected to such concentrated loading. The researchers also assumed an equivalent cantilever action as shown in Figure 2.1 (d) to utilize Hillerborg's strip method to analyze the problem using plastic theories.

Lower Bound Limit Analysis Theory for Slabs

The lower bound theory is based on the work by Hillerborg (1956). Some of the key aspects of the lower bound theory are discussed as follows. The moment distribution is found for the plate when all points in the plate satisfy the equilibrium conditions; No point on the plate exceeds the yield line criterion that defines the strength of the elements in the plate; and the solution is in compliance with the boundary conditions.

(a) Folded plate mechanism evident due to crack patterns in the infill region.

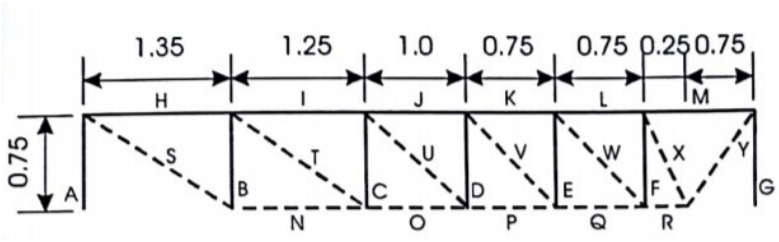

(b) Enlargement of folded plate mechanism, with yield lines: ---=negative; —=positive

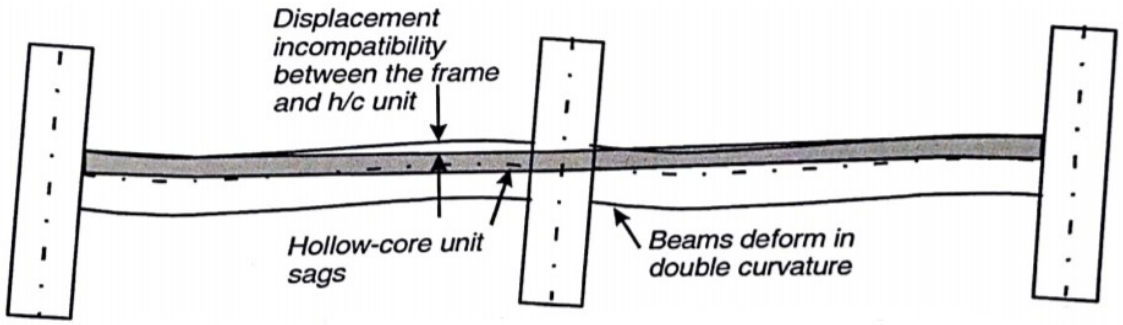

(c) Displacement incompatibility between frame and hollow-core units

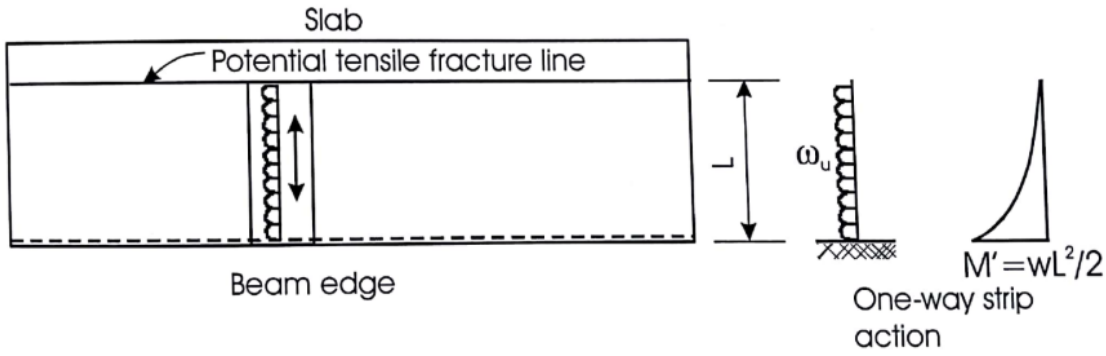

(d) Simplified post-failure assessment of infill slab by Hillerborg's strip method
Source: Lindsay (2004)

Figure 2.1. Folded Plate Theory for Infill Slab Capacity

The plate is assumed to be rigid and perfectly plastic. Hillerborg (1956) referred to the lower bound method as the *"equilibrium theory,"* and suggested that the basis of the design method is, *"If a distribution of moments can be found which satisfies the plate equilibrium equation and boundary conditions for a given external load, and if the plate is at every point able to carry these moments, then the given external load will represent a lower limit of the carrying capacity of the plate,"* (Park and Gamble 2000). This load gives a conservative estimate of the capacity of the slab. Wood (1961) revealed that elastic theory moment distribution generates satisfactory minimization solutions in terms of steel economy and serviceability requisites. This is because uniform steel stress with no locally sharp increase in values is observed at service load. However, moment redistribution precedes the reaching of the ultimate load if elastic moment distribution based on a complex stiffness distribution in slabs following concrete cracking at intensely stressed areas is not selected.

The strength of a slab element is defined by the yield criterion when a moment field is applied in it (Park and Gamble 2000). The yield criterion relates the ultimate moments (internal capacity) per unit width of the slab (m_{ux} and m_{ux} = ultimate internal resistance in the x-, y-directions, respectively) to the applied moments due to the external load at yielding of the element (m_x, m_y, m_{xy} and m_{yx} = bending moments in the x- and y- directions, respectively, and the torsional moment acting on the face of element in x-, y- directions, respectively.) Johansen's yield line criterion assumes that the reinforcement bars in the x- and y- directions attain yield strength when these cross the yield line (Johansen 1962). The yield line is defined in Park and Gamble (2000) as *"a line in the plane of the slab about which plastic rotation occurs, and across which the reinforcing bars are yielding."* The experimental results by Jain and Kennedy (1974), Lenkei

(1967), Lenschow and Sozen (1967) and Cardenas and Sozen (1973) proved that Johansen's yield line criterion can satisfactorily be used where planar forces in slabs are absent (Johansen 1962).

Hillerborg (1956) suggested a simplified approach to the lower bound method to design slabs by the elimination of the use of the torsional moments for the derivation of the design moments. The name of this strip method originates from the so-called consideration of the slab as a system of perpendicular strips that can be solved using the statics for the strips under equilibrium (Hillerborg 1956; Hillerborg 1960; Park and Gamble 2000). He also developed the *"advanced strip method"* for dealing with slabs of more complex shapes and support conditions (Hillerborg 1964). A detailed usage of the strip method can be found in the works of Crawford (1964), Hillerborg (1956), translated by Blakey, Kemp (1962), Wood (1961), Armer (1968) and Shukla (1973).

2.5. Application of Plastic Theory to Bridge Systems

Yield line theory and its application for the analysis of bridges to predict the overstrength capacity and its usage as a design tool is evaluated by Middleton (1997), Middleton (2008), Mander et al. (2010), Pirayeh Gar et al. (2014), Jiang (2015) and Barnard et al. (2010). These shall be reviewed later in detail in this and the following sections.

Middleton (2008) has stated that there is an indiscriminate allocation of large sums of funds on the maintenance and repairs of bridges based on a highly generalized assumption that all the bridges are equally at risk of failure. He reminded that many bridges have survived successfully despite their predicted failure by elastic analysis methods because elastic methods fail to consider that the overall structural system may still continue to function despite the failure of an individual member. In light of the gross economic loss occurring due to *"unwanted remedial"* maintenance

measures and unnecessary load traffic restriction, Middleton (2008) advocates the use of ultimate strength as the primary criterion to judge whether the structure is likely to fail or not. He advocates that elastic philosophy is practicable in design due to the relatively lower cost incurred due to conservatism. However, same is not true when it comes to the analysis of the load carrying capacity. The expenditure estimated for the allocation of the maintenance of short-span concrete bridge decks reported by the Highways Agency in England, forces engineers to evaluate the choice of elastic analyses (PB December 2003). Additionally, Haque (1997) mentioned that the supervision of a complex bridge system is a challenging task; one involving intense inspections and data management. One of the pivotal aspects of rehabilitation or repair measures is the identification of the bridges and/or their elements that need attention, and this may only be accomplished by a proper understanding of the structural behavior. Thus, the maintenance of bridge systems puts extreme pressure on the administrative transportation authorities.

Middleton (2008) pointed out the effects of redistribution of stresses under ultimate conditions that takes place for slabs with sufficient ductility. Thus, linear elastic methods may not be a suitable choice for the analysis of these bridges to capture the nonlinear behavior when the slab is in the post-elastic stage. For slabs that are critical in ductile failure mechanism, the collapse criterion may be given precedence over the serviceability criterion that is applicable for flexural failures. Among the prevalent methods of limit analyses, Middleton (2008) favored yield line for practical use over the Nonlinear Finite Element programs due to the higher cost and complexity of the latter. He suggested that since yield line analysis is prescribed in most of the standard building codes globally, it should be promoted at an industry level and not just be limited to research and academic level. Some of the reasons for the reluctance of the use of yield line theory on a practical

basis are stated as follows: (i) since the method uses hand-calculations, it can be considered tedious for complicated loading, geometry, and support conditions to iterate the various possible mechanism in the process of postulating the critical mechanisms; (ii) the method is viewed with apprehension since it is an upper bound solution, which is why lower bound theories are suggested to be further investigated as a check; (iii) the assumption of ductility must hold for the analysis to be applied.

The concerns can be dealt with if adequate care is taken. For example, the method can be used confidently when the ductility of the members is ensured by sufficient shear reinforcement. For the prevention of shear failure, an elastic shear analysis is recommended. Moreover, most bridge decks are safe in shear action. There is experimental evidence, as discussed in the earlier section, that yield line predicts fairly safe capacities since additional reserve strength is reflected from the slab performance, that can be explained by the *"compressive membrane or arching action"* and marginally due to the strain hardening effects of steel reinforcement. Lastly, the process of postulating the mechanisms can be undertaken using the existing experimental crack patterns available and by expediting the analyses and geometric calculations in a spreadsheet program for faster iterations and minimization analysis to generate critical collapse mechanism. Middleton (2008) developed a program named Concrete Bridge Assessment Program (COBRAS) (Thoft-Christensen et al. 1997) to analyze short-span bridges incorporating yield line theory at Department of Engineering at Cambridge University for a project funded by the Highways Agency. This research showed that there is still a need for the yield line investigation of longer-span bridges.

Mander et al. (2010) investigated the load-carrying capacity for full-depth precast concrete of overhang panels in bridge decks. The authors derived a modification to the yield line theory to account for the flexural and shear combination that is observed to govern the strength of the system. This was carried out by allowing for the mild steel reinforcement to yield. Experimental tests were conducted to corroborate the results of the yield line analysis under the application of load on the edge of the seam. The specimens of the bridge deck used were 4.9 m x 5.5 m and 200 mm thick for the full-depth region. The partial depth transverse panel-to-panel seam was studied in detail to postulate the modified mixed-shear yield line mechanism. It was observed that partial shear failure occurred along the seam line in the partial depth region of 100 mm. and not in the full-depth panel-to-panel seam of 200 mm. The experimental results show that loading the edge of the seam causes a flexural failure of the loaded panel and a shear failure of the seam. The theoretical failure load analyses, both the classical yield line and modified yield line, were conducted and compared with experimental test data for several load cases. The experimental load to theoretical load ratios showed that the results of the modified analytical models that were enhanced to simulate the behavior more accurately were closer to the experimental failure loads (within 1-6% of the observed results), with the exception of the conventional panel that proved to be weak for some unidentified reason.

Pirayeh Gar et al. (2014) examined bridge deck slabs with Fiber Reinforced Polymer (FRP) bars to assess whether or not yield line theory can be applied to find the load carrying capacity, due to lack of discernable plateau of the moment-curvature response of such FRP sections of concrete (prestressed and reinforced). This problem was tackled by assuming an equivalent plastic moment capacity (elasto-plastic behavior) for the FRP sections so as to apply yield line theory to

deck slabs of such bridges. The analytical results were experimentally validated by the results from a full-scale testing of precast panels that were reinforced and prestressed using Aramid Fiber Reinforced Polymer (AFRP). The tests were conducted under various combinations of wheel and axle positioning for a 200 mm. thick bridge deck slab of cross-sectional dimensions 5.5 m x 4.9 m. The load capacities calculated from yield line theory showed that the results were accurate within 3% of the experimental results. The authors recommended that the transfer length and the development length in case of prestressing and reinforcing bars, respectively, should be properly accounted for, so as to avoid overestimation of the internal work done (and the consequent load carrying capacity), in case of cantilever or overhang bridge systems.

Jiang (2015) postulated and implemented critical yield line mechanisms for several load cases for two realistic and novel spread slab-beam bridge prototypes with spans of length greater than 13.7 m, namely the Riverside Bridge and the US 69 bridge of the TxDOT project 0-6722. The overstrength factors of the cases were found for the selected bridges using yield line theory and strip method (modeled through equivalent grillage analysis). The limiting behavior of the slab-on-beam bridge deck system is evaluated for different collapse mechanisms such as weak slab-strong beam and strong slab-weak beam mechanisms. The failure modes of slab flexure, slab shear, compound shear-flexure slab mechanisms, beam only failure and mixed beam-slab failures are explained in detail (Jiang 2015). The results from the two methods were observed to agree, except for the slight differences that can be explained by the different assumptions associated with the 2 methods. It is observed that this research exhibited the immense scope for further development of mixed slab-beam solutions, particularly for bridge systems.

2.6. Technical Needs

Although efforts have been made to use yield line theory for analyzing the bridge systems by Middleton (2008), Jiang (2015) and Barnard et al. (2010), there still exists the need to develop this methodology further to account for the load carrying capacity of the bridges and for their subsequent design. This research aims to explore the true potential of the plastic theories to assess the maximum load carrying capacity of the bridge system. It is an independently convenient method (once the mechanism is correctly postulated for a typical class of bridge system) and the upper bound and lower bound theories offer a range of the load carrying capacity that can readily serve as a check for the computational methods such as the nonlinear finite element analysis and the grillage methods.

This research aims to evaluate the application of the plastic theories by analyzing STTG bridges whose outer tub-girder is assumed to be fractured along its depth for the assessment of the veracity of the classification of STTG bridges as fracture critical since colossal expenditure occurs due to the elaborate inspections. If these bridges have an internal redundancy in the system, these may not be fracture critical, and thus, should be declassified from the category of bridges that are mandated to undergo biannual inspections and maintenance. If these bridges are found to have a load carrying capacity greater than the expected applied load when the outer girder is fully fractured, these bridges can be stated to have sufficient redundancy for their declassification. Such a declassification can prevent depletion of funds on unnecessary maintenance procedures, ensuring the proper allocation of funds of the transportation departments.

Based on this literature review, the following questions arise:

Q1. Is it possible to develop the upper bound and lower bound solutions for the bridges?

Q2. Is it possible to derive a beam-slab mechanism to adequately simulate the structural behavior of the bridge?

Q3. Can the shear studs that connect the girder and the deck slab be incorporated in the failure mechanism?

Q4. How can the tensile failure of the studs be mathematically expressed using the principle of virtual work?

Q5. How can the combination of the deck-slab, girder and stud failure be modeled?

Q6. How does the mechanism vary from a uniform sand loading to point loading due to wheels?

Q7. How much does the catenary effect and the strain hardening effect impact the results?

Q8. How may the upper bound and lower bound methods be modified according to the geometry of different bridges and the varying boundary conditions?

Q9. Can the bridges be subjected to a more advanced investigation to evaluate the declassification or should they remain classified as fracture critical?

Q10. Can recommendations be made for limiting the span length, widths or radii of curvature of the bridges to favor declassification.

CHAPTER III

VERIFICATION OF PLASTIC METHODS APPLIED TO STEEL TWIN-TUB GIRDER BRIDGE STRUCTURE

3.1. Chapter Summary

The previous work conducted to incorporate the limit analyses to bridges has not been able to present a definitive solution to the problem of failure analysis of bridges. Moreover, there is very limited research conducted on a large-scale implementation of the yield line method for bridges of longer spans. The existing analysis done in the past to implement the yield line method for finding the collapse load of a decommissioned Steel Twin-Tub Girder (STTG) bridge with a fracture critical condition imposed by fracturing the web and the bottom flange of the outermost girder showed the potential of this method to successfully predict the actual collapse load. It is, therefore, an essential step in the application of plastic limit methods for the analysis of such bridges to postulate a mechanism that captures the problem accurately. The actual experimental loading conditions are modeled and modifications are implemented in the mechanism to establish the flexural and shear failure likely to cause a collapse in the case under consideration. The analytical result generated from the postulated mechanism is under 1.4% error from the experimentally obtained results.

3.2. Introduction

The primary goal of yield line analysis is to validate the results from the static load test conducted experimentally during a previous TxDOT research project (Barnard et al. 2010). The full-scale testing of a typical STTG bridge was conducted as part of TxDOT Research Project 9-5498, and the experimental static ultimate load capacity of the bridge was reported. To develop a grasp over

the plastic theories and their application to bridge decks, it is imperative to check the analysis using the existing experimental data. Therefore, a test bridge from the TxDOT 9-5498 project is analyzed under the experimental loading conditions since this bridge span is a quintessential STTG single-span simply-supported bridge. Several analyses are conducted to postulate the mechanism that gives the critical mechanism for the test loading conditions.

In the present task, the yield line analysis of the same bridge was undertaken to validate the failure mechanism with the experimental results. The failure mechanism of the bridge is studied in detail to analyze the load path when the exterior girder is fractured along the depth of its webs and its bottom flange. The problem is evaluated in the light of various conditions, such as reduction in capacity due to the fracture of the outer girder, the contribution of the stud failure on the overall load carrying capacity, the capacity of the deck slab, and the impact of the external loads applied. The TxDOT 9-5498 research project evaluated the yield line theory under an equivalent truck load. However, the experiment was conducted using sand load and was perhaps not simulated accurately due to a simplified point loading used in yield line analysis and the calculated load was 22.5% lower than the actual load. The current research (TxDOT 0-6937) postulates yield theory for the exact loading conditions as the experimental test using shape functions to account for the complexity arising due to schematic uniform loading as shown in Figure 3.1

The deflections under the uniform loading of sand is a three-dimensional computation that can be solved using shape functions. The shape function used to find the deflection at any point $P(x,y)$ is given by

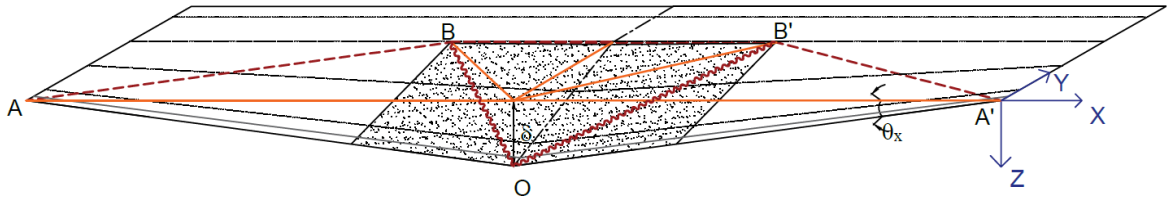

(a) Deflection of deck slab under uniformly distributed loading (schematic).

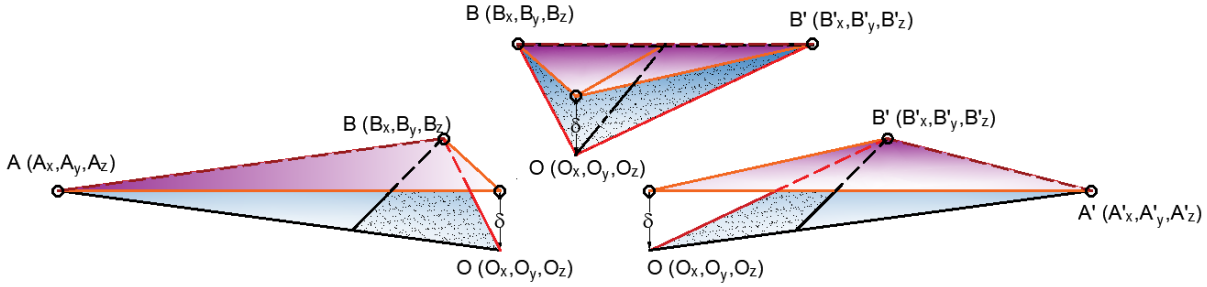

(b) Linear triangular elements formed between the yield lines.

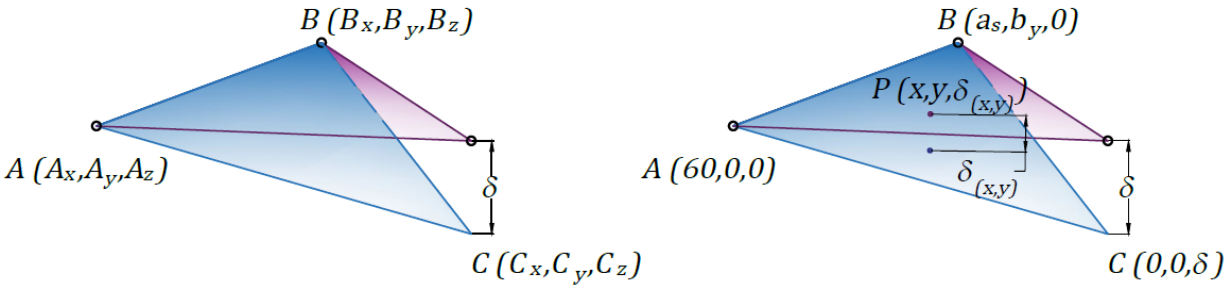

(c) Zoomed in view to demonstrate the shape function used for deflections.

Figure 3.1. Computation of Deflection of the Slab under Uniformly Distributed Loading

$$\delta_{(x,y)} = \begin{bmatrix} 1 & A_x & A_y \\ 1 & B_x & B_y \\ 1 & C_x & C_y \end{bmatrix} \quad (3.1)$$

where *P(x,y)* = any arbitrary point on the deck slab; $\delta_{(x,y)}$ = deflection of the slab at point *P(x,y)*, under the influence of sand loading; A_x, B_x and C_x are the x-coordinates of the points *A*, *B*, and *C*, respectively; and A_y, B_y and C_y are the y-coordinates of the points *A*, *B*, and *C*, respectively. The shear studs were not accounted for in the yield line solution in the TxDOT 9-5498 analysis. A modification is proposed in the current research that accounts for the internal capacity of the shear studs indicating a higher collapse load than that obtained from an analysis that does not include the enhanced capacity due to the shear studs. It should also be noted that the current research utilized the measured strength of the deck as stated in (Barnard et al. 2010) in the computations. The strengths of the steel are as specified by the design drawing of the test bridge (Neuman 2009). The result of this yield line analysis is 2.75% lower than the loads reported by the testing agency that can be attributed to the catenary action of the slab (Pirayeh Gar et al. 2014). The analysis procedures and results are discussed in the following sections.

3.3. Yield Line Theory

The governing equation for the yield line analysis establishes the overstrength factor as follows

$$\Omega EWD = IWD \quad (3.2)$$

where EWD = external work done by the factored loads based on 1.25DL + 1.75(LL + IM); IWD = internal work done on the yield lines in the deck, work done by plastic moments in the steel tub flanges (of the fractured girder), and work done by the pullout of shear studs between the

tub flanges and reinforced concrete deck slab; and Ω is an overstrength factor necessary to give equivalence with IWD.

3.3.1. Internal Work Done

The internal work done due to the deck, flanges of the fractured girder, exterior guardrail, and the studs can be computed as follows:

$$IWD = \sum m_x \theta_x y + \sum m_y \theta_y x + \sum W_{\text{stud}} \delta_{\text{stud}} \tag{3.3}$$

where $\sum m_x \theta_x y$ = the summation of the internal work done due to the moment capacity of the deck in the longitudinal direction, the internal work done due to the guardrail, and the internal work done due to the fractured girder; $\sum m_y \theta_y x$ = the internal work done due to the moment capacity of the deck in the transverse direction; $\sum W_{\text{stud}} \delta_{\text{stud}}$ = the internal work done due to the studs; m_x and m_y = the longitudinal and the transverse moment capacity, respectively; θ_x and θ_y = the angular deflection of the plane segments of the deck slab along the longitudinal and transverse directions, respectively; y and x = the distances along which the moment capacities act in the longitudinal and transverse directions, respectively; W_{stud} = the internal work done by the group of studs connecting the deck slab and the twin tub girders; and δ_{stud} = the deflection of the center of gravity of that length along which the girder flanges are assumed to separate from the deck slab according to the geometry of the mechanism selected.

3.3.2. External Work Done

The loading that was applied in the experimental study of the bridge at the Ferguson Structural Engineering Laboratory, University of Texas at Austin, has been recreated in terms of distributed loads. The girders forming the boundary enclosure for the sand are termed as *"sand bin,"* and the

applied sand load increasingly added until failure of the bridge takes place has been modeled as accurately as possible from the data available. The applied sand load is known to exert a load of 1615 kN from the experimental results. The external work done due to the self-weight of each component, such as the deck slab, the fractured girder, and guardrail has been computed. The work done due to the sand bin girders and the sand has been computed using the following expression.

$$EWD = \sum w_{\mathrm{d}} A_{\mathrm{d}} \delta_{\mathrm{d}} + \sum w_{\mathrm{load}} A_{\mathrm{load}} \delta_{\mathrm{load}} \tag{3.4}$$

in which $\sum w_{\mathrm{d}} A_{\mathrm{d}} \delta_{\mathrm{d}}$ = the total external work done due to the self-weight of the bridge components and $\sum w_{\mathrm{load}} A_{\mathrm{load}} \delta_{\mathrm{load}}$ = the total external work done due to the externally applied load of the sand bin girders and the sand; where w_{d} = the self-weight of the structure components expressed as an area load; A_{d} = the area of the respective components whose self-weight is w_{d}; δ_{d} = the deflection of the center of gravity of the region whose area is A_{d}; w_{load} = the external load applied due to the sand bin girders and the sand, expressed as an area load; A_{load} = the area of the applied load; and δ_{load} = deflection of the center of gravity of the region whose area is A_{load}.

Equations (3.3) and (3.4) are obtained in terms of the deflection (δ) that occurs at the location of maximum sagging. The principle of virtual work facilitates the computation of the load of sand needed to be added to reach the collapse of the bridge by equating Equations (3.3) and (3.4).

3.4. Validation of Yield Line Analysis with Experimental Results

This section gives a detailed analysis of the experimentally tested STTG bridge, which formerly was a single-lane, high-occupancy-vehicle (HOV) flyover exit-ramp of the interchange between IH 10 and Loop 610 in Houston, Texas as shown in Figure 3.2. The yield line analysis was validated using the experimental results from the TxDOT Research Project 9-5498.

(a) Experimental test bridge of TxDOT 9-5498 Project

(b) Applied sand loading for full-scale testing of TxDOT 9-5498 Project

Source:(Neuman 2009)

Figure 3.2. Experimental Test Bridge

3.4.1. Bridge Specifications and Details

This section describes the properties of the experimental test bridge under consideration used for the validation of the plastic limit analysis. Prior to the testing, this span was part of a single-lane, HOV flyover exit-ramp of the interchange between IH 10 and Loop 610 in Houston, Texas.

Material Properties

The deck slab was uniformly reinforced in each direction. The average cylindrical compressive strength of concrete in the deck slab was 6.70 MPa, and that in the exterior guardrail was also 6.70 MPa. The reinforcement in the longitudinal direction of the deck slab was provided with 13 mm diameter bars at 229 mm. on-center spacing with a nominal yield strength of 413.70 MPa at the top and 16 mm diameter bars at 152 mm on-center spacing with a nominal yield strength of 468.80 MPa at the bottom. The reinforcement in the transverse direction of the deck slab was provided with 16 mm diameter bars at 152 mm. on-center spacing with a nominal yield strength of 468.80 MPa at top and bottom. The nominal yield strength of the steel twin tub girders was 344.74 MPa. The modulus of elasticity of the steel is taken as 199945 MPa (Neuman 2009).

Bridge Properties

The bridge deck was 36.6 m long, 7.1 m wide, and 203 mm thick. Figure 3.3(a), (b), and (c) present the dimensions of the steel tub girder, the shear stud connection detail, and the guardrails, respectively. The web of the girder was 1448 mm deep and 13 mm thick. The flanges were 305 mm wide and 16 mm thick, spaced at 1.8 m on-center. The bottom flange steel plate was 1194 mm wide and 19 mm thick. A 76 mm haunch was provided between the reinforced concrete deck, and the deck was flanked by T501 guardrails on both sides longitudinally (Neuman 2009).

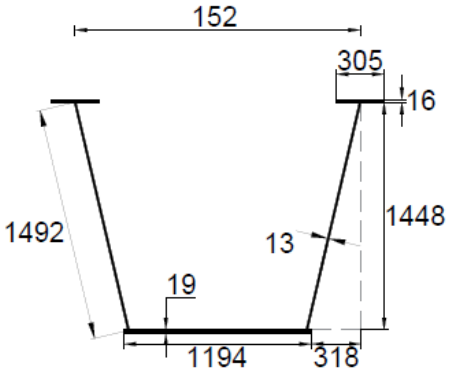

(a) Dimensions of steel tub girder

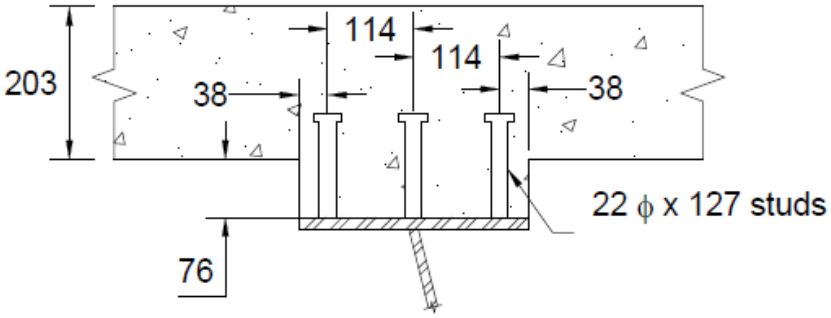

(b) Shear stud connection detail

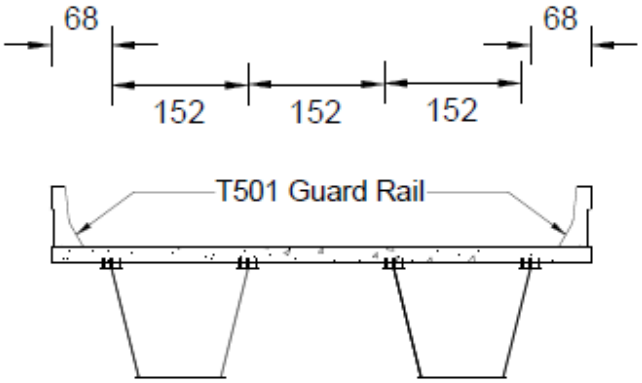

(c) Cross-section showing T501 guardrails

(all dimensions are in mm)

Figure 3.3. Bridge Properties.

Member Capacity

The internal work done computations are based upon the moment capacities of the various member components engaged in the failure mechanism of the bridge, such as the transverse and longitudinal deck-slab sections of unit foot width, the guardrail, and the flanges. These capacities are obtained using the standard U.S. code-based ultimate strength (Mn), using the yield strengths of steel and the characteristic strength of concrete as specified. These computations do not consider the effects of strain hardening. The flexural capacity of the railing was calculated by considering it as a regular doubly reinforced beam. The moment capacity of the flanges at the fractured section at mid-span was computed such that the compressive strength due to deck slab was not double counted.

The positive longitudinal moment capacity of the deck slab was m_x =72 kN-m/m; the negative longitudinal moment capacity per unit width of the deck slab was m'_x =48 kN-m/m; the positive transverse moment capacity per unit width of the deck slab was m_y =111 kN-m/m; and the negative transverse moment capacity per unit width of the deck slab was m'_y =88 kN-m/m. The moment capacity of the flanges of the fractured girder was M_f = 68 kN-m, and the moment capacity due to the T501 guardrail was M_{rail}= 55 kN-m. The pullout capacity of the shear studs was found to be 71 kN following the methods specified in ACI-318 (2017) and modified as per the recommendations from the experimental research conducted by Sutton (2007) and Mouras et al. (2008).

3.4.2. General Overview of Collapse Mechanism

An upper-bound yield line or plastic analysis solution may lead to a sufficient and economical treatment to address the reserve strength of bridges. A general treatise of plastic and yield line

methods may be found in (Park and Gamble 2000) . Plastic methods aim to identify the inherent reserve capacity of the structure that will be higher than the strength calculated from an elastic analysis. Elastic analysis is only able to identify the loads necessary to achieve first yield, whereas plastic methods provide the limit load that leads to a collapse mechanism. This rigid-plastic solution utilizes the equations of equilibrium or the virtual work equations; the former method is generally used for lower-bound strip methods, whereas the latter is used for upper-bound solutions. The assumed virtual deflection eventually gets eliminated from the solution equations, thereby producing a single equation in terms of the collapse load. This solution provides the mechanism by which yield lines and plastic hinges form and significant plastic deformation occurs. Such a plastic analysis approach provides a rapid procedure in contrast with computational solutions like the FEM solutions since plastic methods are essentially hand-calculation methods. The success of the upper-bound plastic solutions, however, rests largely on identifying the correct yield line pattern forming the collapse mechanism.

3.4.3. Potential Collapse Mechanisms for the Experimental Bridge

Various yield line collapse mechanisms may be postulated, and the collapse load is determined using either a virtual work or an equilibrium analysis. The correct mechanism provides the minimum collapse load. The most admissible mechanism is identified from the various possibilities such that the boundary conditions of the bridge and the deck slab are suitably modeled. The loading of the bridge influences the formation of the yield line pattern. The concrete beams that form a rectangular bin at the mid-span along the outer edge of the bridge are formed to pour the sand in the critical region above the fractured girder. The barrier dimensions impact the crack formation and the governing mechanism due to the added stiffness from the concrete girders.

Consider the experimental twin tub bridge span tested at the University of Texas (Barnard et al. 2010; Neuman 2009). Figure 3.4 illustrates the possible failure mechanisms that may occur due to the sand loading described in Neuman (2009) when the bending of the deck slab is on the longitudinal axis passing through the girder of the sand bin positioned at the nonfractured girder's interior flange. The different variables assigned for the dimensions of the bridge are needed for the computation of the load. The transverse dimensions are represented with b_e, b_g, b_s, b_r, and b'_y. The variables b_e, b_g, and b_s represent the width of the edge from the outer flange of the fractured girder, the overall width of each twin tub girder, and the spacing between interior flanges of the outer and inner girders, respectively; b_r = width assumed for the railing, and b'_y = the transverse distance from the outer edge of the bridge at which the horizontal yield line lies. The longitudinal dimensions are represented with X_x, a_e, a_s and a_b. X_x, a_e, a_s and a_b denote the distance of the point of intersection of the negative inclined yield line and the axis along the outer edge of the bridge from the mid-span, the length of half-span, the length of half of the negative horizontal yield line, and the length of half of the sand bin, respectively (Neuman 2009).

Solutions are presented for the variations of collapsed loads with the yield line geometry for different mechanisms and compared in Figure 3.5 (a). The graph shows the variation of the ultimate collapse load as the dimension of half of the horizontal negative yield line, a_s, varies from 0 m to 18.3 m. Figure 3.4 (a) (*Yield Line Mechanism [YLM] 1*) gives the overall minimum solution. However, it is eliminated as inadmissible because the girder is required to twist significantly, and this twist cannot be achieved unless the girder yields plastically. Figure 3.4 (b) (*YLM 2*) assumes the girder is seated at the center of the tub. This feature was not strictly the case in the tests, so it is eliminated.

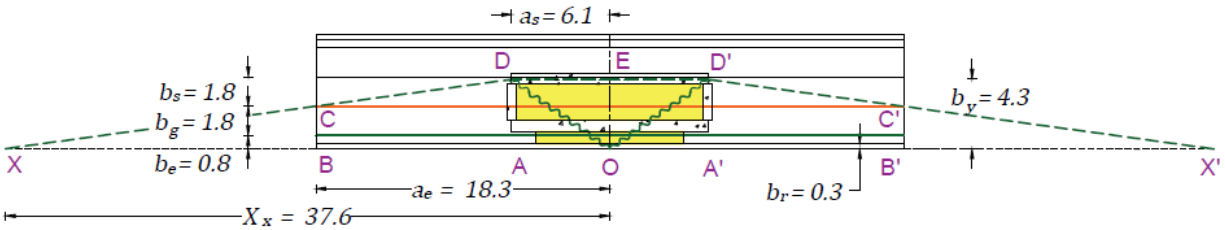

(a) YLM-1, Negative YL through interior flange of OG, Ultimate Collapse Load = 1036 kN

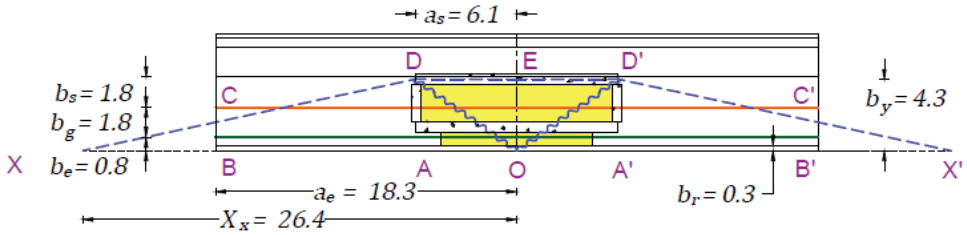

(b) YLM-2, Negative YL through mid-width of OG, Ultimate Collapse Load = 1320 kN

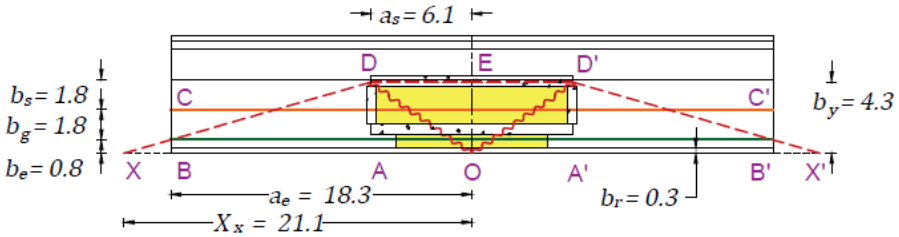

(c) YLM-3, Negative YL through exterior flange of OG, Ultimate Collapse Load = 1570 kN

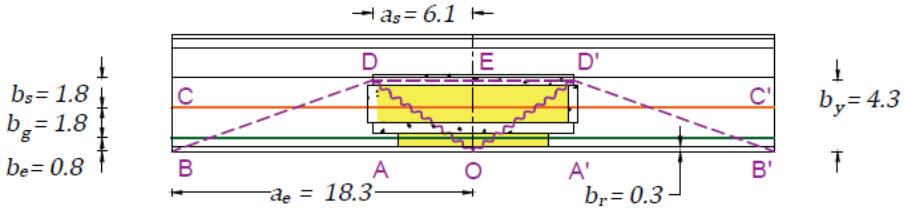

(d) YLM-4, Negative YL through edge of OG, Ultimate Collapse Load = 1780 kN

Note: YLM = yield line mechanism; YL = yield lines; OG = outside girder.
The colors distinguish different locations through which diagonal negative YL pass:
Green: passing through interior flange of OG; Blue: passing through mid-width of OG;
Red: passing through exterior flange of OG; Purple: passing through mid-width of OG.

Figure 3.4. Different Probable Yield Line Mechanisms to study the model that best represents Collapse Mechanism taking place in experimental sand loading test.

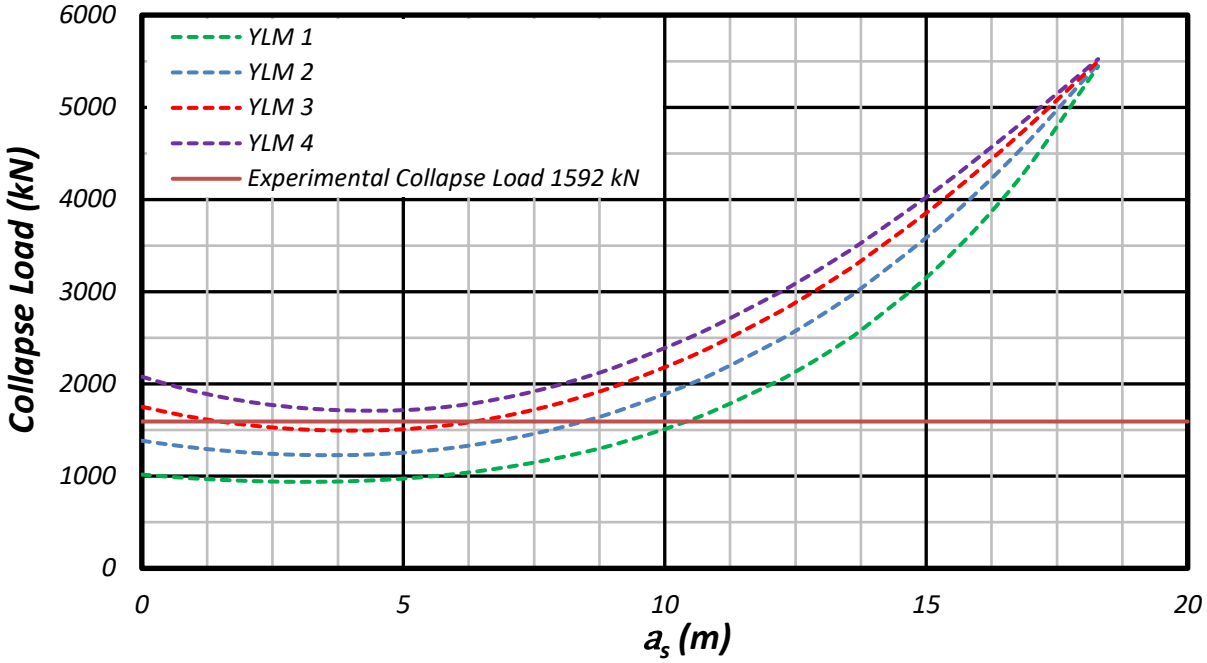

(a) Mechanisms 1 to 4, to be read in conjunction with Figure 3.4.

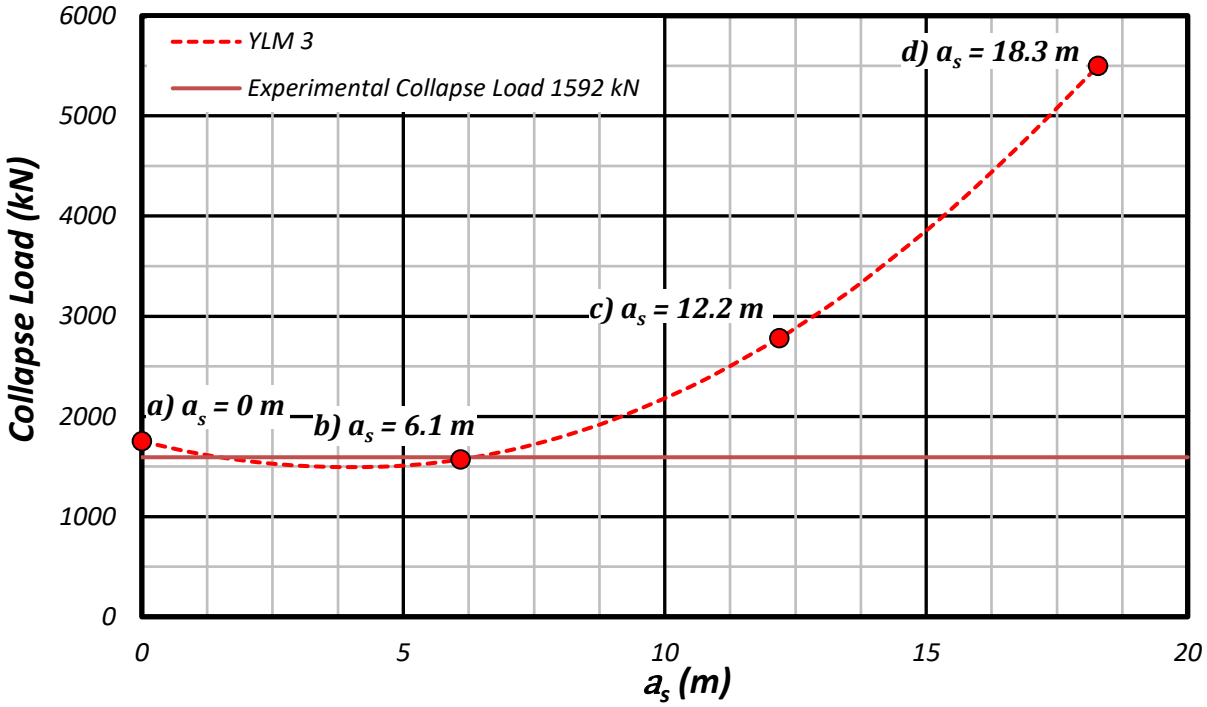

(b) Mechanism 3 showing the different solutions given in Figure 3.6

Figure 3.5. Minimization Curves of Ultimate Static Load Generated for Sand Load on TxDOT Research Project 9-5498.

Figure 3.4 (c) (*YLM3*) assumes the fractured girder is seated over its entire width. Displacement compatibility along the length of the girder is violated, requiring some of the shear studs to pull out. Indeed, this was the case in the reported tests, and accordingly this work has been incorporated into the analysis.

Similarly, *YLM 4*, shown in Figure 3.4 (d), requires stud pullout, but it should be noted that none of the *YLM 4* solutions in Figure 3.5(a) are critical, which leaves mechanism *YLM3* as the remaining viable mechanism. Among the various mechanisms, the case where the negative yield line passes through the exterior flange of the fractured outside girder is found to be the minimum. For this critical case, two of the values of a_s were short-listed such that the solutions resulting from these values encompass all possible mechanisms. Figure 3.5(b) illustrates the critical mechanism, with the loading for key a_s values indicated by red circles and pictorially represented in Figure 3.6

Figure 3.6 (a) and (b) illustrate two of the key mechanisms that form the extremities of the possible a_s values for *YLM3*. The parts (c) and (d) illustrate an intermediate case for a_s and a limiting case of X_x, which denotes the distance from mid-span to the location where diagonal negative yield lines intersect the point where the elevations meet at the zero-deflection datum. It is essential to carefully judge the admissibility of each mechanism in accordance with the boundary conditions and with the rules governing deformation compatibility. Several admissible collapse mechanisms were postulated in the given research. Since this is an upper-bound solution, the veracity of the critical collapse load must be thoroughly checked. Solution (b) shown in Figure 3.5(b), where a_s = 6.1 m, which is the half-length of the stiff barrier at the back of the sand heap, was adopted because it constrained the mechanism shown in Figure 3.6 (b).

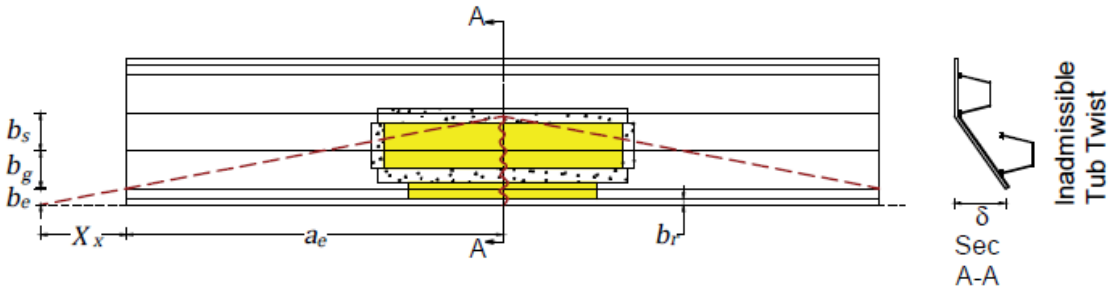

(a) Limiting case with a_s = 0 m

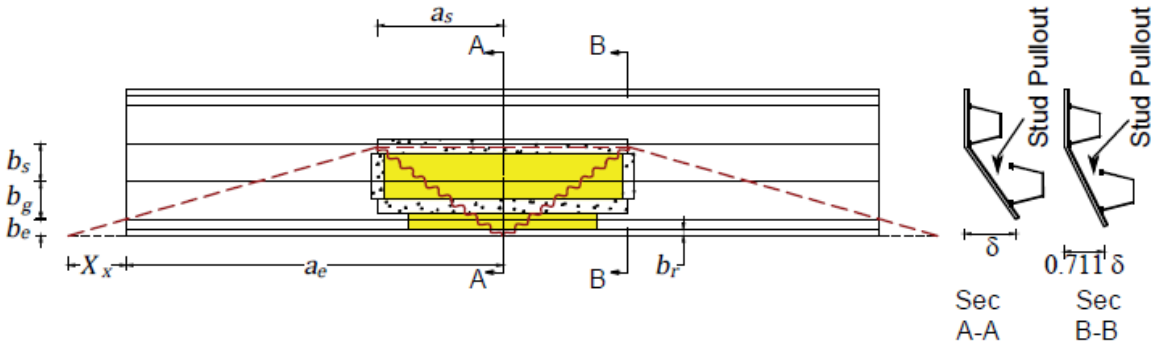

(b) Sand Bin constraint on a_s

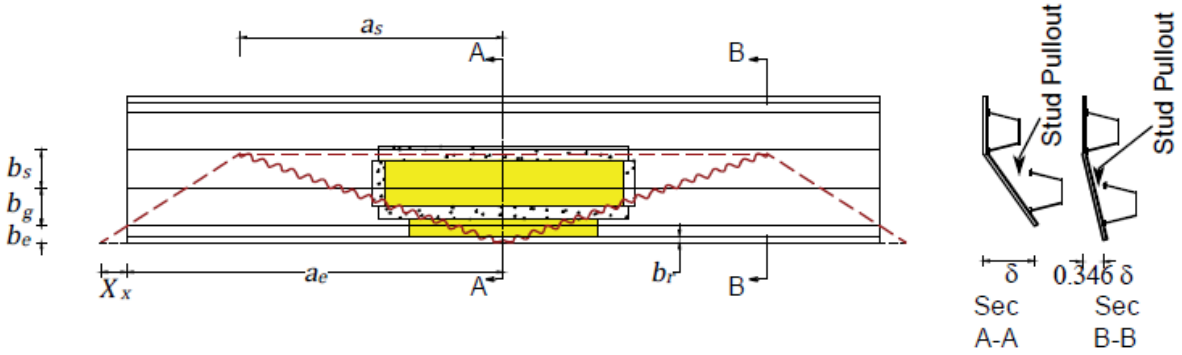

(c) Intermediate case encompassing all admissible values of a_s

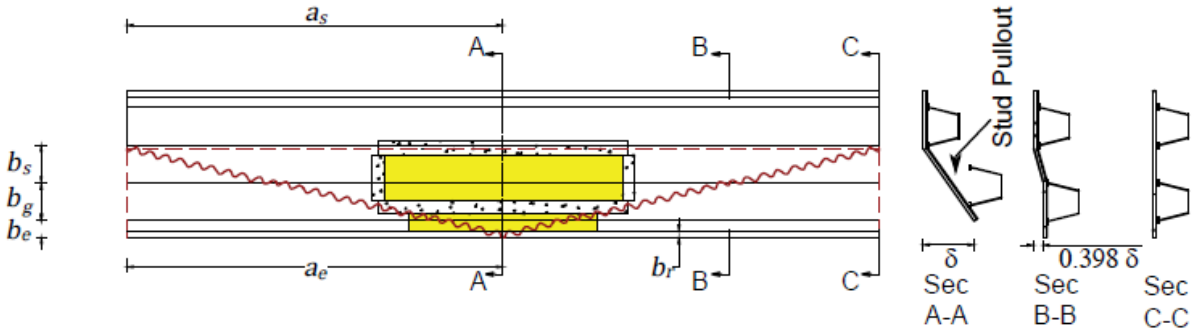

(d) Limiting case with a_s running along the span length

Figure 3.6. Probable Mechanisms Postulated.

3.4.4. Ultimate Collapse Load

Figure 3.7 illustrates the yield line mechanism chosen for the sand loading. The negative yield lines follow a trapezoidal shape due to spreading of the sand load over the deck slab. This pattern is corroborated well by the crack lines observed during the experimental testing for TxDOT Research Project 9-5498. The loading was recreated for the manual analysis of the experimental bridge using yield line theory. The sand loading was modeled to capture the effects on deck slab as accurately as possible by accounting for the geometry in which the sand was accumulated around and inside the concrete girders forming the periphery. The load primarily affects the mid-span since it was concentrated within the sand bin area. To account for this sagging behavior, the positive yield lines (represented by the wiggly lines), form a V-shape at the mid-span region. The minimization trials conducted as mentioned in Section 3.4.3. resulted in the optimal mechanism in which the diagonal negative yield lines passes through the outer flange of the fractured outside girder before it terminates at the point where the elevations meet at the zero- deflection datum, located at a certain distance X_x on either side of the mid-span. The ultimate collapse load computation consists of the internal and external work done calculations. The internal work done due to the slab (that has been divided into segments), the rail along the outer edge of the bridge, and the fractured outside girder are tabulated in Table 3.1. The internal work done due to the studs can be computed based on the assumption that the work is done due to the separation of the deck slab along the two flanges of the outside fractured girder following a constant angular deflection, ϕ, that can be expressed in terms of the deflection, δ.

$$\phi = \frac{\delta}{X_x} \tag{3.5}$$

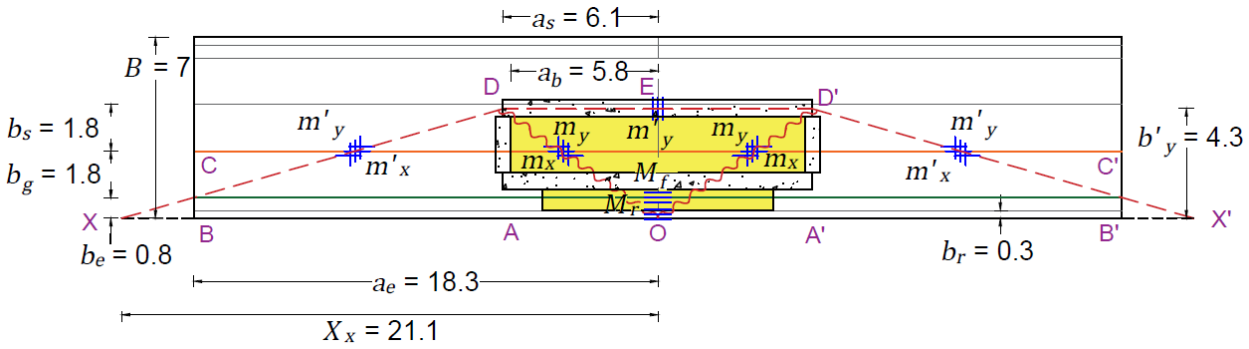

(a) Plan view of the bridge with the postulated yield line mechanism under experimental sand loading

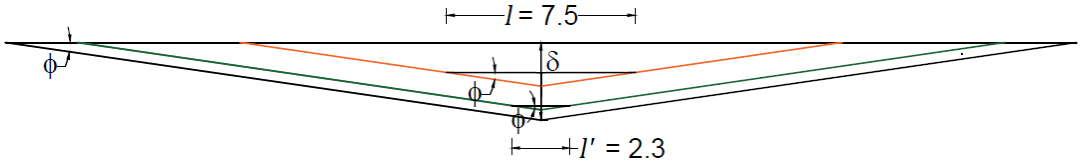

(b)Profile with angular deflections and assumed separation of the deck and flanges of outside girder (OG)

Figure 3.7. Critical Mechanism with the Inclined Negative Yield Lines passing through Exterior Flange of the Outside Girder at the Supports.

Table 3.1. Internal Work Done Due to Deck Slab, Fractured Outside Girder, and Rail.

Segment	Angular Deflection		Internal Work Done	
	$\boldsymbol{\theta_x}$	$\boldsymbol{\theta_y}$	$(\boldsymbol{m_x})(\boldsymbol{\theta_x})(\boldsymbol{y})$	$(\boldsymbol{m_y})(\boldsymbol{\theta_y})(\boldsymbol{x})$
OABCD, OA'B'C'D'	$\frac{\delta}{X_x}$	$\frac{\delta}{b'_y} - \frac{a_s}{b'_y(Xx)}\delta$	$2\left\{\begin{matrix}(m'_x)\left(\frac{\delta}{X_x}\right)(b'_y - b_e) \\ +(m_x)\left(\frac{\delta}{X_x}\right)(b'_y)\end{matrix}\right\}$	$2\left\{\begin{matrix}(m'_y)\left(\frac{\delta}{b'_y} - \frac{a_s}{b'_y X_x}\delta\right)(a_e - a_s) \\ +(m_y)\left(\frac{a_s}{b'_y X_x}\delta\right)(a_s)\end{matrix}\right\}$
DOE, D'OE	0	$\frac{\delta}{b'_y}$	0	$2\left\{(m'_y)\left(\frac{\delta}{b'_y}\right)(a_s)\right\}$
Rail	$\frac{\delta}{X_x}$	0	$2\,M_r\frac{\delta}{X_x}$	0
Girder	$\frac{\delta}{X_x}$	0	$2M_f\frac{\delta}{X_x}$	0
Total Internal Work Done			$2\left\{\begin{matrix}(m'_x)\left(\frac{\delta}{X_x}\right)(b'_y - b_e) \\ +(m_x)\left(\frac{\delta}{X_x}\right)(b'_y)\end{matrix}\right\}+ 2\left(\frac{\delta}{X_x}\right)(M_r + M_f)$	$2\left\{\begin{matrix}(m'_y)\left(\frac{\delta}{b'_y} - \frac{a_s}{b'_y X_x}\delta\right)(a_e - a_s) \\ +(m_y)\left(\frac{a_s}{b'_y X_x}\delta\right)(a_s)\end{matrix}\right\}+ 2\left\{(m'_y)\left(\frac{\delta}{b'_y}\right)(a_s)\right\}$

The design concrete breakout strength of the stud group N_{cbg} is computed to be 71 kN. The length of separation of the deck along the interior and exterior flanges of the outside fractured girder are denoted by l and l', respectively. The average separation between the deck slab and the interior and exterior flanges of the outside fractured girder are represented as δ_l and $\delta_{l'}$, given by the following equations.

$$\delta_l = 0.5\frac{l}{2}\phi \tag{3.6}$$

$$\delta_{l'} = 0.5\frac{l'}{2}\phi \tag{3.7}$$

The stud spacing is denoted by $s_{stud}$and is considered in meters. The internal work done due to studs is given as

$$IWD_{stud} = N_{cbg}s_{stud}(\delta_l l + \delta_{l'}\, l') \tag{3.8}$$

The external virtual work done by the deck slab, the girder, the guardrail, the girders forming the concrete bin girders, and the applied sand load can be expressed as

$$EWD = w_d A_d \delta_d + W_g \delta_g + W_r \delta_r + W_{cbg}\delta_{cbg} + w_s A_s \delta_s \tag{3.9}$$

where w_d = weight of deck slab per unit area; W_g = weight force of the fractured outside girder; W_r = weight force of the outer rail; W_{cbg} = weight force of the concrete bin girders; w_s = weight of sand load per unit area; A_d = area of the deck slab that undergoes deflection for the assumed yield line mechanism; A_s = area of the region in which the sand is poured; δ_d = deflection of the center of gravity of the area A_d; δ_g = deflection of the center of gravity of the fractured outside girder; δ_r = deflection of the center of gravity of the outer rail; δ_{cbg} = deflection of the center of gravity of the concrete bin girders; and δ_s = deflection of the center of gravity of the area A_s.

The sand load, w_s, is the unknown that can be solved by equating the internal work done and the external work done. Using the critical mechanism from the minimization curves and applying the concepts discussed in Section 3.4, the ultimate collapse load is computed to be 1570 kN. This compares well with the experimental collapse load of 1615 kN. It is to be noted that the experimental value reported includes the total weight of the sand poured. However, for this analysis, the entire sand does not contribute to the work done in causing virtual deflection because some of the sand that is spilled out of the deflecting region of the deck slab does no work for the assumed yield line mechanism.

Deducting that volume of the sand load from the reported collapse load, the failure load is calculated as 1592 kN. The analytical yield line result of W_{yield} = 1570 kN is quite close to the revised experimental outcome of W_{yield} = 1570 kN. The overall concept of the plastic yield line mechanism analysis is thus considered validated. The yield solution is expected to be an upper-bound solution, as suggested by (Park and Gamble 2000). However, the exception to this solution is that when deflections are extremely large and tensile, membrane forces may arise from a catenary action. For such action, the rigid-plastic theory adopted herein breaks down (Pirayeh Gar et al. 2014).

3.5. Chapter Findings

The problem of failure load analysis under uniform sand loading as per the TxDOT 9-5498 project was analyzed using the yield line analysis. Critical mechanism was finalized after the evaluation of the problem with all possible mechanisms. The load carrying capacity was computed after simulating the loading conditions according to the experimental details and it was necessary to modify the classical yield line theory to represent the capacity due to flexural strength of the deck

and beam combination and the tensile (pull-out) strength of the shear studs connecting the deck and beam. The shortcomings of the previously attempted yield line analysis to recreate the test problem were addressed by this modification of representing the internal work done due to studs as a tensile contribution in addition to the flexural contribution by the deck slab and the girder. The experimentally tested results show that a load of 1592 kN was applied in the form of sand load to cause the collapse of the bridge, although the value of collapse load mentioned in the report was 1615 kN. It is to be noted that the value reported is inclusive of the entire volume of sand that was added to the deck. However, the load that actually participated in the work done to cause failure was calculated to be 44 kN short of the reported load. Therefore, it was concluded that the postulated mechanism captures the failure mechanism with reasonable accuracy and yield line theory may be a viable tool for the assessment of such bridges.

CHAPTER IV

PLASTIC ANALYSIS THEORY TO IDENTIFY RESERVE CAPACITY AFTER ONE GIRDER HAS FRACTURED

4.1. Chapter Summary

There is a need for the development of the yield line limit analysis method to solve the problem of analyzing Steel Twin-Tub Girder (STTG) bridges under the standard American Association of State Highway and Transportation Officials (AASHTO) loading. The complexity of the bridge geometry is to be assessed in accordance with the behavior of structural elements under the given loading. The upper bound and lower bound theories are developed to establish a general solution for capturing the failure mechanism. The upper bound method is formulated for the critical path flanked by the girders, that undergoes a combination of flexural and torsional bending. Virtual work equations are used to generate expressions for reserve capacity for several possible admissible mechanisms. The minimization of all these solutions is conducted to generate the critical solution for the strip of the bridge under consideration. The solutions are further extended and applied to the full bridge, after accounting for the curvature of the spans. The spans of different boundary conditions are treated individually in detail to develop case-wise expressions of reserve capacity. These expressions will aid in the preliminary assessment of the reclassification of such bridges from their fracture critical status. The ease and nature of this computation makes this method very economic and, therefore, has the potential to save the transportation authority from spending millions of dollars in unwarranted inspections. The findings are concluded by comparing the deflection contours of the yield line analysis with the Finite Element Method (FEM) generated deflection maps.

4.2. Introduction

This section presents the theory behind postulated collapse mechanism for HL-93 load case using the method of virtual work. A derivation is given for a critical folded plate yield-line mechanism that is representative of expected limit behavior in a certain class of bridge deck systems. General equations are then derived for the overstrength factor of fracture critical bridges. The establishment of the yield line theory with the equivalent torsional mechanism is challenging and is accompanied by a supplementary strip method solution to obtain a range of upper bound and lower bound solutions. These solutions are necessary to give an estimate of the reserve capacity of the bridges under the extreme case of outer girder completely fractured. The derivation of the two solutions helps in quantifying the underlying differences in the contribution to inherent strength and stability of a redundant system for the methods. The solutions are modified to account for the curvature of the bridges.

The establishment of the solution aims to equip bridge engineers with a simple yet effective tool to initiate the process of reclassification of bridges as fracture critical. The solutions give a range of expected values within which the overstrength factor will lie and will also indicate whether or not a more advanced analysis such as FEM or Grillage analysis is needed to be undertaken.

4.3. Virtual Work Equations

Bridge decks supported by fracture critical girders are analyzed by yield-line theory using the equations of virtual work. In the upper-bound method of plastic collapse mechanism analysis, any kinematically admissible mechanism may be postulated. The mechanism with the lowest collapse load is then the theoretically correct mechanism.

Figure 4.1 presents a folded plate mechanism (Lindsay et al. 2004) with N yield lines zigzagging between the unfractured and fractured girders, where N is an unknown number of diagonal yield lines but determined by a load minimization procedure. The degree of an equivalent distributed load that may be placed over the fractured girder, W_e, and its magnitude is found via a virtual work analysis. Consider a folded plate mechanism supported on three sides, with the fourth side supported by a torsionally restrained beam with a central hinge, as shown in Figure 4.1(a). Note that negative (hogging) yield lines are dashed, while wiggly solid yield lines are positive (sagging) moments. The long edge with double hatching is fully fixed (clamped against rotation) while the ends are simply supported (free to rotate). The figure also shows the transverse angular deflections along the D-D, E-E, and F-F profiles.

Figure 4.1(b) depicts the side elevation illustrating the deflection profiles along Sections A-A, B-B, and C-C. Figure 4.1(c) and (d) show the geometry of the folded plate mechanisms with deflections, from which the internal work done is derived by considering the half-span of a bridge, as shown. Displacing the fractured girder downward by unit displacement (δ = 1) at mid-span, the external work done is given by

$$EWD = W_e L_x \frac{\delta}{2} = 0.5 W_e L_x \tag{4.1}$$

The internal work done is computed for the cases obtained by incrementing the number of diagonal yield lines in multiples of four, and a pattern emerges that is used for expressing the internal work done in terms of N. The internal work done is thus expressed as

$$IWD = \sum (m'_x + m_x)(\theta_x)(y) + \sum (m'_y + m_y)(\theta_y)(x) \tag{4.2}$$

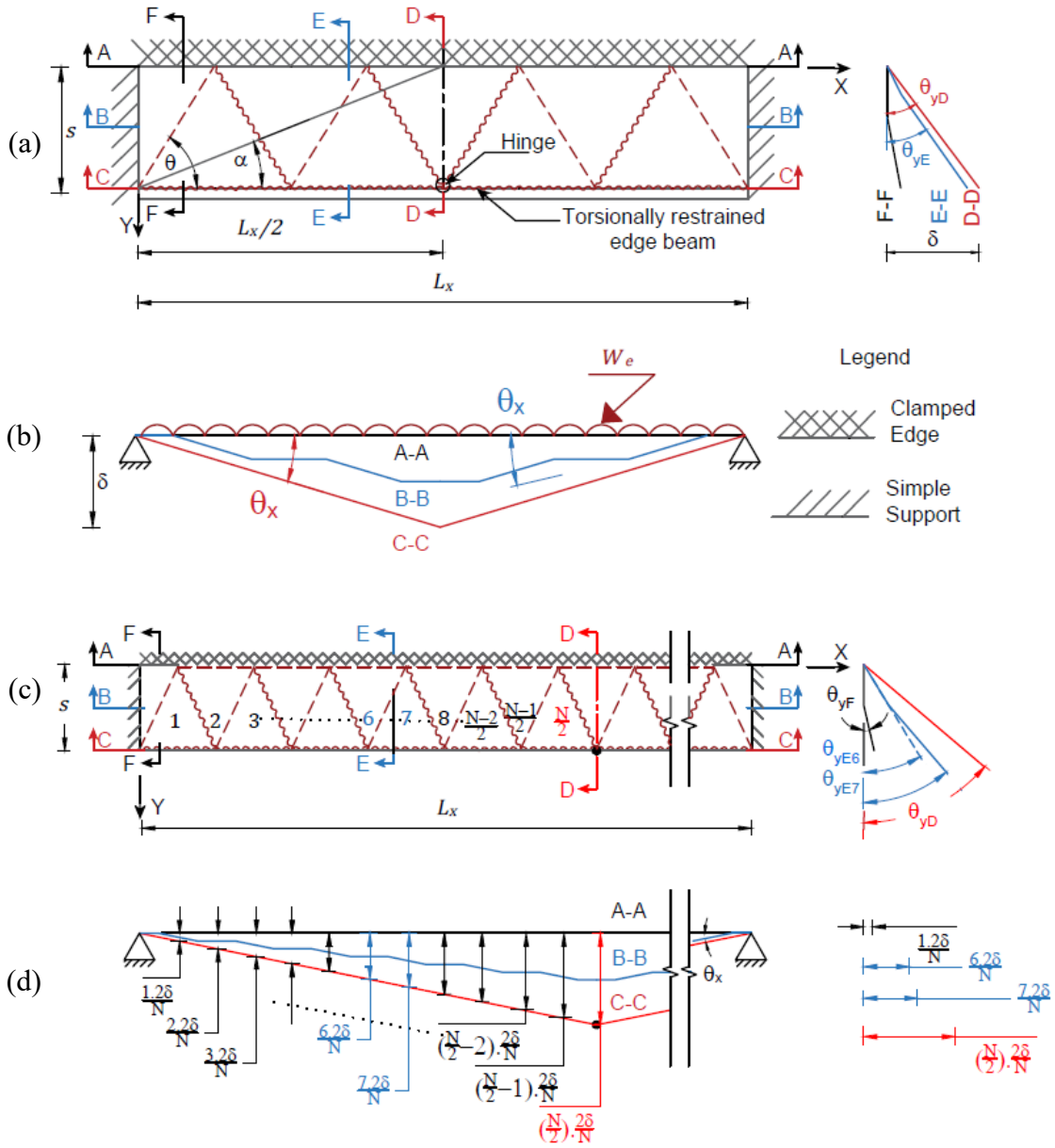

Figure 4.1. Folded Plate Mechanism for N diagonal yield lines showing (a) Plan View and Side Elevation with deflection profiles along D-D, E-E, and F-F; (b) Side Elevation with deflection profile along Sections A-A, B-B, and C-C; (c) Plan View focusing on half bridge with N Diagonal yield lines and Side elevation with transverse angular deflection; and (d) Side View with deflection profiles with longitudinal deflections along Profile C-C.

The deflection profile C-C shows a linear variation from zero at the supports to δ at the fracture location (mid-span). The angle of rotation in the longitudinal direction is a constant given by the slope of the section along C-C. Observing the section profile B-B, the section plateaux out between the alternate triangular segments formed between the zigzag yield lines. Therefore, the internal work done due to the longitudinal reinforcement for each of the triangular segment under consideration for half the span length is considered. Since the rotation takes place alternately, the summation is carried out $N/4$ times for the half span of the bridge.

$$\frac{1}{2} IWD_x = \frac{N}{4} (m'_x + m_x) \left(\frac{2\delta}{L_x}\right) (s) \tag{4.3}$$

Twice the summation of the term in Equation (4.3) simplifies to the following expression for internal work done due to longitudinal reinforcement for the entire span as

$$IWD_x = (m'_x + m_x) \left(\frac{\delta}{L_x}\right) (sN) \tag{4.4}$$

The rotation of the slab in the transverse direction is not constant since it depends on the deflection of the slab along the C-C section, which linearly varies. Figure 4.1(c) and (d) show the deflection at every $1/N$ th segment, where each segment's length is L_x/N. It is observed that the deflection of the ith segment is the ith multiple of $2\delta/N$, which implies a maximum deflection at the mid-span when i = $N/2$. The angle of rotation in the transverse direction is the ratio of the ith deflection to the spacing, s. At section F-F, the rotation takes place once by the negative diagonal yield line and is calculated to be $(1 \times 2\delta)/sN$ over a distance of L_x/N. Along section E-E, the horizontal negative yield line rotates the slab by $(6 \times 2\delta)/sN$ over a distance of $2L_x/N$. The negative diagonal yield line causes a rotation of $(7 \times 2\delta)/sN$ over a distance of L_x/N. The horizontal

positive yield line plateaux the slab from a rotation of $(7 \times 2\delta)/sN$ over a distance of $2L_x/N$. Similar rotations take place for each section passing through the negative diagonal yield lines. Similarly, positive rotations pass through the sections with positive diagonal yield lines. An exception is the triangle shown at D-D. Since this analysis solves the problem using symmetry, care must be taken that the horizontal negative yield line rotates the slab in a similar way, with a rotation of $(0.5N \times 2\delta)/sN$, but for a distance of L_x/N.

The internal work done is calculated along all the yield lines, and it is observed from the terms of the expression that the deflections form an arithmetic progression (AP) from 1 to $N/2$ terms. Using the result of the sum of first *"n"* natural numbers of an AP, $n(n+1)/2$ and substituting in terms of the problem parameters, the expression of the internal work done due to transverse reinforcement for each of the triangular segment under consideration for half the span length is given by

$$\sum IWD_{y.i} = \sum_{i=1}^{N/2} (m'_y + m_y)\left(\frac{i.2\delta}{sN}\right)\left(\frac{L_x}{N}\right) \tag{4.5}$$

Twice the summation then provides the internal work done due to the transverse reinforcement of deck-slab for the entire span as follows

$$IWD_y = \left(\frac{m'_y + m_y}{2s}\right)\left(\frac{0.5N+1}{0.5N}\right)\delta L_x \tag{4.6}$$

Substituting Equations (4.4) and (4.6) in Equation (4.2), the total internal work done due to the folded plate mechanism is given as the summation of IWD_x and IWD_y, thus expressed as

$$IWD = \left[\left(\frac{m'_y + m_y}{2s}\right)\left(1+\frac{2}{N}\right)L_x + \left(\frac{m'_x + m_x}{L_x}\right)sN\right]\delta \tag{4.7}$$

where m'_y and m_y are the negative and positive moment capacities per unit width in the y-direction, respectively, and m'_x, and m_x are the negative and positive moment capacities per unit width in the x-direction, respectively; N = the number of diagonal yield lines in the area under consideration; L_x = the length of the span of the bridge; and s = the width of the area of the slab along which the mechanism under consideration is applied.

Equating the external and internal work, $EWD = IWD$, gives an expression for finding N, the derivation of which is shown in the following equations

$$W_e L_x \frac{\delta}{2} = \left[\left(m'_y + m_y\right)\left(\frac{L_x}{2s}\right) + \left(m'_y + m_y\right)\left(\frac{L_x}{sN}\right) + \left(m'_x + m_x\right)\left(\frac{sN}{L_x}\right)\right]\delta \tag{4.8}$$

from which the equivalent collapse load on the girder can be determined as follows:

$$W_e = \frac{2}{L_x}\left[\left(m'_y + m_y\right)\left(\frac{L_x}{2s}\right) + \left(m'_y + m_y\right)\left(\frac{L_x}{sN}\right) + \left(m'_x + m_x\right)\left(\frac{sN}{L_x}\right)\right]\delta. \tag{4.9}$$

The line load W_e, will have a minimum value when $\frac{dW_e}{dN} = 0$, as follows:

$$\frac{dW_e}{dN} = -\left(m'_y + m_y\right)\left(\frac{L_x}{sN^2}\right) + \left(m'_x + m_x\right)\left(\frac{s}{L_x}\right) = 0 \tag{4.10}$$

$$\frac{\left(m'_y + m_y\right)}{\left(m'_x + m_x\right)} = \left(\frac{s^2N^2}{{L_x}^2}\right) \tag{4.11}$$

Upon solving, the minimum value of N is obtained such that

$$N = \frac{L_x}{s}\sqrt{\frac{m'_y + m_y}{m'_x + m_x}} \tag{4.12}$$

Back-substituting N into Equation (4.9) gives the equivalent collapse line load as shown

$$W_{e\,min} = \frac{4}{L_x}\sqrt{(m'_x + m_x)(m'_y + m_y)} + \frac{(m'_y + m_y)}{s} \tag{4.13}$$

It is also of interest to note the geometry of yield lines. From Figure 4.1(a), the angle θ may be found using trigonometry.

$$\tan\theta = \frac{sN}{L_x} = \sqrt{\frac{m'_y + m_y}{m'_x + m_x}} \tag{4.14}$$

where θ is the angle of the diagonal yield lines with the horizontal. Therefore, Equation (4.13) may be further simplified to give alternate forms for expression for $W_{e\,min}$.

$$W_{e\,min} = \frac{(m'_y + m_y)}{s} + 4\left(\frac{m'_x + m_x}{L_x}\right)\tan\theta \tag{4.15a}$$

or

$$W_{e\,min} = \frac{(m'_y + m_y)}{s}\left[1 + \frac{4s}{L_x}\cot\theta\right] \tag{4.15b}$$

Note that for isotropic reinforcement, $m_x = m_y$ and $m'_x = m'_y$, θ = 45°. A similar result to Equation (4.14) is given in Park and Gamble (2000) based on the Affinity Theorem for orthotropic plates.

The aforementioned theory was applied to the test bridge from TxDOT Research Project 9-5498 and the minimum equivalent lane load was computed. Figure 4.2 presents a graph plotting the minimization of the distributed load, W_e, with respect to the number of diagonal yield lines, N.

Consider an area load of w acting on the trapezoidal region of the slab shown in Figure 4.1. The virtual work done by the load will be the product of the load, the area on which it acts, and the virtual deflections of the center of gravity of that area.

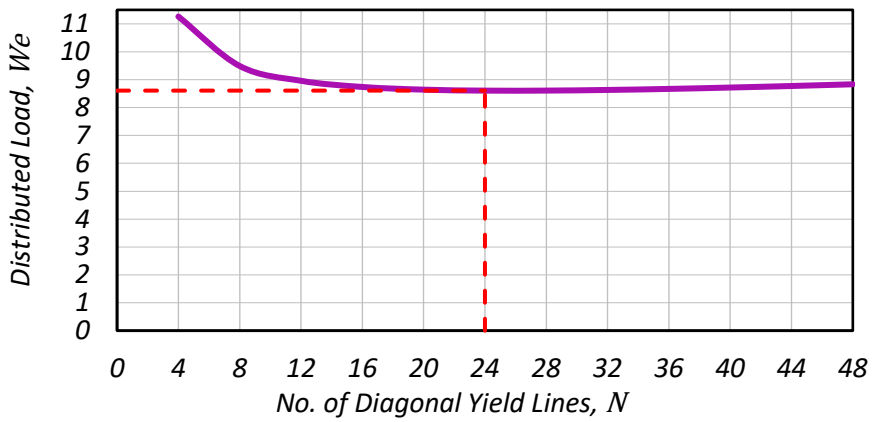

Figure 4.2. Variation of Distributed Load with Number of Diagonal Yield Lines.

From Figure 4.1(a), it can be observed that the diagonal yield lines divide the slab into triangular segments that undergo deflection. The virtual deflections of the triangular segments alternate as follows. Considering half the span, as shown in Figure 4.1(c), and starting from the supports, the centroidal deflection is the i^{th} multiple of $4/3N$, where i = 1, 3, 5, … (0.5 N-1)—in other words, a set of odd integers from 1 to (0.5 N-1); and it is the j^{th} multiple of $2/3N$, where j = 2, 4, 6, … (0.5 N-2), or a set of odd integers from 2 to (0.5 N-2). This encompasses the centroidal deflections of all the triangular segments from the support till the mid-span except the half triangle at section D-D. The areas of all these segments are Ns/L_x. As seen in the case of the internal work done, an exception is the triangle at section D-D, with an area of $Ns/2L_x$ and a centroidal deflection of 1/3. A pattern emerges from several computations of the external work done by incrementing the number of diagonal yield lines in multiples of 4, similar to that observed from the calculations of the internal work. The alternate centroidal deflections from the supports to the mid-span form two series of arithmetic progression, one of first $N/4$ odd numbers, from 1 to

(0.5 N-1), and the other of first (.25N-1) even numbers, from 2 to (0.5 N-2). The sum of each series is obtained using the expression for the sum of first n terms of an AP, $0.5n\,(a_1 + a_n)$, where $a_1$and a_n are the first and n^{th} terms of the AP, respectively.

The summation of the product of the areas of each segment for half the span with their respective centroidal deflections is given as $sL/12$ for the odd numbered segments, (N-4) $sL_x/24N$ for the even numbered segments, and $sL/6\,N$ for the triangle at D-D section. For the full span, the summation of the product of slab segment and the centroidal deflection is $sL_x/4$. The external work done due to area load w is given by $EWD_{trapezium}$.

$$EWD_{trapezium} = wsL_x/4 \tag{4.16}$$

4.3.1. Upper-Bound Solution

From the yield line solution from Equation (4.8), the total load on the girder can be set as $W_T = L_x W_e$. Then, equating external and internal work done (with δ = 1) yields the following

$$0.5W_T = \left[\left(m'_y + m_y\right)\left(\frac{L_x}{2s}\right) + \left(m'_y + m_y\right)\left(\frac{L_x}{sN}\right) + \left(m'_x + m_x\right)\left(\frac{sN}{L_x}\right)\right] \tag{4.17}$$

where W_T = total ultimate load at the bridge participating in the collapse mechanism.

The internal work done may be rewritten by substituting Equation (4.12) in Equation (4.7) and further simplified using Equation (4.14). For the next step, put in the $IWD = EWD$ format using Equation (4.15a) as shown

$$\Omega 0.5W_T = \Omega 0.5W_e L_x = 2\left(m'_x + m_x\right)\tan\theta + \left(m'_y + m_y\right)\frac{L_x}{2s} \tag{4.18}$$

$$\Omega 0.5W_T = \left(m'_y + m_y\right)\frac{L_x}{2s}\left[1 + 2\left(\frac{2s}{L_x}\right)\left(\frac{m'_x + m_x}{m'_y + m_y}\right)\tan\theta\right] \tag{4.19}$$

Define angle α, as shown in Figure 4.1(a), such that

$$\frac{s}{L_x/2} = \tan\alpha \tag{4.20}$$

Then, by using Equation (4.14), Equation (4.19) may be recast as

$$\Omega 0.5W_T = \left(m'_y + m_y\right)\cot\alpha\left[1 + 2\frac{\tan\alpha}{\tan\theta}\right] \tag{4.21}$$

Thus, the system upper-bound overstrength factor is given as follows

$$\Omega_{Upper} = \frac{IWD}{EWD} = \frac{\left(m'_y + m_y\right)[\cot\alpha + 2\cot\theta]}{0.5W_T} \tag{4.22a}$$

or

$$\Omega_{Upper} = \frac{\left(m'_y + m_y\right)\left(\frac{L_x}{2s}\right)\left[1 + 2\frac{\tan\alpha}{\tan\theta}\right]}{0.5W_T} \tag{4.22b}$$

4.3.2. Lower-Bound Solution

The governing moment equation that satisfies the equilibrium of a 2D plate type structure is given by:

$$\frac{\partial^2 m_x}{\partial x^2} + 2\frac{\partial^2 m_{xy}}{\partial x \partial y} + \frac{\partial^2 m_y}{\partial y^2} = -w \tag{4.23}$$

where m_x, m_y = the bending moments per unit width in the x- and y- directions, respectively; $m_{xy} = m_{yx}$ = torsional moments per unit width acting on the faces of the infinitesimal slab element of dimensions d_x and d_y in the x- and y- directions, respectively, if the complementary shear stresses are equal in magnitude, but directionally opposite in nature.

A (conservative) lower bound solution is to ignore the torsional resistance m_{xy} and m_{yx} of cracked concrete as this resistance becomes very small the more concrete behaves in a highly cracked fashion. Thus, Equation (4.23) may be simply recast as

$$\frac{\partial^2 m_x}{\partial x^2} + \frac{\partial^2 m_y}{\partial y^2} = q_x + q_y = w \tag{4.24}$$

where $q_x = \frac{\partial^2 m_x}{\partial x^2}$ is the load carried by strips oriented in the x-direction and $q_y = \frac{\partial^2 m_y}{\partial y^2}$ represents the load carried in the y-direction. This forms the basis of the strip method.

A stringent limit analysis considers a moment distribution that leads to the highest (most accurate) ultimate load. Elastic theory moments, unlike the plastic theory moment distributions, are unique (meaning only one distribution exists) since these are proportional to the curvatures at the slab section. A lower-bound solution may also be formed using a strip method (Park and Gamble 2000).

Figure 4.3 illustrates the lower-bound solution via strips in equilibrium in the x- and y-directions, respectively, where W_x and W_y are the uniformly distributed loads on the longitudinal and transverse strips, respectively.

Consider the W_y strips (assuming $L_x = s$):

$$\left(m'_y + m_y\right) = 2W_y \frac{L_x}{4} = 2W_y \frac{2s}{4} = W_y s \tag{4.25}$$

$$\therefore W_y = \frac{\left(m'_y + m_y\right)}{s} \tag{4.26}$$

Distributed load by W_x strips:

$$(m'_x + m_x) = \frac{W_x}{s}\frac{{L_x}^2}{8} \text{ Thus, } W_x = \frac{8s}{{L_x}^2}\ (m'_x + m_x) \tag{4.27}$$

$$W_e = W_x + W_y = \frac{8s}{{L_x}^2}(m'_x + m_x) + \frac{\left(m'_y + m_y\right)}{s} \tag{4.28}$$

$$\Omega 0.5 W_T = \Omega 0.5 W_e L_x = \left(m'_y + m_y\right)\frac{L_x}{2s} + \frac{4s}{L_x}(m'_x + m_x) \tag{4.29}$$

but, $\frac{s}{L_x/2} = \tan\alpha$, therefore by inversion it is substituted into Equation (4.29):

$$\Omega 0.5W_T = \left(m'_y + m_y\right)\cot\alpha + 2(m'_x + m_x)\tan\alpha \tag{4.30}$$

$$\Omega 0.5W_T = \left(m'_y + m_y\right)\left[\cot\alpha + 2\left(\frac{m'_x + m_x}{m'_y + m_y}\right)\tan\alpha\right] \tag{4.31}$$

$$\Omega 0.5W_T = \left(m'_y + m_y\right)[\cot\alpha + 2\cot^2\theta\tan\alpha] \tag{4.32}$$

Solving gives the lower-bound overstrength factor as follows

$$\Omega_{Lower} = \frac{\left(m'_y + m_y\right)[\cot\alpha + 2\cot^2\theta\tan\alpha]}{0.5W_T} \tag{4.33a}$$

or

$$\Omega_{Lower} = \frac{\left(m'_y + m_y\right)\left(\frac{L_x}{2s}\right)\left[1 + 2\frac{\tan^2\alpha}{\tan^2\theta}\right]}{0.5W_T} \tag{4.33b}$$

4.3.3. Generalized Plastic Solution

By harmonizing the upper- and lower-bound solutions, a general solution covering the two distinct approaches is as follows

$$\Omega = \frac{\left(m'_y + m_y\right)\left(\frac{L_x}{2s}\right)k_{bound}}{0.5W_T} \tag{4.34}$$

in which

$$k_{bound}^{upper} = \left[1 + 2\frac{\tan\alpha}{\tan\theta}\right] = 1 + \frac{4s}{L_x}\sqrt{\left(\frac{m'_x + m_x}{m'_y + m_y}\right)} \tag{4.35}$$

and

$$k_{bound}^{lower} = \left[1 + 2\frac{\tan^2\alpha}{\tan^2\theta}\right] = 1 + \frac{8s^2}{{L_x}^2}\left(\frac{m'_x + m_x}{m'_y + m_y}\right) \tag{4.36}$$

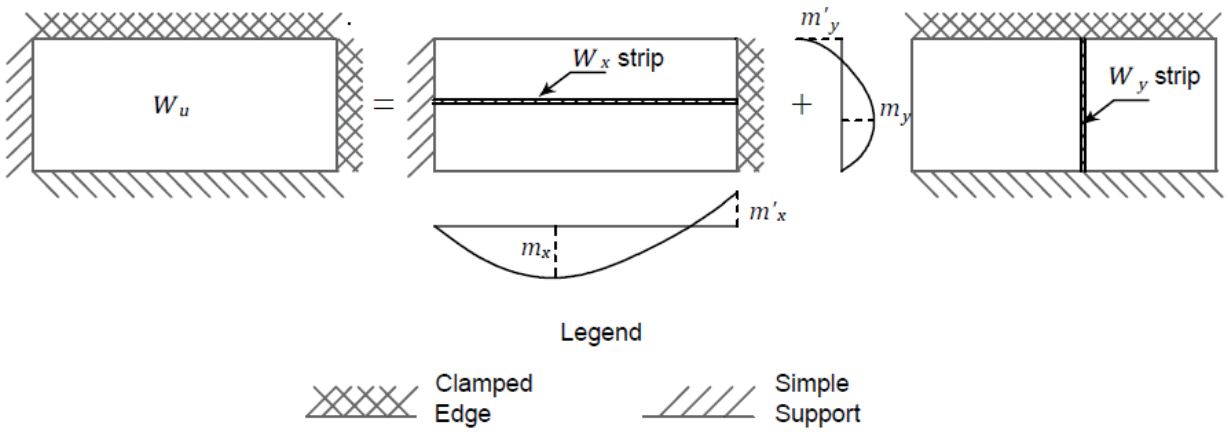

(a) Basic illustration of Strip Method for slabs with varying boundary conditions.

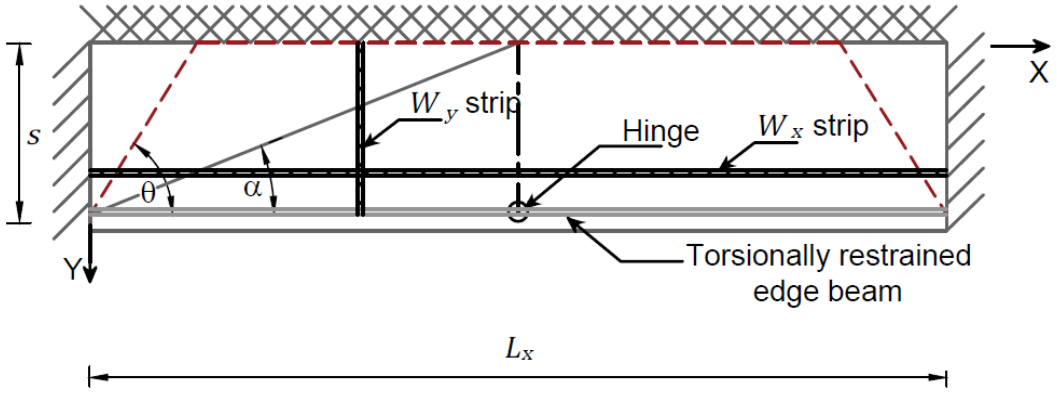

(b) Plan view of interior slab with a central fracture on the edge beam.

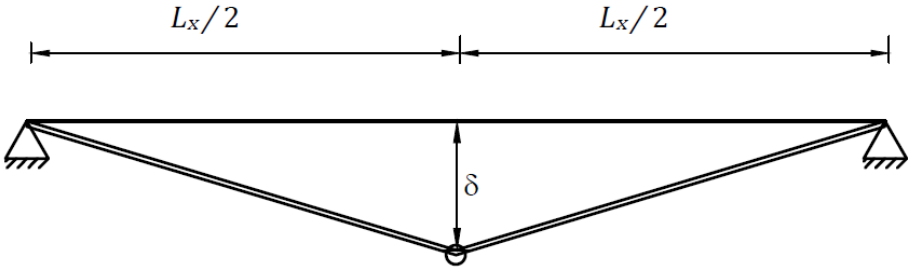

(b) Side elevation of the mechanism.

Figure 4.3. Strip Equivalent Mechanism.

4.3.4. Accounting for the Effect of the Horizontal Curve of a Bridge

Figure 4.4 presents a schematic representation of a generic curved bridge in plan view. Since the bridges are curved in reality, with a centerline radius of curvature $R_{℄}$, arched at an angle ω, with a centerline length, L_x, and breadth, B, the length of the innermost edge progressively increases as a function of $R_{℄}$ and ω.

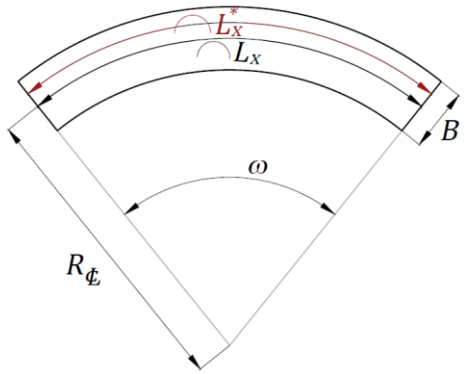

Figure 4.4. Layout of a Generic Curved Bridge in Plan.

Since the internal work done is primarily contributed by the trapezoidal band that is equidistant from the centerline of the bridge at a distance of $s/2$, the increase and decrease of the arc lengths of this folded plate mechanism are compensated. Therefore, the span length L_x used for the internal work done calculations for the trapezoidal region refers to the length of the centerline of the bridge span. However, since the outer region primarily contributes toward the external work done for the yield line mechanism under consideration and the internal work done by the region beyond the trapezoidal band, the span length used in those computations refers to the length of the outer region of the curved bridge.

$$L_x^* = (R_{℄} + 0.25B)\omega \tag{4.37}$$

$$\omega = \frac{L_x}{R_{℄}} \tag{4.38}$$

$$L_x^* = \left(1 + \frac{B}{4R_{℄}}\right) L_x \tag{4.39}$$

4.4. Overstrength Capacity for Factored Applied Loads for Single-Span Bridge

The HL-93 loading consists of HS-20 trucks having 36 kN, 142 kN, and 142 kN axle loads spaced 4.3 m apart along the bridge span and placed centrally such that the load is concentrated above the fracture. These concentrated point loads are the resultant load of each of the 1.8 m wide axles. Additionally, a congested traffic load is applied as a uniformly distributed load of 9.33 kN/m spread across a width of 3 m. Each lane consists of a congested lane load and the truck, and each lane is specified to have an equivalent width of 3.7 m according to AASHTO (2017) specifications. Figure 4.5 presents a generic bridge loaded with two HL-93 vehicular load models.

Figure 4.6 presents the implementation of the yield line mechanism postulated for the HL-93 loading on a typical single-span bridge. The internal work done due to the trapezoidal region can be obtained from Equation (4.34). Assuming a unit virtual deflection and further simplifying gives

$$IWD = \left(m_y^{'} + m_y\right)\left(\frac{L_x}{2s}\right) k_{bound} \tag{4.40}$$

The internal work done due to the rectangular part of the deck slab and the fractured outside girder is due to the hinge formation at the mid-span that causes a rotation of $4/L_x$ by the positive longitudinal reinforcement m_x along a width b as shown

$$IWD = 4m_x\left(\frac{b}{L_x^*}\right) \tag{4.41}$$

rearranging more specifically, in terms of the moment at the central hinge region, is represented as

$$IWD = \frac{4}{L_x^*}(m_x b) \tag{4.42}$$

This constitutes the total internal work done for the assumed yield line mechanism when the outside girder is fully fractured. The external work done is due to the virtual work done by the deck slab, the girder and the guardrail, and the HL-93 loading. The external work done due to the live load (HL-93) is considered due to the lane load that is increased by 75 percent to account for live load allowance and due to the wheel loads of the trucks that are increased by 75 percent to account for the live load factor, and it is increased by 33 percent to account for the impact factor as specified by AASHTO (2017).

For the sake of convenience, an approximation is implemented wherein the lane load is considered spread across the deck, similar to the self-weight per unit area. This measurement is achieved by applying the lane load for a width of the HL-93 lane of 3.7 m. Thus, the distributed lane load is w_l of 2.55 kN/m^2 and considered to act with the area load of reinforced concrete deck slab, w_c. The equivalent combined area load is denoted by w_u. This assumption is justified because the lane load is considered to act over an area beyond the actual loaded area. In accordance with the LRFD loads, (AASHTO (2017), the dead loads are increased by 25 percent.

The external work done due to an area load w_u is derived using Equation (4.16):

$$EWD_{w_u} = w_u L_x^*\left(\frac{b}{2} + \frac{s}{4}\right) \tag{4.43}$$

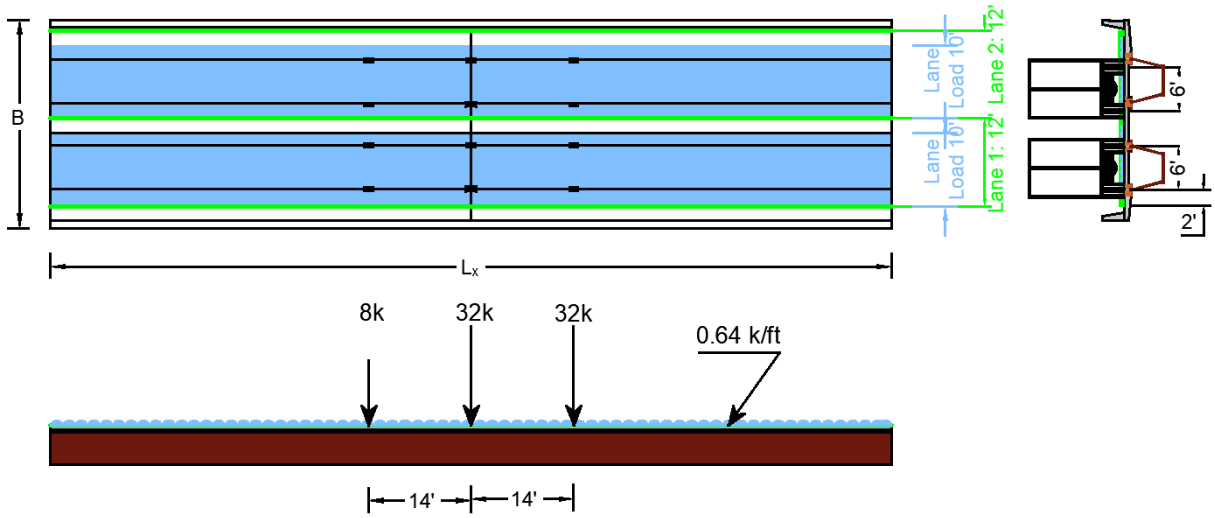

Figure 4.5. HL-93 Load Position for Two-Lane Loaded Case.

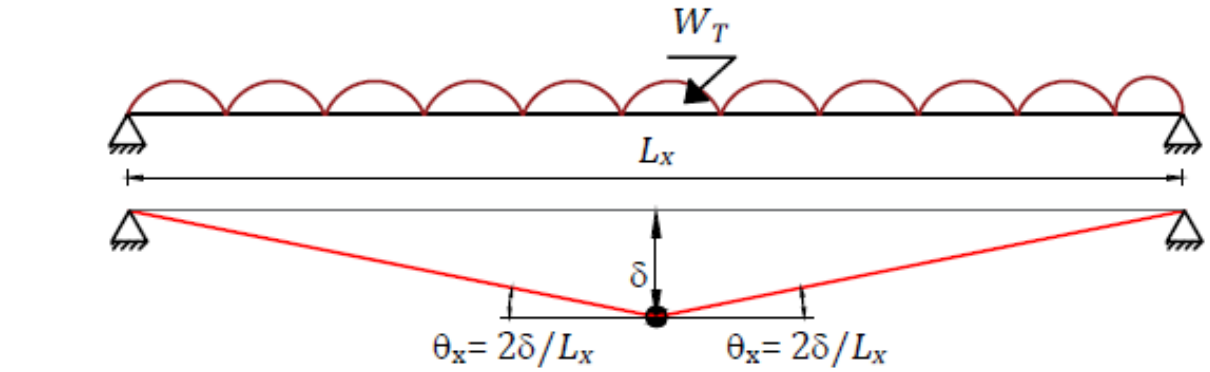

(a) Single-Span Support Conditions

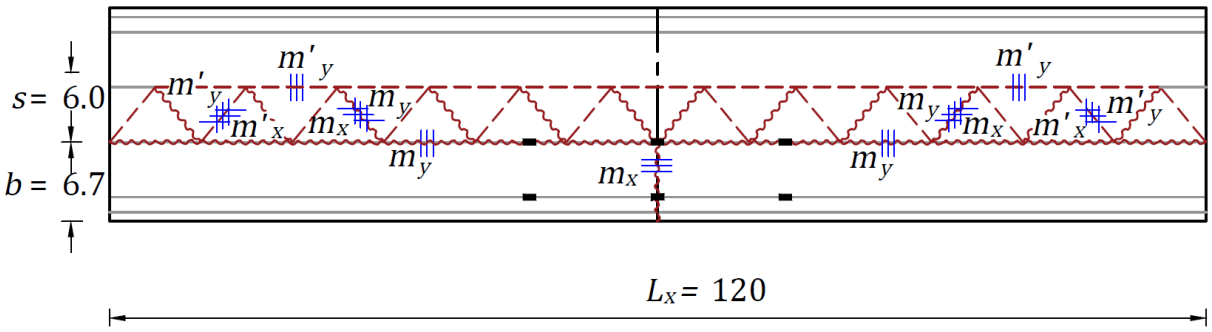

(b) Layout of a Typical Single Span with Yield Line Mechanism

Figure 4.6. Critical Yield Line Mechanism for a Fractured Single-Span (9-5498).

The external work done due to the combined weight of the fractured outside girder and the outer guardrail, W_x, is given by

$$EWD_{W_x} = \frac{W_x L_x^*}{2} \tag{4.44}$$

The deflections under each wheel load are computed using similar triangles and are multiplied with the factored loads of each wheel to obtain the external virtual work done by the HS-20 truck.

$$EWD_{HS20} = \left(168 - \frac{2613}{L_x^*}\right) \tag{4.45}$$

For a wider bridge, the second lane of trucks may participate (in part) in the collapse mechanism. The axle loads are therefore required to be increased proportionally to their deflection with respect to the truck position over the fractured girder. Thus, the lane load requires modification through the scalar K_{lane}. For one line of truck wheels participating, the factor is given by

$$K_{lane} = 1 + 0.5\,\frac{y}{s} \tag{4.46}$$

in which y = distance measured from the intact (unfractured) girder to the line of wheels.

The following expression is used if both lines of wheels are participating in the mechanism:

$$K_{lane} = 1 + \frac{y}{s}\,;\, K_{lane} \leq 2 \tag{4.47}$$

where y = distance to the centerline of the truck. Thus, the total external work done is given by

$$EWD = w_u L_x^*(0.5b + 0.25s) + 0.5 W_x L_x^* + \left(168 - \frac{2613}{L_x^*}\right) K_{lane} \tag{4.48}$$

and may be contracted to the following

$$EWD = 0.5W_T \tag{4.49}$$

where W_T = total ultimate load at the bridge participating in the collapse mechanism, represented by

$$W_T = w_u L_x^*(b + 0.5s) + W_x L_x^* + \left(336 - \frac{5226}{L_x^*}\right) K_{lane} \tag{4.50}$$

Solving for the overstrength factor $\Omega = IWD/EWD$ for the simply supported span is given by

$$\Omega = \frac{\left(m'_y + m_y\right)\left(\frac{L_x}{2s}\right) k_{bound} + (m_x b)\left(\frac{4}{L_x^*}\right)}{0.5W_T} \tag{4.51}$$

where m'_y and m_y are the negative and positive moment capacities per unit width in the y-direction, respectively, and m'_x, and m_x are the negative and positive moment capacities per unit width in the x-direction, respectively; L_x = the centerline length of the span of the bridge; L_x^* = the length of the outer region of the bridge, factored for curvature; s = the width of the area of the slab along which the mechanism under consideration is applied; b = the transverse distance of the interior flange of the fractured girder from the outer edge of the bridge; w_u = the area load consisting of self-weight of the reinforced concrete deck slab and the applied lane load; and W_x = the line load consisting of the self-weight of the fractured tub girder and the guardrail.

When implemented for the bridge of TxDOT Research Project 9-5498, the upper-bound and lower-bound overstrength factors are found—using Equation (4.51)—to be Ω_{Upper} = 1.46 and Ω_{Lower} = 1.28. Note that in the bridge is narrow and can only accommodate a single HS-20 truck load alone.

4.5. Analysis for Spans with Plastic End Moments

Consider now the general case for spans that possess a measure of fixity at their ends due to the presence of continuity via the adjacent spans, as shown in Figure 4.7 (a).

Equating the factored external work done to the internal work done as shown

$$\Omega\, 0.5W_T = 0.5M_{p1}^{-}\theta + 0.5M_{p2}^{-}\theta \tag{4.52}$$

$$\Omega\, 0.5W_T = \left(0.5M_{p1}^{-} + 0.5M_{p2}^{-}\right)\left(\frac{2}{L_x^*}\right) \tag{4.53}$$

Thus, the overstrength factor for the intact case is given by

$$\Omega = \frac{\left(0.5M_{p1}^{-} + 0.5M_{p2}^{-}\right)\left(\frac{2}{L_x^*}\right)}{0.5W_T} \tag{4.54}$$

where $0.5M_{p1}^{-}$ and $0.5M_{p2}^{-}$ are the plastic moment capacities of the composite deck participating in the overall plastic mechanism (0.5 is used since the outside girder alone takes part in the critical mechanism).

This result may now be incorporated into the overall solution for the fractured girder case. Thus, the overall effective weight, W_{ET}, used in the plastic analysis is given by

$$W_{ET} = w_u L_x^*(b + 0.5s) + W_x L_x^* + \left(336 - \frac{5226}{L_x^*}\right)K_{lane} \tag{4.55}$$

Adding the effect of end moments, the overall collapse overstrength capacity is given by

$$\Omega = \frac{\left(m_y^{'} + m_y\right)\left(\frac{L_x}{2s}\right)k_{bound} + \left(\frac{4m_x b}{L_x^*}\right) + \left(0.5M_{p1}^{-} + 0.5M_{p2}^{-}\right)\left(\frac{2}{L_x^*}\right)}{0.5W_{ET}} \tag{4.56}$$

For the end-spans in multi-span bridges as well as two-span continuous bridges, either $0.5M_{p1}^{-}$ or $0.5M_{p2}$ is set to zero at the outermost abutments, as shown in Figure 4.8.

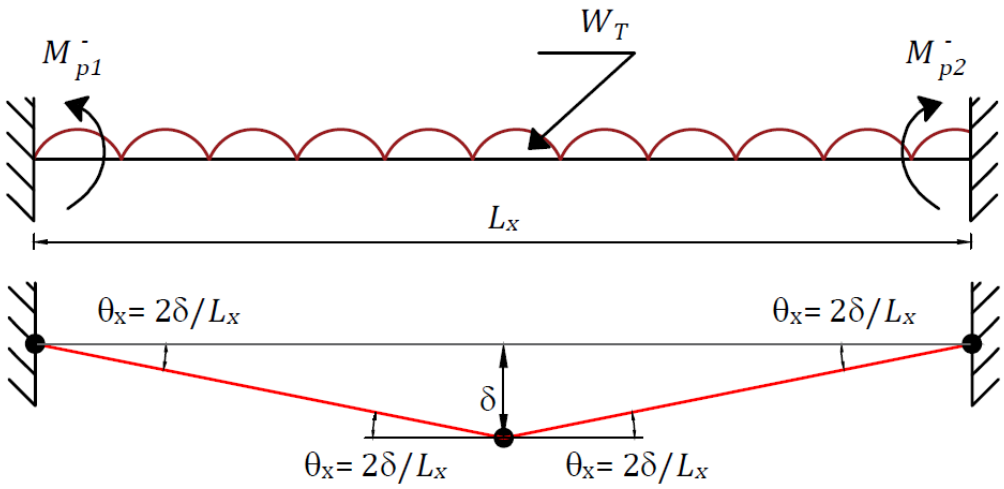

(a) Continuous Bridge Span with End Moments

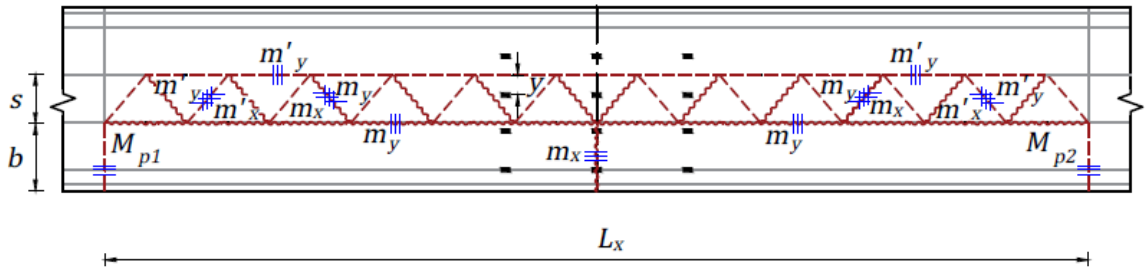

(b) Layout of a Typical Interior Span with Yield Line Mechanism

Figure 4.7. Collapse Load Analysis of Interior Span of Continuous Bridges.

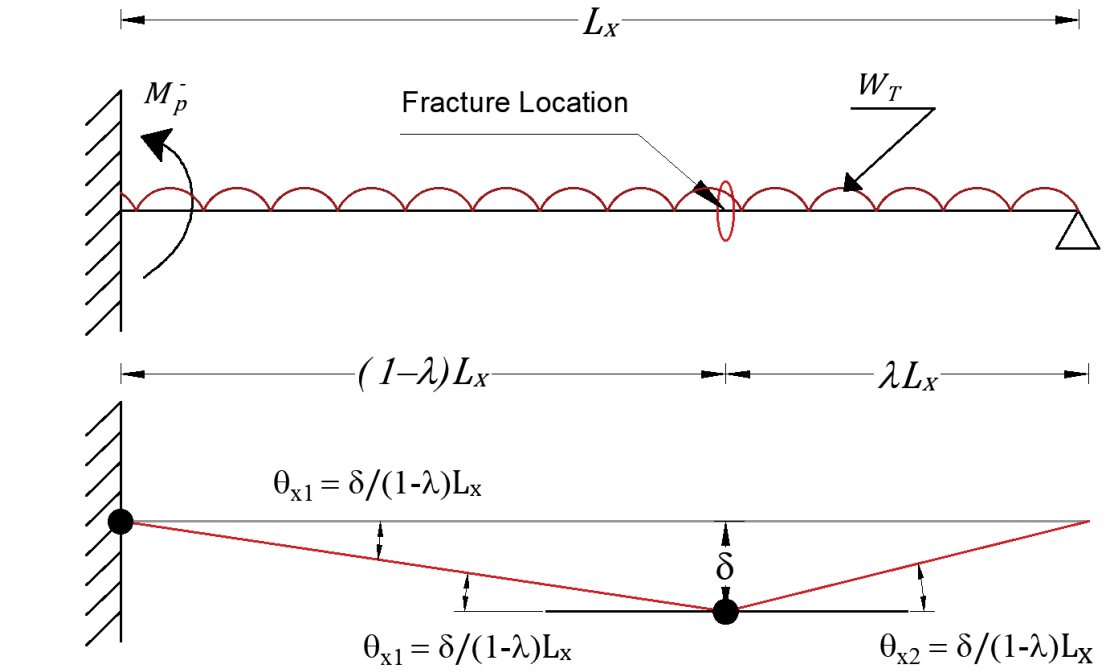

(a) End-Span of Bridge

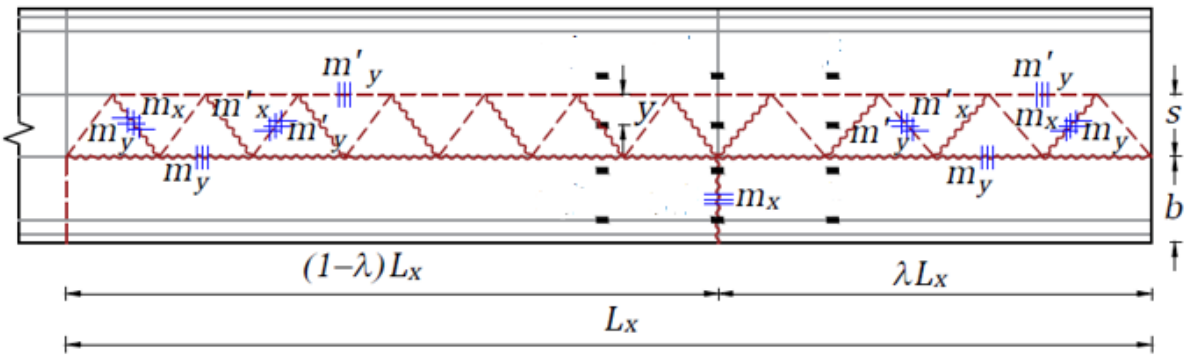

(b) Layout of a Typical Interior Span with Yield Line Mechanism

Figure 4.8. Collapse Load Analysis of End-Spans of Continuous Bridges.

The overstrength factor of the system due to the moment, $0.5M_p^-$, at the continuous interior support is given as

$$\Omega = \frac{\left(0.5M_p^-\right)\left(\frac{1}{(\lambda-1)L_x^*}\right)}{0.5W_T} \tag{4.57}$$

where $0.5M_p^-$ = the plastic moment capacities of the composite deck participating in the overall plastic mechanism at the supports, and λ = fraction of span length from the simply supported end of the span at which the steel twin tub girder is fractured. The overall effective weight, W_{ET}, used in the plastic analysis, is given as

$$W_{ET} = w_u L_x^*(b + 0.5s) + W_x L_x^* + \left(336 - \frac{523}{\lambda L_x^*} - \frac{2091}{(1-\lambda)L_x^*}\right)K_{lane} \tag{4.58}$$

The critical case in which the external work done, $0.5W_{ET}$, is set to be the maximum by positioning the 36 kN load at the side of the fracture that is nearer to the simply supported end of the span is considered in Equation (4.58).

This result may now be incorporated into the overall solution for the fractured girder case.

$$\Omega = \frac{\left(m_y^{'} + m_y\right)\left(\frac{L_x}{2s}\right)k_{bound} + \left(\frac{m_x b}{(\lambda-\lambda^2)L_x}\right) + \left(\frac{0.5M_p^-}{(1-\lambda)L_x}\right)}{0.5W_{ET}} \tag{4.59}$$

4.6. Location of Maximum Positive Moment for Collapse Analysis of Fractured Girder

The location of the maximum positive moment within the end-span region of multi-span continuous bridge structures depends on several factors:

- The stiffness (length) of the adjoining span or spans.
- The relative positive to negative moment capacities, as designed and constructed.
- The relative proportion of distributed loads to point loads.

To illustrate the significance of the above, consider the following scenarios depicted in Figure 4.9 where the location of the maximum positive moment is expressed as a fraction of the span length, λ.

Figure 4.9(a) and (b) respectively show the extreme cases for a multi-span bridge with full fixity (where M^F=$wL^2/8$) and for a two-span structure with partial fixity where only one span is fully loaded. For an elastic design, moment capacities are proportionately tuned to the elastic bending moment diagram. Thus, for Figure 4.9(a) and (b), λ = 0.375 (full fixity) and λ = 0.4375 (partial fixity), respectively. Figure 4.9(c) and (d) present the location of the maximum positive moment under the moving concentrated load with full fixity (where M^F= $(\lambda - \lambda^3)PL/2$) and partial fixity for a two-span structure. The maximum positive moment occurs where λ = 0.366 (full fixity) and λ = 0.5536 (partial fixity). For plastic analysis and design, in both the cases of Figure 4.9(a) and (b), λ = 0.414 if the beam has the same positive and negative moment capacity as shown in Figure 4.9(e). Figure 4.9(f) indicates that the maximum moment occurs at the location where the concentrated load acts.

The critical location in the end spans in continuous bridges will be at that location where fracture critical (welded joint) details exist closest to the maximum positive moment region. Because this may vary from structure to structure, for simplicity it may be assumed to be in the vicinity of λ = 0.40. Such high moments are assumed to be capable of initiating fracture at that location. Therefore, for consistency, in this study the location of fractures in the end-spans of multi-span continuous bridges shall be taken herein as λ = 0.40.

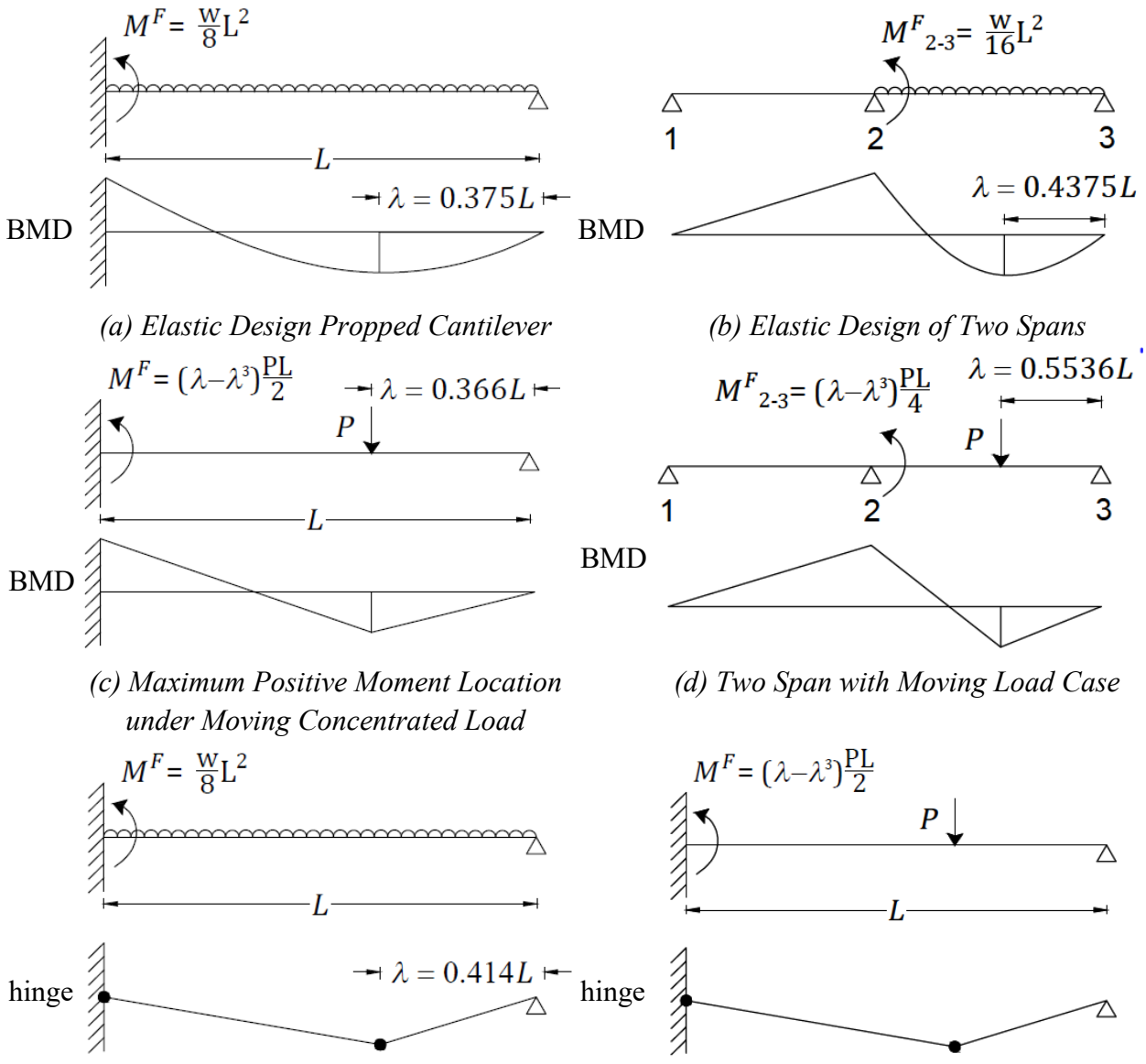

(a) Elastic Design Propped Cantilever

(b) Elastic Design of Two Spans

(c) Maximum Positive Moment Location under Moving Concentrated Load

(d) Two Span with Moving Load Case

(e) Uniformly Distributed Load

(f) Concentrated Moving Load

Figure 4.9. Different Scenarios Used to Determine the Location of Maximum Positive Moment for Collapse Analysis.

To check the veracity of this assumption, the overstrength factors of the fifteen pre-selected bridges were calculated using the exact λ value found in the following formula.

$$\lambda = \frac{\sqrt{\mu + 1} - 1}{\mu} \tag{4.60}$$

where μ represents the ratio of the negative and positive bending moment ($\mu = M_p^- / M_p^+$) of the composite bridge section at support and at mid-span, respectively. These *"exact"* values of λ range from 0.37 to 0.42 for the different bridges under consideration and presented in Table 4.1. The overstrength factors have also been calculated by setting $\lambda = 0.4$ and $\lambda = 0.5$. To assess the significance of the differences in overstrength factors, ratios, R have been formed using the following expression.

$$R = \frac{\Omega(\lambda)}{\Omega(\lambda_{exact})} \tag{4.61}$$

Results are shown for these ratios plotted as a cumulative distribution in Figure 4.10. A lognormal distribution has also been fitted to the data points for the two cases where $\lambda = 0.4$ and $\lambda = 0.5$. The median values of the distributions show that when $\lambda = 0.4$, there is only a very slight bias of 0.73 percent, whereas the bias (error) increases markedly to 11 percent when $\lambda = 0.5$. This simply means that $\lambda = 0.5$ is not the most appropriate or adverse location to assume the existence of a girder fracture in end-span positive moment regions. It is therefore evident that in lieu of a more precise minimization analysis, one can confidently adopt $\lambda = 0.4$ as being an appropriate location to assume fractures in end-spans of the continuous bridges. Using $\lambda = 0.4$ means that any error introduced into the Ω factor will be less than 3 percent.

Table 4.1. Comparison of Overstrength Factors for Exterior Spans, Ω.

ID	L_x (m)	λ_{exact}	B (m)	Ω λ_{exact}	Ω at λ=0.4	Ω at λ=0.5
B4S1	40	0.39	8.5	1.79	1.80	1.98
B4S2	39	0.39	8.5	1.83	1.85	2.03
B5S1	43	0.41	9.1	1.41	1.40	1.53
B5S2	43	0.41	9.1	1.40	1.39	1.52
B6S1	43	0.40	11.6	1.63	1.62	1.81
B6S2	43	0.40	11.6	1.63	1.62	1.81
B7S1	67	0.40	8.5	1.45	1.45	1.57
B7S2	58	0.37	8.5	1.64	1.69	1.86
B8S1	81	0.41	8.5	1.35	1.34	1.44
B8S2	90	0.42	8.5	1.26	1.25	1.33
B9S1	43	0.41	8.5	1.57	1.56	1.71
B9S3	38	0.41	8.5	1.69	1.68	1.86
B10S1	45	0.39	9.1	1.96	1.98	2.23
B10S3	58	0.37	9.1	1.62	1.67	1.85
B11S1	68	0.37	8.5	1.71	1.75	1.97
B11S3	72	0.37	8.5	1.61	1.65	1.85
B12S1	43	0.38	8.5	1.73	1.75	1.91
B12S3	44	0.38	8.5	1.69	1.71	1.87
B13S1	46	0.37	9.1	1.38	1.41	1.57
B13S3	46	0.37	9.1	1.37	1.40	1.55
B14S1	46	0.40	8.5	1.63	1.63	1.77
B14S3	46	0.40	8.5	1.63	1.63	1.77
B15S1	61	0.39	8.5	1.69	1.70	1.85
B15S3	61	0.39	8.5	1.69	1.69	1.85

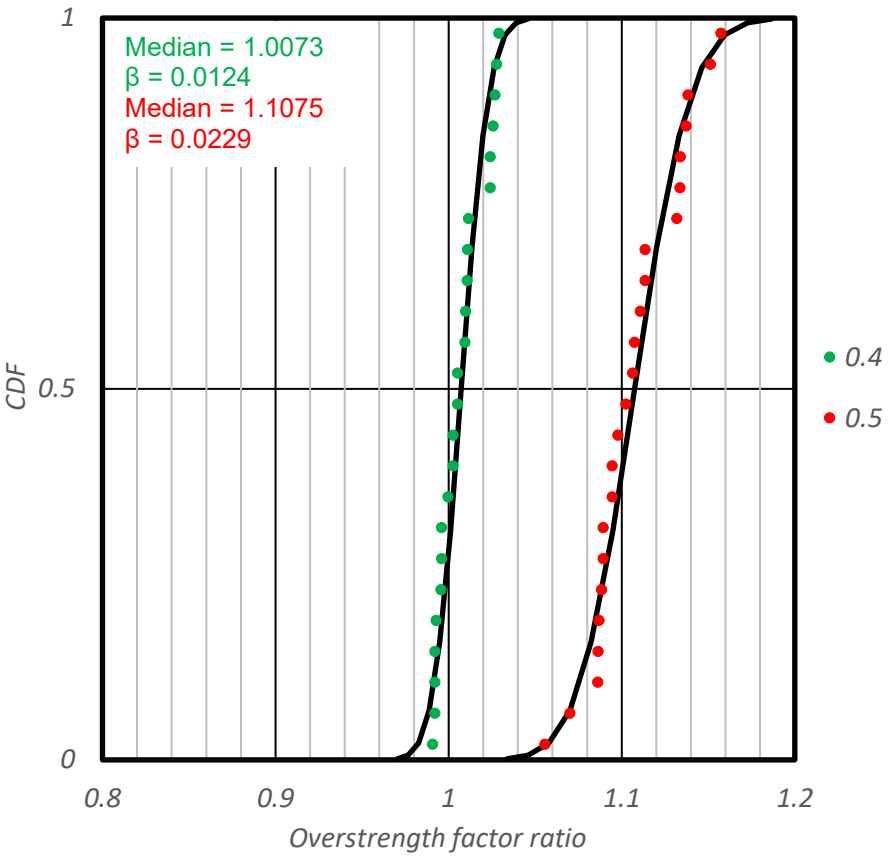

Figure 4.10. Cumulative Distribution for λ = 0.4 and λ = 0.5.

4.7. Chapter Findings

The limit analysis was conducted to assess the application of the plastic methods to STTG bridges. The upper bound and lower bound theories were established to formulate expressions to calculate the reserve capacity of bridges when it is assumed that the outer girder is fully fractured. The critical mechanism was postulated by considering several admissible mechanisms for the given loading, after undertaking minimization study to attain the optimal number of diagonal yield lines that should be formed in the yield pattern taking place in the patch of the bridge lying between the two girders. This region of the slab faced flexural and torsional bending as a result of the HL-93 loading. The curvature of the bridges was incorporated in the solution by a suitable modification. The formulae for computing the overstrength capacity of each span were formulated so as to encompass the various possibilities arising from the boundary conditions and geometry of the bridges such that the theory may be easily applied to any bridge belonging to this class of bridges.

Figure 4.11 illustrates the comparison of the deflection contours generated from the yield line mechanism with the deflection mapping obtained from the FEM results (Hurlebaus et al. 2018). The details of the FEM analysis of all the bridges discussed in this research may be found in technical report of TxDOT 0-6937 project. The comparison displays a good agreement between the two independently conducted analyses. It is noteworthy that the FEM results are highly sophisticated and result from a complex computational program such as ABAQUS (2014). Thus, this comparison was essentially a reasonable validation of the postulated mechanism.

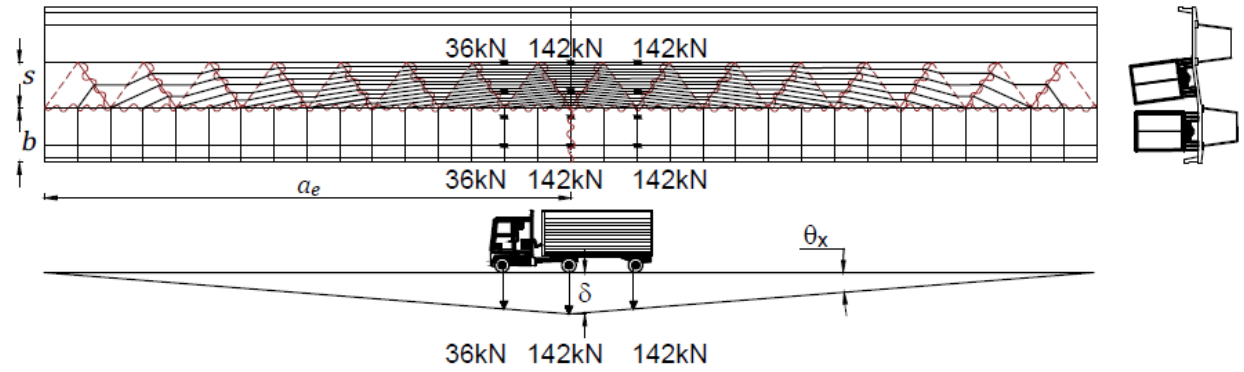

(a). Deflection contours plotted by mapping the deflections of the postulated yield line mechanism

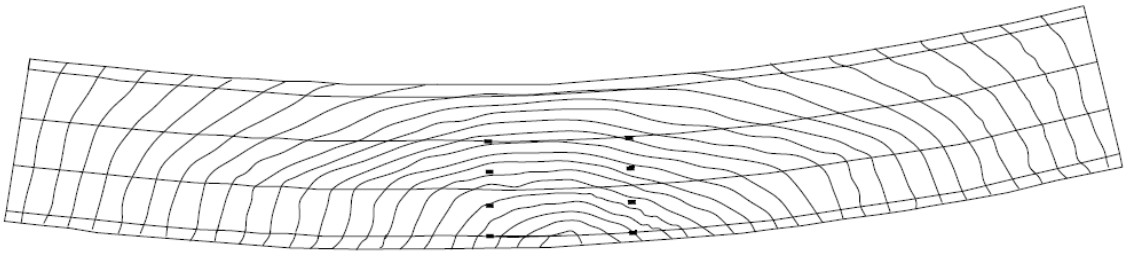

(b). Deflection contours generated by the FEM analysis in ABAQUS. Source TxDOT 0-6937 (Hurlebaus et al. 2018)

Figure 4.11. Comparison of Deflection Contours of Yield Line Analysis and FEM Results

CHAPTER V

APPLICATION TO SELECTED TYPES OF BRIDGES

5.1. Chapter Summary

The upper bound and lower bound theories are derived with the help of the postulated yield line mechanism. These theories are evaluated in detail with a purely computational focus so as to develop a step-by-step procedure for calculating the overstrength capacity of Steel Twin-Tub Girder (STTG) bridges under the influence of standard American Association of State Highway and Transportation Officials (AASHTO) HL-93 loading. The application of the theories is briefly described to develop a general equation that can be used for different boundary conditions, thus, essentially merging the three cases into a universal solution with modification factors incorporated within a single equation. The suite of 15 selected STTG bridges include three distinct kinds of spans based on their boundary conditions. This chapter provides detailed analysis guidelines for spans of each kind through the following examples.

- Single-span bridges: Bridge 2 is used as an example that has no support fixity.
- Two-span or greater continuous bridges: Both exterior spans of Bridge 11, with one fixity over the interior support, and one interior span of Bridge 10, with fixity over both the interior supports, are provided as examples.

5.2. Introduction

As described in Park and Gamble (2000), the overstrength factor is calculated using virtual work analysis by equating the factored external work to the internal work when a maximum deflection of unity takes place:

$$\Omega EWD_U = IWD_N \tag{5.1}$$

in which IWD_N = internal work done based on nominal material properties; EWD_U = external work done by factored ultimate design load; and Ω=overstrength factor.

The external work done is calculated as follows:

$$EWD_U = W_{ET} L_x^* \frac{\delta}{2} = 0.5 W_{ET} L_x^* \tag{5.2}$$

in which W_{ET} = the total load that effectively participates in the collapse mechanism; δ = 1 = virtual displacement; and L_x^* = the span length under consideration measured on the centerline (CL) of the collapse mechanism, such that:

$$L_x^* = \left(1 + \frac{B}{4R_{℄}}\right) L_x \tag{5.3}$$

where L_x = CL of the bridge (midway between the twin tubs); B = the width of the bridge; and $R_{℄}$ = the radius of curvature measured along the CL of the bridge deck for a straight bridge $L_x^* = L_x$.

5.3. Unifying Plastic Solutions Developed for Three Different Cases

In order to derive a general solution that encompasses all the different boundary conditions and geometric parameters, a combined equation with suitable modifiers is developed based on the principle of virtual work done.

For AASHTO HL93 truck and lane loads, this results in:

$$W_{ET} = w_u L_x^* (b + 0.5s) + W_x L_x^* + \left(1494 - \frac{709}{\lambda L_x^*} - \frac{2835}{(1-\lambda) L_x^*}\right) K_{lane} \tag{5.4}$$

where s = the width of the area of the slab along which the mechanism under consideration is applied; b = the transverse distance of the interior flange of the fractured girder from the outer edge of the bridge; w_u = the area load consisting of self-weight of the reinforced concrete deck

slab and the applied lane load (kN/m^2); W_x = the line load consisting of the self-weight of the fractured tub girder and the guardrail (kN/m); and λ = the critical location factor for the hinge to occur, normally at the location of maximum moments. For simply supported spans and the interior spans of three- or more-span continuous bridges, $\lambda = 0.5$, whereas for two-span bridges or the end span for three- or more-span bridges, $\lambda = 0.4$.

Thus, for simply supported spans and for interior spans ($\lambda = 0.5$):

$$W_T = w_u L_x^* (b + 0.5s) + W_x L_x^* + \left(1494 - \frac{7086}{L_x^*}\right) K_{lane} \tag{5.5}$$

For the end spans of continuous bridges (2 spans or greater, where $\lambda = 0.4$).

$$W_T = w_u L_x^* (b + 0.5s) + W_x L_x^* + \left(1494 - \frac{6498}{L_x^*}\right) K_{lane} \tag{5.6}$$

For a wider bridge, the second lane of trucks may participate (in part) in the collapse mechanism, as depicted in Figure 5.1.

The axle loads are required to be increased proportionally to their deflection with respect to the truck position over the fractured girder. Thus, the lane load requires modification through the scalar K_{lane}. For one line of truck wheels participating:

$$K_{lane} = 1 + 0.5\,\frac{y}{s} \tag{5.7}$$

in which y = distance measured from the intact (unfractured) girder to the line of wheels. If both lines of wheels are participating in the mechanism, then:

$$K_{lane} = 1 + \frac{y}{s}\,; \qquad K_{lane} \leq 2 \tag{5.8}$$

where y = distance to the CL of the truck.

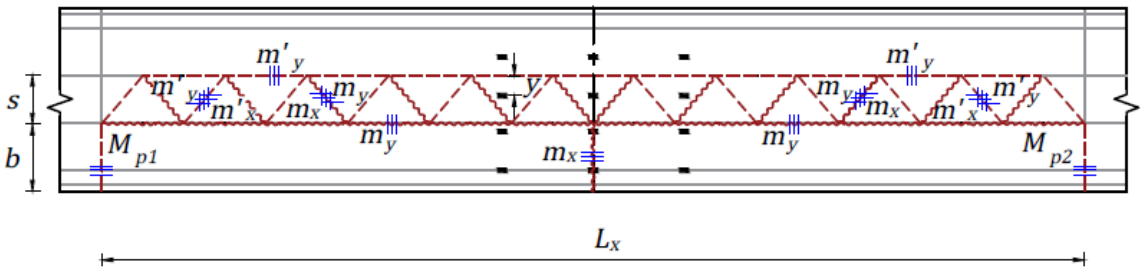

Figure 5.1. Layout of typical interior span with yield line mechanism.

The internal work done is calculated as follows:

$$IWD_N = (m'_y + m_y)\left(\frac{L_x}{2s}\right)k_{bound} + \left(\frac{m_x b}{\lambda(1-\lambda)L_x^*}\right) + \left(\frac{0.5M_{p1}^-}{(1-\lambda)L_x^*}\right) + \left(\frac{0.5M_{p2}^-}{(1-\lambda)L_x^*}\right) \quad (5.9)$$

where m'_y and m_y are the negative and positive moment capacities per unit width in the y direction, respectively, and m'_x, and m_x are the negative and positive moment capacities per unit width in the x direction, respectively (units k-in./in. = k-ft/ft, or kN m/m or N-mm/mm); M_{p1}^- and M_{p2}^- are the plastic moment capacities of the composite deck and the intact girders at the ends of the span in consideration (0.5 is used since the outside girder alone takes part in the critical mechanism); and λ = the critical location factor for the hinge to occur, normally at the location of maximum moments, as defined above.

Note that for simply supported spans, there is no end fixity; therefore, M_{p1}^- and M_{p2}^- are set to zero, whereas exterior spans of the two-span and of the three-span bridges have one fixity at the end support; therefore, one of the M_{p1}^- and M_{p2}^- are set to zero for that case, and interior spans have fixity at both the ends, implying that both M_{p1}^- and M_{p2}^- are non-zero.

For simply supported spans and the interior spans of three-or-more-span continuous bridges ($\lambda = 0.5$):

$$IWD_{Simple\ Spans} = \left(m'_y + m_y\right)\left(\frac{L_x}{2s}\right)k_{bound} + \frac{4}{L_x^*}(m_x b) \tag{5.10}$$

$$IWD_{Int.Spans} = \left(m'_y + m_y\right)\left(\frac{L_x}{2s}\right)k_{bound} + \left(\frac{4m_x b}{L_x^*}\right) + \left(0.5M_{p1}^- + 0.5M_{p2}^-\right)\left(\frac{2}{L_x^*}\right) \tag{5.11}$$

For two-span bridges or the end-span for three- or more-span bridges ($\lambda = 0.4$):

$$IWD_{Ext.Spans} = \left(m'_y + m_y\right)\left(\frac{L_x}{2s}\right)k_{bound} + \left(\frac{25m_x b}{6L_x}\right) + \left(\frac{25M_{p1}^-}{12L_x^*}\right) \tag{5.12}$$

The term k_{bound} represents the modifier term representing the upper and lower-bound solutions, as follows:

$$k_{bound}^{upper} = \left[1 + 2\frac{\tan\alpha}{\tan\theta}\right] = 1 + \frac{4s}{L_x}\sqrt{\left(\frac{m'_x + m_x}{m'_y + m_y}\right)} \tag{5.13}$$

and:

$$k_{bound}^{lower} = \left[1 + 2\frac{\tan^2\alpha}{\tan^2\theta}\right] = 1 + \frac{8s^2}{{L_x}^2}\left(\frac{m'_x + m_x}{m'_y + m_y}\right) \tag{5.14}$$

where:

$$\tan\alpha = \frac{s}{L_x/2} \tag{5.15}$$

and:

$$\tan\theta = \frac{sN}{L_x} = \sqrt{\frac{m'_y + m_y}{m'_x + m_x}} \tag{5.16}$$

The overstrength factors are computed using Equation (5.1).

$$\Omega_{Yield\ Line} = \frac{IWD_N}{EWD_U} = \frac{\left(m'_y + m_y\right)\left(\frac{L_x}{2s}\right)k_{bound} + \left(\frac{m_x b}{\lambda(1-\lambda)L_x^*}\right) + \left(\frac{M_{p1}^- + M_{p2}^-}{2L_x^*(1-\lambda)}\right)}{0.5W_{ET}} \tag{5.17}$$

For simply supported spans:

$$\Omega_{Simply\ Supported} = \frac{\left(m'_y + m_y\right)\left(\frac{L_x}{2s}\right)k_{bound} + \frac{4}{L_x^*}(m_x b)}{0.5W_{ET}} \tag{5.18}$$

For interior spans:

$$\Omega_{Interior} = \frac{\left(m'_y + m_y\right)\left(\frac{L_x}{2s}\right)k_{bound} + \left(\frac{4m_x b}{L_x^*}\right) + \left(0.5M_{p1}^- + 0.5M_{p2}^-\right)\left(\frac{2}{L_x^*}\right)}{0.5W_{ET}} \tag{5.19}$$

For exterior spans:

$$\Omega_{Exterior} = \frac{\left(m'_y + m_y\right)\left(\frac{L_x}{2s}\right)k_{bound} + \left(\frac{25m_x b}{6L_x}\right) + \left(\frac{25M_{p1}^-}{12L_x^*}\right)}{0.5W_{ET}} \tag{5.20}$$

The longitudinal and transverse moment (positive and negative) capacities of the deck slab and the positive capacities of the composite intact section are computed based on the standard U.S. code procedure using the specified compressive strength of concrete and specified or as-built if known) yield strength of reinforcing steel in the deck and the guardrail and of the structural steel of the twin tub girders. The negative capacities of the composite intact section are computed using plastic analysis of sections via the equal area method, assuming that the concrete has cracked completely and does not contribute to tension. Since the fractured outside girder alone takes part in the postulated critical mechanism, the negative moment capacity of half the section is used for the computation of the overstrength factor of the exterior spans.

The tabulations in the examples in sections that follow are presented such that the input values to be used depend on bridge geometry, the material properties of the deck and the guardrail, the reinforcement, and the structural steel. They are indicated by yellow highlighting of the corresponding row number, with the value itself in boldface. Similarly, the values that need to be

solved for to ensure equilibrium and the corresponding equilibrium checks are indicated by blue highlighting of the corresponding row number, with the value itself in boldface.

The other rows can be automated by feeding the formulae presented in the column named FORMULA/DEFINITION/EQUATION, which also mentions the conditions for which each formula is applicable. Since Bridge 2 does not have support fixity at all, the moment calculations for the positive and negative composite deck and the intact girders are irrelevant for this bridge, and are therefore not included in this section. The results are presented in boldface. It is to be noted that the step-wise calculations are presented in the format of *"engineering computation sheets"* for ease of understanding and presentation.

5.4. Yield Line Analysis Example of Bridge 2

This section presents the stepwise procedure of the yield line analysis conducted to establish the upper-bound and lower-bound solution range for the overstrength factor that is in conjunction with the theory of plastic analysis in Section 5.3. Figure 5.2 presents the dimensional details of the simply supported span of Bridge 2. The moment capacities (longitudinal and transverse) of the deck slab are calculated using the standard US code-based procedure following the Whitney's stress block approach. The capacities are calculated for one meter wide cross-section of the bridge.

The geometric parameters namely $B =$ the total width (breadth) of the deck slab, $t =$ thickness and b = the width of each cross-section are noted from the structural plans. The various material properties of concrete and steel are obtained through the bridge plans and the reports associated with the respective bridges. These properties include f_c' = the specified compressive strength of concrete, ε_{cu} = the maximum strain at the extreme concrete compression fiber (computed as per Section 22.2.2 of ACI-318 (2017) which states the

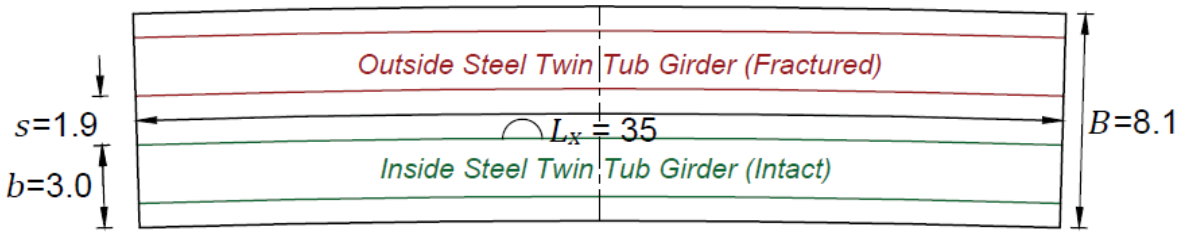

Figure 5.2. Schematic Diagram of Bridge 2 (R_L = 582 m, L_x = 35 m).

"assumptions for concrete."), f_y = the yield strength of steel of the reinforcement bars, E = the Young's modulus of steel and ε_y = the yield strain that is the ratio of yield strength and Young's modulus of steel in the reinforcement. β_1 = the factor relating depth of equivalent rectangular compressive stress block to depth of neutral axis which is computed using Table 22.2.2.4.3 of ACI-318 (2017). The formula applicable for the strength of concrete used in this study is as follows

$$\beta_1 = 0.85 - 0.05(f_c' - 28) \tag{5.21}$$

where f_c' is in MPa.

The details of the reinforcement such as $\#_{bar}$ = the number of bars per one meter wide section (for the longitudinal capacities) or s = the on-center spacing (for the transverse capacities), d_b = the diameters of the bars, A_s the corresponding areas of steel, cc = the clear cover (from the bridge drawings) and d and d' = the subsequently computed effective depths of the tensile and compressive zones respectively, are recorded. ε_{top} and ε_{bot} = the net tensile strain in the extreme tension reinforcement at the top and bottom of the section respectively, are determined from a linear distribution (ACI-318 2017).

The section of concrete is considered to be divided into compressive and tensile zones by a neutral axis that is located at a depth c from the top fiber. The compressive force due to concrete (with a negative sign) is found using the formula

$$C_c = 0.85 f_c' \mathrm{b} \beta_1 \mathrm{c} = 0.85 f_c' \mathrm{b} a \tag{5.22}$$

where $a = \beta_1 \mathrm{c}$

If the reinforcement steel is in compression, the compressive force due to compression steel is denoted by a negative sign, as follows

$$T_{top/bottom} = -(A_s f_s - 0.85 f_c' A_s) \tag{5.23}$$

The tensile force due to the steel reinforcement is given by

$$T_{top/bottom} = A_s f_s \tag{5.24}$$

To ensure that the computation of the forces considers whether or not the steel has yielded, the following formula is used for the strength of steel at the extreme fiber of reinforcement

$$f_s = \frac{E \varepsilon_{top/bottom}}{\left\{1 + \left|\frac{E \varepsilon_{top/bottom}}{f_y}\right|^{20}\right\}^{0.05}} \tag{5.25}$$

The depth of neutral axis, c (indicated by blue highlighting) is obtained by equating the tensile and compressive forces. The moment capacities are found by taking moments of forces about the neutral axis.

The computation of the overstrength factor is based on the procedure explained in the Section 5.3. The data necessary for the calculations such as the geometric details, the moment capacities, the volume of girder and area of cross-section of rail are listed as input values indicated by yellow highlighting. The parameters needed to solve the equations in Section 5.3 are computed

using the formulae and allowance factors for dead load, live load and the weight of the stiffeners. The parameters and their corresponding formulae and values are tabulated in a sequential order and can be regenerated using any spreadsheet program.

The following series of engineering computations tabulate the entire procedure of finding out the reserve capacity of Bridge 2 such that the same method may be replicated for other simply supported spans with similar characteristics. The computations are styled in the format that may be easy to follow and to regenerate the steps in a spreadsheet format such that the analytical check may be conducted very quickly by changing the data according to bridge specifications.

Care should be taken such that the data is input in the appropriate units so that all the computations are consistent. It should also be noted the results reported in the following tables are for the full span-length. The results of internal work done reported in the tables of Chapter 7 belong to the upper bound solution data. More examples of such analysis guidelines may be found in the guidelines of TxDOT 0-6937 project (Hurlebaus et al. 2018).

The following engineering computation sheets 5-1a to d enclose the yield line analysis summary for Bridge 2.

Sheet 5-1 a		MOMENT CAPACITY OF DECK SLAB (BRIDGE 2)					1 / 4
		Description	Parameter	Data			
DECK SECTION	1	Total Width	B mm	**8051.8**			
	2	Thickness	t mm	**203.2**			
	3	Section width	b mm	1000			
CONCRETE MATERIAL	4	Characteristic Compressive Strength					
	5		f_c Mpa	28			
	6	Strain	β_1	0.85			
REBAR MATERIAL	7	Yield Strength	ε_{cu}	0.003			
	8	Young's Modulus					
	9	Strain	f_y MPa	414			
		Moment Computations		Longitudinal		Transverse	
	10			m'_x	m_x	m'_y	m_y
	11			Top	Bottom	Top	Bottom
REINFORCING BAR DETAIL	12	Bar No.		**5**	**5**	**5**	**5**
	13	Diameter of Bar	d_b mm	15.875	15.875	15.875	15.875
	14	Area of Bar	A_Φ mm^2	197.93	197.93	197.93	197.93
	15	Spacing	s mm	-	-	**127**	**127**
	16	No. of Bars	$\#_{bar}$	**38**	**32**	-	-
	17	Area of Steel	A_s mm^2	934	787	1559	1559
	18	Clear Cover	cc mm	**50.8**	**31.75**	**50.8**	**31.75**
	19	Effective depth (tension)	d mm	128.5875	147.6375	144.4625	163.5125
	20	Effective depth (comp.)	d' mm	55.5625	74.6125	39.6875	58.7375
	21	Depth of NA	c mm	**34.19**	**35.72**	**36.48**	**45.72**

Sheet 5-1 b		MOMENT CAPACITY OF DECK SLAB (BRIDGE 2)					2/4
		Moment Computations		Longitudinal		Transverse	
	22			m'_x	m_x	m'_y	m_y
	23			Top	Bottom	Top	Bottom
STRAIN	24		ε_{top}	0.008282	0.003266	0.008880	0.000854
	25		ε_{bot}	0.001875	0.009398	0.000264	0.007730
	26	$\beta_1 c$	a mm	29.06	30.37	31.01	38.86
FORCES	27	Compression-Concrete	C_c N	-681324.36	-711847.42	-726908.63	-910964.82
	28	Tension / Compression-Steel	T_{top} N	386431.46	386431.46	644730.38	266234.44
	29		T_{bot} N	294892.90	325415.97	82178.25	644730.38
	30	Equilibrium Check	T-C N	**0.00**	**0.00**	**0.00**	**0.00**
RESULTS	31	Moment	M N-mm	56174222	66068202	85130609	103359338
			M_n kN-m	56	66	85	103

Remarks:

Top Yielded	Top Yielded	Top Yielded	Top Not Yielded
Bottom Not Yielded	Bottom Yielded	Bottom Not Yielded	Bottom Yielded
Both steel in Tension	Both steel in Tension	Both steel in Tension	Both steel in Tension

Note: The moment capacities are calculated for 1-meter section.

Sheet 5-1 c		COMPUTATION OF OVERSTRENGTH FACTOR SINGLE SPAN CASE (BRIDGE 2)		3 / 4
		Parameter	Formula/Definition/Equation	Data
GEOMETRY	1	L_x	Span length (center line)	**35.05** m
	2	R_{CL}	Radius of center line	**582.168** m
	3	B	Width	**8.1** m
	4	L_x^*	Outer region length $L_x^* = \left(1 + \frac{B}{4R_{C_L}}\right) L_x$	**35.17** m
	5	s	Inter-Girder Spacing	**1.9** m
	6	b	Width of Girder + Edge	**3** m
	7	t	Deck Thickness	**203** mm
INTERNAL WORK DONE, IWD	8	m_x	Longitudinal Positive Moment per m	**67** kN-m/m
	9	m'_x	Longitudinal Negative Moment per m	**57** kN-m/m
	10	m_y	Transverse Positive Moment per m	**104** kN-m/m
	11	m'_y	Transverse Negative Moment per m	**86** kN-m/m
	12	$\tan\theta$	$\tan\theta = \sqrt{\frac{m'_y + m_y}{m'_x + m_x}}$	**1.24** (Θ=50.8°)
	13	$\tan\alpha$	$\tan\alpha = \frac{2s}{L_x}$	**0.11** (Θ=6.0°)
	14	k_{bound}^{upper}	$\left[1 + 2\frac{\tan\alpha}{\tan\theta}\right] = 1 + \frac{4s}{L_x}\sqrt{\frac{m'_x + m_x}{m'_y + m_y}}$	**1.17**
	15	k_{bound}^{lower}	$\left[1 + 2\frac{\tan^2\alpha}{\tan^2\theta}\right] = 1 + \frac{8s^2}{{L_x}^2}\sqrt{\frac{m'_x + m_x}{m'_y + m_y}}$	**1.01**
	16	IWD_{upper}	$\left(m'_y + m_y\right)\left(\frac{L_x}{2s}\right)k_{bound}^{upper} + \frac{4m_x b}{L_x}$	**2126** kN-m[*1]
	17	IWD_{lower}	$\left(m'_y + m_y\right)\left(\frac{L_x}{2s}\right)k_{bound}^{lower} + \frac{4m_x b}{L_x}$	**1846** kN-m[*1]

Note: *[1]: A unit deflection (δ=1) is considered, therefore, the external work unit is in kN-m.

Sheet 5-1 d		COMPUTATION OF OVERSTRENGTH FACTOR SINGLE SPAN CASE (BRIDGE 2)		4 / 4
		Parameter	Formula/Definition/Equation	Data
EXTERNAL WORK DONE, EWD	18	DL	Dead Load Factor	**1.25**
	19	LL	Live Load Factor	**1.75**
	20	SAF	Stiffener Allowance Factor	**1.15**
	21	γ_c	Unit weight of reinforced concrete	**23.56** kN/m^3
	22	w_u	Area load due to reinforced concrete + lane load $\boldsymbol{DL\gamma_c \frac{t}{1000} + LL \cdot 2.55}$	**10.45** kN/m^2
	23	γ_s	Unit weight of steel	**76.97** kN/m^3
	24	V_g	Volume of Girder	**4** m^3
	25	A_r	Area of Rail Cross-Section SSTR	**0.26** m^2
	26	V_r	Volume of Rail $= L_x A_r$	**9** m^3
	27	W_x	$1.25\left(1.15V_g\gamma_s + V_r\gamma_c\right)/L_x$	**20.67** kN/m
	28	y (Lane 2)	$(b+s-4.6)$ *for (b+s)<6.4* $(b+s-5.5)$ *for (b+s)>6.4*	**0.38** m
	29	K_{lane}	$1+0.5\frac{y}{s}$ *for (b+s)<6.4;* $1+\frac{y}{s}$ *for (b+s)>6.4*	**1.10**
	30	$EWD_{HS\text{-}20}$	$\left(747-\frac{3543}{L_x}\right)K_{Lane}$	**713** kN/m
	31	W_{ET}	$w_u L_x(b+0.5s) + W_x L_x + 2EWD_{HS20}$	**3634** kN-m
	32	EWD	$0.5\ W_{ET}$	**1817** kN-m[*1]
RESULTS	33	Ω_{upper}	IWD_{upper}/EWD	**1.17**
	34	Ω_{lower}	IWD_{lower}/EWD	**1.02**

Note: *[1]: A unit deflection (δ=1) is considered, therefore, the external work unit is in kN-m.

5.5. Yield Line Analysis Example of Bridge 11

Figure 5.3 shows the schematic diagram of all the spans of Bridge 11. This section presents the stepwise procedure to establish the upper-bound and lower-bound solution range for the overstrength factor for Bridge 11, that is in conjunction with the theory of plastic analysis in Section 5.3. The moment capacities of the deck slab and the overstrength factors are computed in the same way as described in Section 5.4. Bridge 11 is a three-span bridge which is why the two exterior spans have one continuous support. It should be noted that in addition to the two typical exterior spans with one support fixity, this bridge consists of one interior span with fixity at both the supports.

The moment capacities of the intact section at the continuous support are computed as the positive and negative moment of the intact section using the similar procedure as that followed for calculating the moment capacities of the deck slab alone (explained in Section 5.4). The difference being the additional elements of the girder cross-section that contribute to the flexural strength. The intact cross-section of the bridge, including the girders, at the continuous supports is considered. The geometric parameters namely $B =$ the total width (breadth) of the deck slab, $t =$ thickness and $h =$ thickness of haunch are noted from the structural plans. The various material properties of concrete and steel are obtained from the bridge plans and the reports associated with the respective bridges. These properties include f_c' = the specified compressive strength of concrete, ε_{cu} = the maximum strain at the extreme concrete compression fiber (computed as per Section 22.2.2 of ACI-318 (2017) which states the *"assumptions for concrete."*), f_y = the yield strength of steel of the reinforcement bars, F_y' = the yield strength of the steel of S TTG, E = the

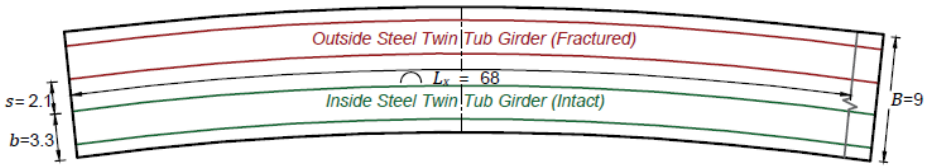

(a) Bridge 11, Span 1 (L_x = 68 m)

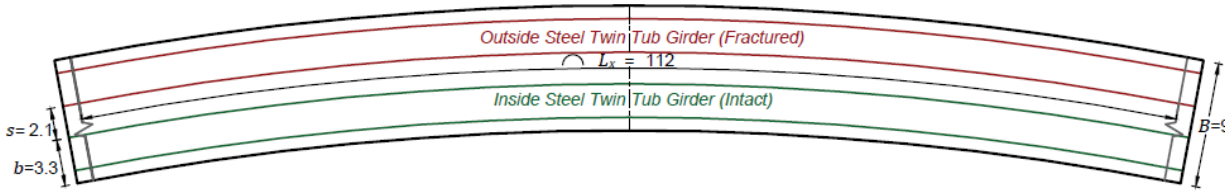

(b) Bridge 11, Span 2 (L_x = 112 m)

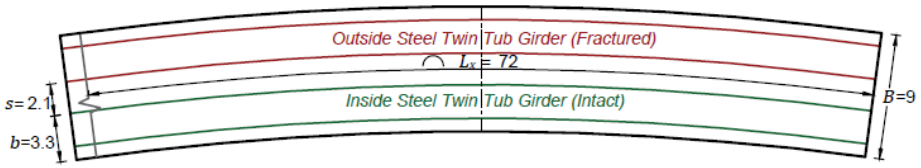

(c) Bridge 11, Span 3 (L_x = 72.m)

Figure 5.3. Schematic Diagrams of Bridge 11 (R_L = 250 m).

Young's modulus of steel of and ε_y and ε_s = the yield strain that is the ratio of yield strength and Young's modulus of steel, of the reinforcement and the SSTG, respectively. There are additional number of bars provided for extra strength at the supports that are denoted by *"bent."* The details of the reinforcement such as $\#_{top\ bars}$ = the number of top bars, $\#_{top\ bars\ bent}$ = the number of top bars at bent, $\#_{bottom\ bars}$ = the number of bottom bars, $d_{b\ top\ tra}$ = the diameters of the transverse top bars, $d_{b\ bot\ tra}$ = the diameters of the transverse bottom bars, $d_{b\ top\ long}$ = the diameters of the longitudinal top bars, $d_{b\ top\ long}{}'$ = the diameters of the longitudinal top bars at bent, $d_{b\ bot\ long}$ = the diameters of the longitudinal bottom bars and the clear cover for each type of bar are recorded with suitable subscript to *cc.* The STTG dimensions such as D_g = depth of girder (overall), b_{tf} = top flange width, t_{tf} = top flange thickness, b_w = web width, t_w = web thickness, b_{bf} = bottom flange width and t_{bf} = bottom flange thickness are also tabulated.

The composite area neutral axis is found by using n which denotes the ratio of yield strength of steel of reinforcement and that of the STTG to express the area computations in terms of an effective area. The positive moment capacity is found by the similar procedure for computing the compressive and tensile forces as explained in Section 5.4 whereas the negative moment capacity is found by using the equal area method of plastic analysis where the areas of compression and tension zones are calculated. The neutral axis for the positive moment capacity is obtained by equating the compressive and the tensile forces while the plastic neutral axis for the negative moment capacity is calculated by equating the areas in compression and tension. The depth of compression zones from the top is denoted by c and is indicated by blue highlighting. y = the portion of the width of web in compression and y' = the portion of the width of web in tension.

The depths of the compressive and tensile forces from the neutral axis are computed for the positive moment capacity while the depths of the center of gravity of compressive and the tensile areas from the plastic neutral axis are calculated for the negative moment capacity. The neutral axis and the plastic neutral axis may lie either in the web or in the top flanges and those sections are denoted by the subscripts 1 and 2 for the top-half and the bottom-half of the element of girder on either side of the neutral axes, respectively.

For the positive moment capacity, the net tensile strain in the extreme steel components of the section respectively, are determined from a linear distribution (ACI-318 2017). The compressive and tensile forces are computed in the similar method explained in Section 5.4. The compressive forces and areas are denoted by a negative sign while the tensile forces and areas are denoted by positive sign. The concrete is assumed to be completely cracked for the negative moment capacity and is not considered for the tensile area. The positive moment capacity is obtained by taking the moments about the neutral axis and negative moment capacity is calculated by taking moments about the plastic neutral axis. The yield line mechanism engages only the outer half of the bridge cross-section. Therefore, only half of the intact moment capacities are used. The positive intact moment capacity is used for obtaining the exact location of fracture in the end spans that is needed to develop the value of the fraction of the span length from the exterior support at which the girder is fractured, λ. The λ is set to 0.4 as a result of a detailed analysis explained in the TxDOT (0-6937) report on Fracture Critical Steel Twin Tub Girder Bridges. The negative intact moment capacity is used for the internal work done at the interior supports. The engineering computation sheets 5-2a to n enclose the detailed analysis results of Bridge 11.

Sheet 5-2 a	MOMENT CAPACITY OF DECK SLAB (BRIDGE 11)				1 / 14
		Description	Parameter	Data	
DECK SECTION	1	Total Width	B mm	**8051.8**	
	2	Thickness	t mm	**203.2**	
	3	Section width	b mm	1000	
CONCRETE MATERIAL	4	Characteristic Compressive Strength	f_c Mpa	28	
	5		β_1	0.85	
	6	Strain	ε_{cu}	0.003	
REBAR MATERIAL	7	Yield Strength	f_y MPa	414	
	8	Young's Modulus	E Mpa	199948	
	9	strain	ε_y	0.002070	

		Moment Computations		Longitudinal		Transverse	
	10			$\mathbf{m'_x}$	$\mathbf{m_x}$	$\mathbf{m'_y}$	$\mathbf{m_y}$
	11			Top	Bottom	Top	Bottom
REINFORCING BAR DETAIL	12	Bar No.		**5**	**5**	**5**	**5**
	13	Diameter of Bar	d_b mm	15.875	15.875	15.875	15.875
	14	Area of Bar	A_Φ mm^2	197.93	197.93	197.93	197.93
	15	Spacing	s mm	-	-	**127**	**127**
	16	No. of Bars	$\#_{bar}$	**38**	**32**	-	-
	17	Area of Steel	A_s mm^2	934	787	1559	1559
	18	Clear Cover	cc mm	**50.8**	**31.75**	**50.8**	**31.75**
	19	Effective depth (tension)	d mm	128.5875	147.6375	144.4625	163.5125
	20	Effective depth (comp.)	d' mm	55.5625	74.6125	39.6875	58.7375
	21	Depth of NA	c mm	**34.19**	**35.72**	**36.48**	**45.72**

Sheet 5-2 b		MOMENT CAPACITY OF DECK SLAB (BRIDGE 11)					2 / 14
		Moment Computations		Longitudinal		Transverse	
	22			$\mathbf{m'_x}$	$\mathbf{m_x}$	$\mathbf{m'_y}$	$\mathbf{m_y}$
	23			Top	Bottom	Top	Bottom
STRAIN	24		ε_{top}	0.008282	0.003266	0.008880	0.000854
	25		ε_{bot}	0.001875	0.009398	0.000264	0.007730
	26	$\beta_1 c$	a mm	29.06	30.37	31.01	38.86
FORCES	27	Compression-Concrete	C_c N	-681324.36	-711847.42	-726908.63	-910964.82
	28	Tension / Compression-Steel	T_{top} N	386431.46	386431.46	644730.38	266234.44
	29		T_{bot} N	294892.90	325415.97	82178.25	644730.38
	30	Equilibrium Check	T-C N	**0.00**	**0.00**	**0.00**	**0.00**
RESULTS	31	Moment	M N-mm	56174222	66068202	85130609	103359338
			M_n kN-m	56	66	85	103

Remarks:				
	Top Yielded	Top Yielded	Top Yielded	Top Not Yielded
	Bottom Not Yielded	Bottom Yielded	Bottom Not Yielded	Bottom Yielded
	Both steel in Tension	Both steel in Tension	Both steel in Tension	Both steel in Tension

Note: The moment capacities are calculated for 1-meter section.

Sheet 5-2 c	POSITIVE AND NEGATIVE MOMENT OF INTACT SECTION (BRIDGE 11, SPAN 1&3)				3 / 14
			Moment			
		Description	Positive		Negative	
DECK SECTION	1	Total width	B mm	**4330.7**	B mm	4330.7
	2	Thickness	t mm	**203.2**	t mm	203.2
	3	Haunch thickness	h mm	**101.6**	h mm	101.6
CONCRETE MATERIAL	4	Characteristic Compressive Strength	f_c Mpa	27.579		
	5		β_1	0.85		
	6	Strain	ε_{cu}	0.003		
REINFORCING BAR DETAILS	7	Yield Strength	f_y Mpa	414	f_y Mpa	414
	8	Strain	Rebar ε_y	0.002070		
	9	No of Bars at Top	# top bars	**14.5**	# top bars	**14.5**
	10	No of Bars at Top Bent			# top bars bent	**14**
	11	No of Bars at Bottom	# bot bars	**18.5**	# bot bars	**18.5**
	12	Clear Cover Top	cc_{top} mm	**50.8**	cc_{top} mm	**50.8**
	13	Clear Cover Bottom	cc_{bot} mm	**31.75**	cc_{bot} mm	**31.75**
	14	Transverse Top Diameter	$d_{b\ top\ tra}$ mm	**15.875**	$d_{b\ top\ tra}$ mm	**15.875**
	15	Transverse Bottom Diameter	$d_{b\ bot\ tra}$ mm	**15.875**	$d_{b\ bot\ tra}$ mm	**15.875**
	16	Longitudinal Top Diameter	$d_{b\ top\ long}$ mm	**15.875**	$d_{b\ top\ long}$ mm	**15.875**
	17	Longitudinal Top Diameter at Bents			$d_{b\ top\ long}'$ mm	**15.875**
	18	Longitudinal Bottom Diameter	$d_{b\ bot\ long}$ mm	**15.875**	$d_{b\ bot\ long}$ mm	**15.875**
	19	Effective Depth Top	d_{top} mm	74.61	d_{top} mm	74.61
	20				$d_{top\ bent}$ mm	74.61
	21	Effective Depth Bottom	d_{bot} mm	147.64	d_{bot} mm	147.64
	22	Area of Steel for #4 Bars	$A_{\#4}$ mm^2	126.677	$A_{\#4}$ mm^2	126.677
	23	Area of Steel for #5 Bars	$A_{\#5}$ mm^2	197.933	$A_{\#5}$ mm^2	197.933
STRUCTURAL STEEL	24	Yield Strength	F'_y Mpa	345	F'_y Mpa	345
	25	Strain	ε_s	0.00172		
	26	Young's Modulus	E Mpa	199948		
	27	f_y/F'_y	n	1.2	n	1.2
	28	Effective Area of Steel for #4 Bars	$A_{\#4.\ eff}$ mm^2	152	$A_{\#4.\ eff}$ mm^2	152
	29	Effective Area of Steel for #5 Bars	$A_{\#5.\ eff}$ mm^2	238	$A_{\#5.\ eff}$ mm^2	238

Sheet 5-2 d	POSITIVE AND NEGATIVE MOMENT OF INTACT SECTION (BRIDGE 11, SPAN 1&3)			4 / 14
		Moment		
	Description	Positive		Negative	
GIRDER DETAILS	30	Girder Depth	D_g mm	2641.60	D_g mm	2743.2
	31	Top Flange Width	b_{tf} mm	**457.2**	b_{tf} mm	**762**
	32	Top Flange Thickness	t_{tf} mm	**25.4**	t_{tf} mm	**76.2**
	33	Web Width	b_w mm	**2590.8**	b_w mm	**2590.8**
	34	Web Thickness	t_w mm	**73.025**	t_w mm	**73.0**
	35	Bottom Flange Width	b_{bf} mm	**1676.4**	b_{bf} mm	**1676.4**
	36	Bottom Thickness	t_{bf} mm	**25.4**	t_{bf} mm	**76.2**
DEPTHS	37	Compression Zone	c mm	**1534.74**	c mm	**1365.82**
	38	b_w in Comp.	y mm	1204.54	y mm	1289.62
	39	b_w in Tension	y' mm	1386.26	y' mm	1301.18
DISTANCES	40	Distances of Compressive Forces and Tensile Forces from Neutral Axis/ Distances of Areas in Tension and Compression from PNA	$d\,C_{conc}$ mm	882.48	$d\,A_{rebar\ top}$ mm	1607.57
	41		$d\,C_{rebar\ top}$ mm	1460.13	$d\,A_{rebar\ top\ bent}$ mm	1607.57
	42		$d\,C_{rebar\ bottom}$ mm	1387.10	$d\,A_{rebar\ bot}$ mm	1534.55
	43		$d\,C_{tf\,1}$ mm	1217.24	$d\,A_{tf}$ mm	1339.28
	44		$d\,C_{w\,1}$ mm	602.27	$d\,A_{w\,1}$ mm	650.59
	45		$d\,T_{w\,2}$ mm	693.13	$d\,A_{w\,2}$ mm	644.81
	46		$d\,T_{bf}$ mm	1398.96	$d\,A_{bf}$ mm	1327.72
STRAIN	47		$\varepsilon\,C_{rebar\ top}$	0.00285		
	48		$\varepsilon\,C_{rebar\ bottom}$	0.00271		
	49		$\varepsilon\,C_{tf}$	0.00238		
	50		$\varepsilon\,C_{w\,1}$	0.00118		
	51		$\varepsilon\,T_{w\,2}$	0.00135		
	52		$\varepsilon\,T_{bf}$	0.00273		

Sheet 5-2 e	POSITIVE AND NEGATIVE MOMENT OF INTACT SECTION (BRIDGE 11, SPAN 1&3)					5 / 14
			Moment			
		Description	Positive		Negative	
FORCE/AREA	53	Compression F_C / Tension A_T Tension F_T/ Compression A_C	$0.85f'_c\beta BT$ N	-17534712	$A_{s\ top}$ mm	2204
	54				$A_{s\ top\ bent}$ mm	3325
	55		$A_{s\ top}F_y$ N	-860165	$A_{s\ bottom}$ mm	4394
	56		$A_{s\ bottom}F_y$ N	-1714769	A_{tf} mm	116129
	57		$2b_{tf1}yF'_y$ N	-8006799	$A_{w\,1}$ mm	190038
	58	Tension F_T/ Compression A_C	$2b_{tf2}y'F'_y$ N	-41411157.15		
	59		$2b_wt_wF'_y$ N	54848471	$A_{w\,2}$ mm	-188349
	60		$b_{bf}t_{bf}F'_y$ N	14679131	A_{bf} mm	-127742
CHECK	61	Equilibrium of Forces/Areas	F_C N	-69527603	A_T mm	316090
	62		F_T N	69527603	A_C mm	-316090
	63		$F_C + F_T$ N	**0**	$A_T - A_C$ mm	**0**
MOMENT	64	(Half Section)	$0.5\ M_p^+$ kN-m	112348	$0.5\ M_p^-$ kN-m	203043
	65	(Full Section)	M_p^+ kN-m	**224696**	M_p^- kN-m	**406086**

Sheet 5-2 f	POSITIVE AND NEGATIVE MOMENT OF INTACT SECTION (BRIDGE 11, SPAN 2)				6 / 14
			Moment		
		Description	Positive		Negative	
DECK SECTION	1	Total width	B mm	**4330.7**	B mm	4330.7
	2	Thickness	t mm	**203.2**	t mm	203.2
	3	Haunch thickness	h mm	**101.6**	h mm	101.6
CONCRETE MATERIAL	4	Characteristic Compressive Strength	f_c Mpa	28		
	5		β_1	0.85		
	6	Strain	ε_{cu}	0.003		
REINFORCING BAR DETAILS	7	Yield Strength	f_y Mpa	414	f_y Mpa	414
	8	Strain	Rebar ε_y	0.002070		
	9	No of Bars at Top	# top bars	**14.5**	# top bars	**14.5**
	10	No of Bars at Top Bent			# top bars bent	**14**
	11	No of Bars at Bottom	# bot bars	**18.5**	# bot bars	**18.5**
	12	Clear Cover Top	cc_{top} mm	**50.8**	cc_{top} mm	**50.8**
	13	Clear Cover Bottom	cc_{bot} mm	**31.75**	cc_{bot} mm	**31.75**
	14	Transverse Top Diameter	$d_{b\ top\ tra}$ mm	**15.875**	$d_{b\ top\ tra}$ mm	**15.875**
	15	Transverse Bottom Diameter	$d_{b\ bot\ tra}$ mm	**15.875**	$d_{b\ bot\ tra}$ mm	**15.875**
	16	Longitudinal Top Diameter	$d_{b\ top\ long}$ mm	**15.875**	$d_{b\ top\ long}$ mm	**15.875**
	17	Longitudinal Top Diameter at Bents			$d_{b\ top\ long}'$ mm	**15.875**
	18	Longitudinal Bottom Diameter	$d_{b\ bot\ long}$ mm	**15.875**	$d_{b\ bot\ long}$ mm	**15.875**
	19	Effective Depth Top	d_{top} mm	74.61	d_{top} mm	74.61
	20				$d_{top\ bent}$ mm	74.61
	21	Effective Depth Bottom	d_{bot} mm	147.64	d_{bot} mm	147.64
	22	Area of Steel for #4 Bars	$A_{\#4}$ mm^2	126.677	$A_{\#4}$ mm^2	126.677
	23	Area of Steel for #5 Bars	$A_{\#5}$ mm^2	197.933	$A_{\#5}$ mm^2	197.933
STRUCTURAL STEEL	24	Yield Strength	F'_y Mpa	345	F'_y Mpa	345
	25	Strain	ε_s	0.00172		
	26	Young's Modulus	E Mpa	199948		
	27	f_y/F'_y	n	1.2	n	1.2
	28	Effective Area of Steel for #4 Bars	$A_{\#4.\ eff}$ mm^2	152	$A_{\#4.\ eff}$ mm^2	152
	29	Effective Area of Steel for #5 Bars	$A_{\#5.\ eff}$ mm^2	238	$A_{\#5.\ eff}$ mm^2	238

Sheet 5-29	POSITIVE AND NEGATIVE MOMENT OF INTACT SECTION (BRIDGE 11, SPAN 2)	7/14

			Moment			
		Description	Positive		Negative	
GIRDER DETAILS	30	Girder Depth	D_g mm	2686.05	D_g mm	2743.2
	31	Top Flange Width	b_{tf} mm	**457.2**	b_{tf} mm	**762**
	32	Top Flange Thickness	t_{tf} mm	**57.15**	t_{tf} mm	**76.2**
	33	Web Width	b_w mm	**2590.8**	b_w mm	**2590.8**
	34	Web Thickness	t_w mm	**73.025**	t_w mm	**73.0**
	35	Bottom Flange Width	b_{bf} mm	**1676.4**	b_{bf} mm	**1676.4**
	36	Bottom Thickness	t_{bf} mm	**38.1**	t_{bf} mm	**76.2**
DEPTHS	37	Compression Zone	c mm	**1547.54**	c mm	**1365.82**
	38	b_w in Comp.	y mm	1185.59	y mm	1289.62
	39	b_w in Tension	y' mm	1405.21	y' mm	1301.18
DISTANCES	40	Distances of Compressive Forces and Tensile Forces from Neutral Axis/ Distances of Areas in Tension and Compression from PNA	$d\,C_{conc}$ mm	889.83	$d\,A_{rebar\ top}$ mm	1607.57
	41		$d\,C_{rebar\ top}$ mm	1472.92	$d\,A_{rebar\ top\ bent}$ mm	1607.57
	42		$d\,C_{rebar\ bottom}$ mm	1399.90	$d\,A_{rebar\ bot}$ mm	1534.55
	43		$d\,C_{tf\,1}$ mm	1214.16	$d\,A_{tf}$ mm	1339.28
	44		$d\,C_{w\ 1}$ mm	592.79	$d\,A_{w\,1}$ mm	650.59
	45		$d\,T_{w\ 2}$ mm	702.61	$d\,A_{w\,2}$ mm	644.81
	46		$d\,T_{bf}$ mm	1424.26	$d\,A_{bf}$ mm	1327.72
STRAIN	47		$\varepsilon\,C_{rebar\ top}$	0.00286		
	48		$\varepsilon\,C_{rebar\ bottom}$	0.00271		
	49		$\varepsilon\,C_{tf}$	0.00235		
	50		$\varepsilon\,C_{w\,1}$	0.00115		
	51		$\varepsilon\,T_{w\,2}$	0.00136		
	52		$\varepsilon\,T_{bf}$	0.00276		

Sheet 5-2 h	POSITIVE AND NEGATIVE MOMENT OF INTACT SECTION (BRIDGE 11, SPAN 2)					8 / 14
			Moment			
		Description	Positive		Negative	
FORCE/AREA	53	Compression F_C / Tension A_T Tension F_T/ Compression A_C	$0.85f_c\beta BT$ N	-17534712	$A_{s\ top}$ mm	2204
	54				$A_{s\ top\ bent}$ mm	3325
	55		$A_{s\ top}F_y$ N	-860165	$A_{s\ bottom}$ mm	4394
	56		$A_{s\ bottom}F_y$ N	-1714769	A_{tf} mm	116129
	57		$2b_{tf1}yF'_y$ N	-18015298	$A_{w\,1}$ mm	190038
	58	Tension F_T/ Compression A_C	$2b_{tf2}y'F'_y$ N	-39786411.21		
	59		$2b_wt_wF'_y$ N	55892658	$A_{w\,2}$ mm	-188349
	60		$b_{bf}t_{bf}F'_y$ N	22018697	A_{bf} mm	-127742
CHECK	61	Equilibrium of Forces/Areas	F_C N	-77911355	A_T mm	316090
	62		F_T N	77911355	A_C mm	-316090
	63		$F_C + F_T$ N	**0**	$A_T - A_C$ mm	**0**
MOMENT	64	(Half Section)	$0.5\ M_p^+$ kN-m	135360	$0.5\ M_p^-$ kN-m	203043
	65	(Full Section)	M_p^+ kN-m	**270720**	M_p^- kN-m	**406086**

Sheet 5-2 i	COMPUTATION OF OVERSTRENGTH FACTOR EXTERIOR: 3-SPAN CASE (BRIDGE 11, SPAN 1)		9 / 14
	Parameter	Formula/Definition/Equation	Data
GEOMETRY 1	L_x	Span Length	**67.97** m
GEOMETRY 2	R_{CL}	Radius of center line	**250** m
GEOMETRY 3	B	Width	**9** m
GEOMETRY 4	L_x^*	Outer region length $L_x^* = \left(1 + \frac{B}{4R_{C_L}}\right) L_x$	68.56 m
GEOMETRY 5	s	Inter Girder Spacing	**2.1** m
GEOMETRY 6	b	Width of Girder + Edge	**3.3** m
GEOMETRY 7	t	Deck Thickness	**203.20** mm
INTERNAL WORK DONE, IWD 8	m_x	Longitudinal Positive Moment per meter	**64** kN-m/m
INTERNAL WORK DONE, IWD 9	m'_x	Longitudinal Negative Moment per meter	**47** kN-m/m
INTERNAL WORK DONE, IWD 10	m_y	Transverse Positive Moment per meter	**91** kN-m/m
INTERNAL WORK DONE, IWD 11	m'_y	Transverse Negative Moment per meter	**74** kN-m/m
INTERNAL WORK DONE, IWD 12	$0.5M_p^-$	Negative Moment at Support	**203043** kN-m
INTERNAL WORK DONE, IWD 13	λ	Fraction of Length from the exterior support at which girder is fractured	0.40
INTERNAL WORK DONE, IWD 14	$\tan\theta$	$\tan\theta = \sqrt{\frac{m'_y + m_y}{m'_x + m_x}}$	1.22 (Θ=52.5˚)
INTERNAL WORK DONE, IWD 15	$\tan\alpha$	$\tan\alpha = \frac{2s}{L_x}$	0.06 (Θ=5.9˚)
INTERNAL WORK DONE, IWD 16	k_{bound}^{upper}	$\left[1 + 2\frac{\tan\alpha}{\tan\theta}\right] = 1 + \frac{4s}{L_x}\sqrt{\frac{m'_x + m_x}{m'_y + m_y}}$	1.10
INTERNAL WORK DONE, IWD 17	k_{bound}^{lower}	$\left[1 + 2\frac{\tan^2\alpha}{\tan^2\theta}\right] = 1 + \frac{8s^2}{{L_x}^2}\sqrt{\frac{m'_x + m_x}{m'_y + m_y}}$	1.01
INTERNAL WORK DONE, IWD 18	IWD_{upper}	$\left(m'_y + m_y\right)\left(\frac{L_x}{2s}\right) k_{bound}^{upper} + \frac{m_x b}{L_x(\lambda - \lambda^2)} + \frac{0.5M_p^-}{(1-\lambda)L_x}$	**7852** kN-m*1
INTERNAL WORK DONE, IWD 19	IWD_{lower}	$\left(m'_y + m_y\right)\left(\frac{L_x}{2s}\right) k_{bound}^{lower} + \frac{m_x b}{L_x(\lambda - \lambda^2)} + \frac{0.5M_p^-}{(1-\lambda)L_x}$	**7595** kN-m*1

Note: *1: A unit deflection (δ = 1) is considered; therefore, the unit of internal work is in kN-m.

Sheet 5-2 j		COMPUTATION OF OVERSTRENGTH FACTOR EXTERIOR: 3-SPAN CASE (BRIDGE 11, SPAN 1)		10 14
		Parameter	Formula/Definition/Equation	Data
EXTERNAL WORK DONE, EWD	20	DL	Dead Load Factor	1.25
	21	LL	Live Load Factor	1.75
	22	SAF	Stiffener Allowance Factor	1
	23	γ_c	Unit weight of reinforced concrete	23.56 kN/m^3
	24	w_u	Area load due to reinforced concrete + lane load $DL\gamma_c \frac{t}{100} + LL \cdot 2.55$	10.454 kN/m^2
	25	γ_s	Unit weight of steel	76.97 kN/m^3
	26	V_g	Volume of Girder	**33** m^3
	27	A_r	Area of Rail Cross-Section (SSTR)	**0.26** m^2
	28	V_r	Volume of Rail = $L_x A_r$	18 m^3
	29	W_x	$1.25\left(1.15V_g\gamma_s + V_r\gamma_c\right)/L_x$	61.41 kN/m
	30	y (Lane 2)	$(b+s-4.6)$ *for (b+s)<6.4* $(b+s-5.5)$ *for (b+s)>6.4*	0.83 m
	31	K_{lane}	$1+0.5\frac{y}{s}$ *for (b+s)<6.4;* $1+\frac{y}{s}$ *for (b+s)>6.4*	1.19
	32	$EWD_{HS\text{-}20}$	$\left(747-\frac{480}{\lambda L_x}-\frac{1921}{(1-\lambda)L_x}\right)K_{Lane}$	835 kN-m
	33	W_{ET}	$w_u L_x(b+0.5s) + W_x L_x + 2EWD_{HS20}$	8985 kN-m
	34	EWD	$0.5\ W_{ET}$	4493 kN-m*1
RESULTS	35	Ω_{upper}	IWD_{upper}/EWD	**1.75**
	36	Ω_{lower}	IWD_{lower}/EWD	**1.69**

Note: *1: A unit deflection (δ = 1) is considered; therefore, the unit of internal work is in kN-m.

Sheet 5-2 k		COMPUTATION OF OVERSTRENGTH FACTOR INTERIOR: 3-SPAN CASE (BRIDGE 11, SPAN 2)		11 / 14	
		Parameters	Formula/Definition/Equation	Data	
GEOMETRY	1	L_x	Span Length	**111.56**	m
	2	R_{CL}	Radius of center line	**250**	m
	3	B	Width	**9**	m
	4	L_x^*	Outer region length $L_x^* = \left(1 + \frac{B}{4R_{C_L}}\right) L_x$	112.52	m
	5	s	Inter Girder Spacing	**2.1**	m
	6	b	Width of Girder + Edge	**3**	m
	7	t	deck thickness	**203**	mm
INTERNAL WORK DONE, IWD	8	m_x	Longitudinal Positive Moment per meter	**64**	kN-m/m
	9	m'_x	Longitudinal Negative Moment per meter	**47**	kN-m/m
	10	m_y	Transverse Positive Moment per meter	**91**	kN-m/m
	11	m'_y	Transverse Negative Moment per meter	**74**	kN-m/m
	12	$0.5M_{p1}^-$	Negative Moment at Support 1	**203043**	kN-m
	13	$0.5M_{p2}^-$	Negative Moment at Support 2	**203043**	kN-m
	14	tan θ	$\tan\theta = \sqrt{\frac{m'_y + m_y}{m'_x + m_x}}$	1.22	(Θ=52.5˚)
	15	tan α	$\tan\alpha = \frac{2s}{L_x}$	0.04	(Θ=3.3˚)
	16	k_{bound}^{upper}	$\left[1 + 2\frac{\tan\alpha}{\tan\theta}\right] = 1 + \frac{4s}{L_x}\sqrt{\frac{m'_x + m_x}{m'_y + m_y}}$	1.06	
	17	k_{bound}^{lower}	$\left[1 + 2\frac{\tan^2\alpha}{\tan^2\theta}\right] = 1 + \frac{8s^2}{{L_x}^2}\sqrt{\frac{m'_x + m_x}{m'_y + m_y}}$	1.00	
	18	IWD_{upper}	$\left(m_y^{'} + m_y\right)\left(\frac{L_x}{2s}\right) k_{bound}^{upper} + \frac{4m_x b}{L_x} + \left(0.5M_{p1}^- + 0.5M_{p2}^-\right)\frac{2}{L_x}$	**11817**	kN-m*1
	19	IWD_{lower}	$\left(m_y^{'} + m_y\right)\left(\frac{L_x}{2s}\right) k_{bound}^{lower} + \frac{4m_x b}{L_x} + \left(0.5M_{p1}^- + 0.5M_{p2}^-\right)\frac{2}{L_x}$	**11554**	kN-m*1

Note: *1: A unit deflection (δ = 1) is considered; therefore, the unit of internal work is in kN-m.

Sheet 5-2 l		COMPUTATION OF OVERSTRENGTH FACTOR INTERIOR: 3-SPAN CASE (BRIDGE 11, SPAN 2)		12 / 14	
		Parameter	Formula/Definition/Equation	Data	
EXTERNAL WORK DONE, EWD	20	DL	Dead Load Factor	1.25	
	21	LL	Live Load Factor	1.75	
	22	SAF	Stiffener Allowance Factor	1.15	
	23	γ_c	Unit weight of reinforced concrete	23.56	kN/m^3
	24	w_u	Area load due to reinforced concrete + lane load $DL\gamma_c \frac{t}{100} + LL \cdot 2.55$	10.45	kN/m^2
	25	γ_s	Unit weight of steel	76.97	kN/m^3
	26	V_g	Volume of Girder	**57**	m^3
	27	A_r	Area of Rail Cross-Section (T4 (S))	**0.26**	m^2
	28	V_r	Volume of Rail = $L_x A_r$	29	m^3
	29	W_x	$1.25\left(1.15V_g\gamma_s + V_r\gamma_c\right)/L_x$	63.93	kN/m
	30	y (Lane 2)	$(b+s-4.6)$ *for (b+s)<6.4* $(b+s-5.5)$ *for (b+s)>6.4*	0.83	m
	31	K_{lane}	$1+0.5\frac{y}{s}$ *for (b+s)<6.4;* $1+\frac{y}{s}$ *for (b+s)>6.4*	1.19	
	32	$EWD_{HS\text{-}20}$	$\left(747-\frac{3535}{L_x}\right)K_{Lane}$	854	kN-m
	33	W_{ET}	$w_u L_x(b+0.5s) + W_x L_x + 2EWD_{HS20}$	13997	kN-m
	34	EWD	$0.5\ W_{ET}$	6999	kN-m*1
RESULTS	35	Ω_{upper}	IWD_{upper}/EWD	**1.69**	
	36	Ω_{lower}	IWD_{lower}/EWD	**1.65**	

Note: *1: A unit deflection (δ = 1) is considered; therefore, the unit of external work is in kN-m.

Sheet 5-2 m		COMPUTATION OF OVERSTRENGTH FACTOR EXTERIOR: 3-SPAN CASE (BRIDGE 11, SPAN 3)		13 14
		Parameters	Formula/Definition/Equation	Data
GEOMETRY	1	L_x	Span Length	**71.63** m
	2	R_{CL}	Radius of center line	**250** m
	3	B	Width	**9** m
	4	L_x^*	Outer region length $L_x^* = \left(1 + \frac{B}{4R_{C_L}}\right) L_x$	72.25 m
	5	s	Inter Girder Spacing	**2.1** m
	6	b	Width of Girder + Edge	**3.3** m
	7	t	Deck Thickness	**203.20** mm
INTERNAL WORK DONE, IWD	8	m_x	Longitudinal Positive Moment per meter	**64** kN-m/m
	9	m'_x	Longitudinal Negative Moment per meter	**47** kN-m/m
	10	m_y	Transverse Positive Moment per meter	**91** kN-m/m
	11	m'_y	Transverse Negative Moment per meter	**74** kN-m/m
	12	M_p^-	Negative Moment at Support	**203043** kN-m
	13	λ	Fraction of Length from the exterior support at which girder is fractured	0.40
	14	$\tan\theta$	$\tan\theta = \sqrt{\frac{m'_y + m_y}{m'_x + m_x}}$	1.22 (Θ=52.5°)
	15	$\tan\alpha$	$\tan\alpha = \frac{2s}{L_x}$	0.06 (Θ=5.9°)
	16	k_{bound}^{upper}	$\left[1 + 2\frac{\tan\alpha}{\tan\theta}\right] = 1 + \frac{4s}{L_x}\sqrt{\frac{m'_x + m_x}{m'_y + m_y}}$	1.10
	17	k_{bound}^{lower}	$\left[1 + 2\frac{\tan^2\alpha}{\tan^2\theta}\right] = 1 + \frac{8s^2}{{L_x}^2}\sqrt{\frac{m'_x + m_x}{m'_y + m_y}}$	1.00
	18	IWD_{upper}	$\left(m'_y + m_y\right)\left(\frac{L_x}{2s}\right) k_{bound}^{upper} + \frac{m_x b}{L_x(\lambda - \lambda^2)} + \frac{0.5M_p^-}{(1-\lambda)L_x}$	**7741** kN-m*1
	19	IWD_{lower}	$\left(m'_y + m_y\right)\left(\frac{L_x}{2s}\right) k_{bound}^{lower} + \frac{m_x b}{L_x(\lambda - \lambda^2)} + \frac{0.5M_p^-}{(1-\lambda)L_x}$	**7483** kN-m*1

Note: *1: A unit deflection (δ = 1) is considered; therefore, the unit of external work is in kN-m.

Sheet 5-2 n		COMPUTATION OF OVERSTRENGTH FACTOR EXTERIOR: 3-SPAN CASE (BRIDGE 11, SPAN 3)		14 / 14
		Parameter	Formula/Definition/Equation	Data
EXTERNAL WORK DONE, EWD	20	DL	Dead Load Factor	1.25
	21	LL	Live Load Factor	1.75
	22	SAF	Stiffener Allowance Factor	1
	23	γ_c	Unit weight of reinforced concrete	23.56 kN/m^3
	24	w_u	Area load due to reinforced concrete + lane load $DL\gamma_c \frac{t}{100} + LL \cdot 2.55$	10.454 kN/m^2
	25	γ_s	Unit weight of steel	76.97 kN/m^3
	26	V_g	Volume of Girder	**35** m^3
	27	A_r	Area of Rail Cross-Section (T4 (S))	**0.26** m^2
	28	V_r	Volume of Rail = $L_x A_r$	18 m^3
	29	W_x	$1.25\left(1.15V_g\gamma_s + V_r\gamma_c\right)/L_x$	61.83 kN/m
	30	y (Lane 2)	$(b+s-4.6)$ for $(b+s)<6.4$ $(b+s-5.5)$ for $(b+s)>6.4$	0.83 m
	31	K_{lane}	$1+0.5\frac{y}{s}$ for $(b+s)<6.4$; $1+\frac{y}{s}$ for $(b+s)>6.4$	1.19
	32	$EWD_{HS\text{-}20}$	$\left(747-\frac{480}{\lambda L_x}-\frac{1921}{(1-\lambda)L_x}\right)K_{Lane}$	838 kN-m
	33	W_{ET}	$w_u L_x(b+0.5s) + W_x L_x + 2EWD_{HS20}$	9415 kN-m
	34	EWD	$0.5\ W_{ET}$	4708 kN-m*1
RESULTS	35	Ω_{upper}	IWD_{upper}/EWD	**1.64**
	36	Ω_{lower}	IWD_{lower}/EWD	**1.59**

Note: *1: A unit deflection (δ = 1) is considered; therefore, the unit of external work is in kN-m.

5.6. Results for Overstrength Factors of Bridges with Intact Girder

A similar analysis was conducted for the same spans of the bridges discussed in this section such that the outer girder is intact. As expected, the analysis of the problem with the assumption that the outer girder is not fractured resulted in overstrength factors higher than that of the case of fractured outer girder. The intact girder analysis showed that the bridge has a much higher reserve capacity and this analysis was conducted for sake of completeness. The intact girder overstrength factors for Bridge 2 are $\Omega_{Upper} = 3.96$ and $\Omega_{Lower} = 3.80$. These values are higher than the overstrength factors of the corresponding fractured girder case by 238% and 274% respectively. The intact girder overstrength for Bridge 11, Span 1 are $\Omega_{Upper} = 3.26$ and $\Omega_{Lower} = 3.21$. The overstrength factors are 87% and 90% higher than the corresponding fractured case, respectively. Similarly, the results of the intact and fractured outer girder cases are summarized in Table 5.1. These results are validated against the FEM analysis conducted for the TxDOT project 0-6937 (Hurlebaus et al. 2018).

Table 5.1. Summary of Overstrength Factors for Single-Span Bridges (Intact and Fractured conditions).

		Ωupper	Ωlower	UB % Increase	LB % Increase
B2S1	**Intact**	3.96	3.80	238	274
	Fractured	1.17	1.02		
B11S1	**Intact**	3.26	3.21	87	90
	Fractured	1.75	1.69		
B11S2	**Intact**	2.37	2.34	41	42
	Fractured	1.69	1.65		
B11S3	**Intact**	2.96	2.91	80	83
	Fractured	1.64	1.59		

Note: Intact and Fractured designate the state of the outer girder of bridge.
The increase or decrease percent is between the intact and fractured cases.

5.7. Chapter Findings

A unified general expression was derived that may be used for any of the spans selected from the suite of 15 bridges. The two bridges selected for establishing the postulated mechanism and the theories for deriving the overstrength capacity of the bridges encompass all the probable boundary conditions present for each of the spans under consideration. Bridges 2 and 11 together comprise of one single-span, simply supported bridge, two exterior spans of the three-span bridge, with one end free and the other end fixed, and one interior span of the three-span bridge with both ends fixed. Therefore, all the various combinations of spans belonging to the suite of 15 bridges were captured in this chapter. Though each of the three distinct spans differ in boundary conditions, the general formula may be employed for the assessment of bridges using limit method by simply following the step wise analysis procedure explained in the following sections. These guidelines serve as an aid for bridge engineers to replicate this analysis for any STTG bridge that have the essential features of the bridges focused in this study.

Since the limit analyses are a simple and independent check for the reserve capacity of the STTG bridges, this analysis will expedite the process of reclassification of bridges. If the reserve capacity is found to be lower than the required capacity after fracture, the need to undertake the more complicated FEM analysis may be dispensed with.

CHAPTER VI

FURTHER APPLICATIONS AND RAMIFICATIONS

6.1. Chapter Summary

The limit analysis solutions are applied to assess the viability of these methods for the purpose of reclassification of the Steel Twin-Tub Girder bridges from their present fracture critical designation. A suite of 15 preselected bridges are analyzed using the solutions that are developed and the results are discussed to bring out the influencing factors for the failure analysis of these bridges. Each span is evaluated based on the boundary condition, the geometrical parameters such as the span length, the inter-girder spacing, the breadth and the radius of curvature. The discussions of the results of each span is conducted and the recommendations based on these methods regarding the redundancy of the bridges and the consequent potential declassification from fracture critical nature are presented.

6.2. Introduction

This section discusses the yield line analysis conducted for the 15 pre-selected bridges. The mechanism that was formulated for the HL-93 loading case with the folded plate mechanism, implemented for the calculation of the overstrength factors of the bridges. The expressions for the overstrength factor derived in Chapter 4, modified according to the boundary conditions of the bridges, namely the simply supported, the pinned-fixed and the fixed-fixed condition, and for the trucks accommodated on the deck under HL-93 loading, are used to obtain the results reported in this section.

The details of geometry, boundary conditions and loading are discussed for each bridge. The results of each span are listed out and the equations used to calculate the upper bound and lower bound solutions are discussed in detail in this chapter. This analysis shall give an overview

of the reserve capacity of the 15 bridges selected for the purpose of reclassification study from their existing fracture critical status. A pattern of redundancy based on the boundary conditions, geometry and loading of each span emerges from the discussions. The behavioral pattern that are observed from this analysis may help in the development of recommendations for a potential reclassification from the fracture critical status.

6.2.1. Bridge 1—NBI #12-102-3256-01-403

The yield line analysis for the first of the bridges is illustrated in Figure 6.1. This is a single-span bridge of 67.1 m span length and 9.8 m width. The upper-bound and lower-bound overstrength factors calculated using an appropriate factor explained in Equation (4.46) to modify Equation (4.51) to account for the addition of the external work done due to inner wheels of the second truck are Ω_{Upper} = 0.62 and Ω_{Lower} = 0.57 for this bridge. In fact, all the STTG bridges selected for this section are wide enough to accommodate two lanes of HL-93 loading, unlike the bridge of TxDOT Research Project 9-5498.

6.2.2. Bridge 2—NBI #12-102-0271-17-530

This is a single-span bridge of 35.1 m span length and 8.1 m width. The upper-bound and lower-bound overstrength factors calculated using Equation (4.51) are Ω_{Upper} = 1.17 and Ω_{Lower} = 1.02 for this bridge. Since the span of this bridge is much less than that of Bridge 1, the overstrength factor is higher. It is to be noted that the dimensions of this bridge are comparable to that of the test bridge, and consequently, so is the overstrength factor.

6.2.3. Bridge 3—NBI #12-102-0508-01-294

This is a single-span bridge of 70.1 m span length and 11.8 m width. The upper-bound and lower-bound overstrength factors calculated using an appropriate factor explained in Equation (4.47) to modify Equation (4.50) to account for the addition of the external work done due to both the lines

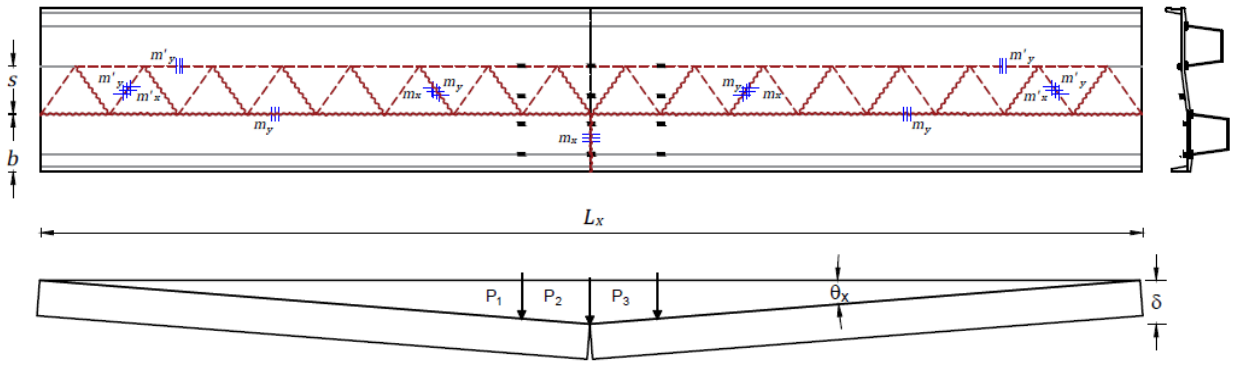

Figure 6.1. Plan, cross-section, and side elevation with HL-93 loading for single-span bridges.

of wheels of the second truck are Ω_{Upper} = 0.51 and Ω_{Lower} = 0.44 for this bridge. Equation (4.47) is applied because the bridge is so wide that the outer wheels also cause a small amount of deflection and, therefore, external work. Since the span length of this bridge is very high, the overstrength factor is low. Table 6.1 summarizes the input values and the results for the overstrength factors of the test bridge of TxDOT Research Project 9-5498 and single-span STTG bridges using the equations mentioned in Section 4.4.

6.2.4. Bridge 4—NBI #12-102-0271-07-637

Bridge 4 is a two-span bridge with an exterior critical span that is 40.2 m long and 8.7 m wide, and it has the upper-bound and lower-bound overstrength factors of Ω_{Upper} = 1.80 and Ω_{Lower}=1.67. The 39 m span is not critical since the upper-bound and lower-bound overstrength factors are Ω_{Upper} = 1.85 and Ω_{Lower} = 1.71. Equation (4.46) was used to modify Equation (4.58). The fixed-end moment causes negative yield line to occur vertically along the width b at the interior continuous support. There will also be additional hinge formation due to the negative moment of the steel tub girder. Both effects are accounted for by the plastic moment capacity of the composite deck at support, M_p^-.

Table 6.1. Summary of Overstrength Factors for Single-Span Bridges.

ID	L_x	R	B	L_x^*	s	b	t	m_x	m'_x	m_y	m'_y	w_u	W_x	IWD	EWD	Ω	Ω
	m	m	m	m	m	m	mm	kN	kN	kN	kN	kN/m^2	kN/m	kN-m	kN-m	UB	LB
9-5498	37	396	7	37	1.8	2.7	203	71	49	111	89	10.53	13.71	2318	1588	**1.46**	**1.28**
B1	67	175	10	68	2.9	3.5	203	44	22	120	93	10.53	50.19	2691	4359	**0.62**	**0.57**
B2	35	582	8	35	1.9	3.1	203	67	58	102	85	10.53	20.72	2126	1819	**1.17**	**1.02**
B3	70	673	12	70	3.8	4.0	229	80	67	120	102	11.01	36.48	2415	4737	**0.51**	**0.44**

Note: UB and LB denote upper-bound and lower-bound overstrength factors, respectively.

6.2.5. Bridge 5—NBI #14-227-0-0015-13-452

This is a two-span bridge whose exterior span is 4 m long and 0.9 m wide. The upper-bound and lower-bound overstrength factors are Ω_{Upper} = 1.40 and Ω_{Lower} = 1.28 for this span. The other exterior span of 42.5 m span length has critical upper-bound and lower-bound overstrength factors of Ω_{Upper} = 1.39 and Ω_{Lower} = 1.28. The calculations use the same procedure as that of Bridge 4.

6.2.6. Bridge 6—NBI #12-102-0271-07-575

This is a two-span bridge whose exterior critical spans are both 42.7 m long and 11.7 m wide. The upper-bound and lower-bound overstrength factors are Ω_{Upper} = 1.62 and Ω_{Lower} = 1.52. Equation (4.58) is modified using the appropriate factor mentioned in Equation (4.47) to account for the external work done due to the second truck since the bridge is so wide that the outer wheels of the second truck also cause a small amount of deflection and, consequently, external work. This modification factor is similar to that used for computing the overstrength factor of Bridge 3.

6.2.7. Bridge 7—NBI #12-102-0177-07-394

This is a two-span bridge whose exterior critical span is 66.8 m long and 8.7 m wide. The upper-bound and lower-bound overstrength factors calculated using Equation (4.59) and Equation (4.46) are Ω_{Upper} = 1.45 and Ω_{Lower} = 1.37 for this span. The upper-bound and lower-bound overstrength factors calculated using the same equation for the 57.9 m span are Ω_{Upper} = 1.69 and Ω_{Lower} = 1.59.

6.2.8. Bridge 8—NBI #12-102-0271-06-661

This is an 8.7 m wide two-span bridge whose exterior critical span is 89.9 m long. The upper-bound and lower-bound overstrength factors calculated using Equation (4.59) are Ω_{Upper} = 1.25 and Ω_{Lower} = 1.18 for this span. The upper-bound and lower-bound overstrength factors calculated using Equation (4.59) for the 80.8 m span are Ω_{Upper} = 1.34 and Ω_{Lower} = 1.27. The modification factor of Equation (4.46) was used.

6.2.9. Bridge 9—NBI #12-102-0177-07-394

This three-span bridge has a width of 8.7 m and an exterior critical span 42.7 m long. The upper-bound and lower-bound overstrength factors are calculated to be Ω_{Upper} = 1.56 and Ω_{Lower} = 1.44 for the exterior critical span and calculated to be Ω_{Upper} = 1.68 and Ω_{Lower} = 1.56 for the other exterior span of 38.4 m. Equation (4.59) and Equation (4.55) were used by modifying with the factor explained in Equation (4.46) to find the overstrength factor of the interior span. The fixed-end moments cause negative yield line to occur vertically along a width of b at the two continuous supports of the interior span. There will also be additional hinge formation due to the negative moment of the steel tub girder. Both of these are accounted for by the plastic moment capacities of the composite deck, M_{p1}^{-} and M_{p2}^{-}, at the continuous supports at the left and right ends of the interior span, respectively. For Bridge 9, the interior continuous span, clamped on both ends, is 46 m long and 8.7 m wide. The upper-bound and lower-bound overstrength factors are Ω_{Upper} = 2.34 and Ω_{Lower} = 2.24.

6.2.10. Bridge 10—NBI # 14-227-0-0015-13-450

This three-span bridge is 9.1 m wide and the exterior critical span is 57.9 m long, and the other exterior span is 45.1 m long. The upper-bound and lower-bound overstrength factors calculated using Equation (4.59) are Ω_{Upper} = 1.67 and Ω_{Lower} = 1.59 for the exterior critical span and Ω_{Upper}

= 1.98 and Ω_{Lower} = 1.88 for the other exterior span. The interior span of length 80.8 m and width 9.1 m has upper-bound and lower-bound overstrength factors of Ω_{Upper} = 1.90 and Ω_{Lower} = 1.84 that were calculated using Equation (4.56).

6.2.11. Bridge 11—NBI #12-102-0271-07-593

This three-span bridge is 8.7 m wide; the critical exterior span is 71.6 m long and the other exterior span is 68 m long. The upper-bound and lower-bound overstrength factors calculated using Equation (4.59) are Ω_{Upper} = 1.65 and Ω_{Lower} = 1.59 for the exterior critical span and Ω_{Upper} = 1.75 and Ω_{Lower} = 1.69 for the other exterior span. The interior span, 112 m long and 9.1 m wide, has upper-bound and lower-bound overstrength factors of Ω_{Upper} = 1.69 and Ω_{Lower} = 1.66 that were calculated using Equation (4.56).

6.2.12. Bridge 12—NBI # 12-102-0271-07-639

This three-span bridge is 8.5 m wide, the critical exterior span is 44.2 m long, and the other exterior span is 42.7 m long. The upper-bound and lower-bound overstrength factors calculated using Equation (4.59) are Ω_{Upper} = 1.71 and Ω_{Lower} = 1.60 for the exterior critical span and Ω_{Upper} = 1.75 and Ω_{Lower} = 1.63 for the other exterior span. The interior span, 54.9 m long and 8.5 m wide, has upper-bound and lower-bound overstrength factors of Ω_{Upper} = 2.20 and Ω_{Lower} = 2.10 that were calculated using Equation (4.56).

6.2.13. Bridge 13—NBI #14-227-0-0015-13-452

This three-span bridge has a width of 9.1 m. Both exterior spans are 46.2 m long, but with differing girder dimensions. The upper-bound and lower-bound overstrength factors calculated using Equation (4.59) are Ω_{Upper} = 1.40 and Ω_{Lower} = 1.30 for the exterior critical span and Ω_{Upper} = 1.41 and Ω_{Lower} = 1.32 for the other exterior span. The 57.9 m long, 9.1 m wide interior span has upper-

bound and lower-bound overstrength factors of Ω_{Upper} = 1.89 and Ω_{Lower} = 1.80 that were calculated using Equation (4.56).

6.2.14. Bridge 14—NBI #18-057-0-0009-11-460

This three-span bridge has a width of 8.5 m; both the exterior spans are 45.7 m long. The upper-bound and lower-bound overstrength factors calculated using Equation (4.59) are Ω_{Upper} = 1.63 and Ω_{Lower} = 1.52 for both. The 57.9 m long, 8.5 m wide interior span has upper-bound and lower-bound overstrength factors of Ω_{Upper} = 2.07 and Ω_{Lower} = 1.98 that were calculated using Equation (4.56).

6.2.15. Bridge 15—NBI #12-102-0271-06-689

This three-span bridge has a width of 8.5 m, and both exterior spans are 61 m long, but with differing girder dimensions. The upper-bound and lower-bound overstrength factors calculated using Equation (4.59) are Ω_{Upper} = 1.69 and Ω_{Lower} = 1.59 for the exterior critical span and Ω_{Upper} = 1.70 and Ω_{Lower} = 1.60 for the other exterior span. The 89.9 m long, 8.5 m wide interior span has upper-bound and lower-bound overstrength factors of Ω_{Upper} = 1.86 and Ω_{Lower} = 1.78 that were calculated using Equation (4.59). It is to be noted that Bridges 9–15 use the modification factor defined in Equation (4.46) for both exterior and interior spans to account for the external work done by the HS-20 truck load of the second lane.

Table 6.2 and Table 6.3 summarize (similar to the Table 6.1) the input values and the results for the bridges to obtain the overstrength factors of the exterior and interior spans of the STTG bridges using the equations mentioned in Section 4.5.

Table 6.2. Summary of Overstrength Factors for Exterior Spans.

ID	L_x	R	B	L_x^*	s	b	t	m_x	m'_x	m_y	m'_y	$0.5M_p^-$	w_u	W_x	IWD	EWD	Ω	Ω
	m	m	m	m	m	m	mm	kN	kN	kN	kN	kN-m	kN/m^2	kN/m	kN-m	kN-m	UB	LB
B4S1	40	59	9	42	2.4	3.2	229	62	58	111	93	46595	11.01	21.01	3999	2220	**1.80**	**1.67**
B4S2	39	59	9	41	2.4	3.2	229	62	58	111	93	46595	11.01	20.72	4003	2166	1.85	1.71
B5S1	43	137	9	43	3.0	3.1	203	53	40	102	85	35866	10.53	13.86	3038	2180	1.40	1.28
B5S2	43	137	9	43	3.0	3.1	203	53	40	102	85	35866	10.53	14.44	3038	2184	**1.39**	**1.28**
B6S1	43	250	12	43	3.0	4.4	203	67	58	129	107	71483	10.53	25.39	4835	2985	**1.62**	**1.52**
B6S2	43	250	12	43	3.0	4.4	203	67	58	129	107	71483	10.53	25.39	4835	2985	**1.62**	**1.52**
B7S1	67	233	9	67	2.1	3.2	203	67	49	89	76	81505	10.53	26.99	4715	3261	**1.45**	**1.37**
B7S2	58	233	9	58	2.1	3.2	203	67	49	89	76	81505	10.53	22.32	4706	2793	1.69	1.59
B8S1	81	269	9	81	2.4	3.0	203	67	53	102	85	94475	10.53	29.47	5236	3897	1.34	1.27
B8S2	90	269	9	91	2.4	3.0	203	67	53	102	85	94475	10.53	31.08	5378	4319	**1.25**	**1.18**
B9S1	43	233	9	43	2.1	3.2	203	67	49	89	76	40374	10.53	19.26	3394	2180	**1.56**	**1.44**
B9S3	38	233	9	39	2.1	3.2	203	67	49	89	76	40374	10.53	19.40	3416	2037	1.68	1.56
B10S1	45	218	9	46	2.4	3.4	203	53	40	93	76	79147	10.53	20.72	4760	2406	1.98	1.88
B10S3	58	218	9	59	2.4	3.4	203	53	40	93	76	87602	10.53	21.30	4813	2882	**1.67**	**1.59**
B11S1	68	250	9	69	2.1	3.3	203	62	49	93	76	203043	10.53	61.42	7852	4493	1.75	1.69
B11S3	72	250	9	72	2.1	3.3	203	62	49	93	76	203043	10.53	61.86	7741	4706	**1.64**	**1.59**
B12S1	43	69	9	44	2.4	3.2	229	58	44	111	93	48114	11.01	21.45	4035	2309	1.75	1.63
B12S3	44	69	9	46	2.4	3.2	229	58	44	111	93	48114	11.01	21.01	4039	2358	**1.71**	**1.60**
B13S1	46	137	9	47	2.7	3.1	203	53	40	93	76	48644	10.53	16.49	3332	2358	1.41	1.32
B13S3	46	137	9	47	2.7	3.1	203	53	40	93	76	48644	10.53	17.65	3332	2384	**1.40**	**1.30**
B14S1	46	308	9	46	2.1	3.3	203	62	44	93	76	42776	10.53	20.43	3732	2291	**1.63**	**1.52**
B14S3	46	308	9	46	2.1	3.3	203	62	44	93	76	42776	10.53	20.43	3732	2291	**1.63**	**1.52**
B15S1	61	247	9	62	2.4	3.1	203	71	62	111	93	82970	10.53	26.70	5178	3047	1.70	1.60
B15S3	61	247	9	62	2.4	3.1	203	71	62	111	93	82970	10.53	26.99	5178	3056	**1.69**	**1.59**

Note: UB and LB denote upper-bound and lower-bound overstrength factors, respectively.

Table 6.3. Summary of Overstrength Factors for Interior Spans.

ID	L_x	R	B	L_x^*	s	b	t	m_x	m'_x	m_y	m'_y	$0.5M_{p1}^-$	$0.5M_{p2}^-$	w_u	W_x	IWD	EWD	Ω	Ω
	m	m	m	m	m	m	mm	kN	kN	kN	kN	kN-m	kN-m	kN/m^2	kN/m	kN-m	kN-m	UB	LB
B9S2	46	233	9	47	2.3	3.2	203	67	49	89	76	40374	40374	10.53	19.99	5418	2313	**2.34**	**2.24**
B10S2	81	218	9	82	2.3	3.4	203	53	40	93	76	79147	87602	10.53	23.49	7206	3785	**1.90**	**1.84**
B11S2	112	250	9	112	2.1	3.3	203	62	49	93	76	203891	203043	10.53	64.34	11817	6999	**1.69**	**1.65**
B12S2	55	69	9	57	2.3	3.2	229	58	44	111	93	48114	48114	11.01	23.49	6156	2798	**2.20**	**2.10**
B13S2	58	137	9	59	2.8	3.1	203	53	40	93	76	48644	48644	10.53	17.65	5249	2780	**1.89**	**1.80**
B14S2	58	308	9	58	2.0	3.3	203	62	44	93	76	42776	42776	10.53	21.16	5623	2718	**2.07**	**1.98**
B15S2	90	247	9	91	2.4	3.1	203	71	62	111	93	82970	82970	10.53	28.74	7807	4199	**1.86**	**1.78**

Note: UB and LB denote upper-bound and lower-bound overstrength factors, respectively.

6.3. Ramifications

In this chapter, yield line theory was applied to twin tub girder bridges with one tub completely fractured. The yield line theory that was developed was implemented by using both upper- and lower-bound approaches for the class of curved twin tub bridges investigated herein. The results of the 15 bridges investigated were tabulated for each span type: (a) simply supported, (b) both ends continuous; and (c) one end continuous plus the abutment simply supported (free).

Some of the conclusions drawn from the results of yield line analysis are as follows:

- The analysis of the bridges under the HL-93 loads results in a mechanism that makes use of torsional folded-plate action. This mechanism ensures the estimation of critical capacity after several trials.
- The overall analysis is conservative because the guardrail is disengaged in this analysis. This assumption is reasonable since the guardrail is not constructed as a uniformly continuous entity due to the presence of expansion joints. Moreover, crushing of the guardrail under compression is reported to have taken place during the failure of the test bridge, as mentioned by Barnard et al. (2010). Therefore, it is reasonable to not count on any strength from the guardrail since it may lead to an incorrectly higher estimate of the strength of the bridge.
- The simple-span bridges with the span lengths of 35.1 m and 36.6 m have upper-bound overstrength factors of 1.17 and 1.46, respectively, while those with the span lengths of 67.1 m and 70.1 m have upper-bound overstrength factors of 0.62 to 0.51, respectively. The exterior spans have upper-bound overstrength factors ranging from 1.25 to 1.98 depending on the

length of the span and the variation of the girder geometry along the span. The interior spans have overstrength factors ranging from 1.69 to 2.34 depending on the length of the span.

- The redundancy owing to the continuity at supports contributes to a greater strength, as evidenced by the higher overstrength factors of the exterior and interior spans when compared to those of the simply supported single spans. The general order is that the interior spans have the most load bearing capacity, the exterior spans have the next highest load bearing capacity, and the single-span bridges are weakest in comparison, especially when the length and width are large, as seen in the case of Bridges 1 and 3.
- The width of the bridge, however, is observed to not have as substantial an impact as that of the length of the span and boundary conditions in the case of yield line analysis. This phenomenon is because the external work done due to the second truck considered for the computation of the overstrength factor of the wider bridges does not change the overall outcome significantly since the deflections under the second HS-20 truck are of smaller magnitude.
- From the results of the analysis, it may be recommended that the single-spans of the simply supported bridges are most susceptible to failure due to the lack of continuity at supports. Therefore, such bridges should continue to remain fracture critical if the span length exceeds 65 m. The width and radius of curvature must also be suitably monitored when these bridges are being considered for a reclassification.
- The interior spans of bridges beyond the span length of 80 m may be recommended to undergo a thorough investigation by more advanced methods since the span length may lead to a failure

in case of a fracture. The interior spans less than 80 m long display high redundancy and are likely have a high overstrength factor by all the methods of analyses.

- Exterior spans of STTG bridges are observed to show fairly high redundancy for span lengths of up to 45 m. The lengths between 45 m to 60 display a slightly lower redundancy compared to ones below the 45 m range. Those spans beyond 60 m length must be assessed with caution during the reclassification investigation since the overstrength factors for such lengths are observed to be the least among the spans of this group.

Table 6.4 summarizes the overstrength factors for the test bridge of TxDOT Research Project 9-5498 and the 15 preselected STTG bridges with the overstrength factors of the critical spans presented in boldface.

Table 6.4. Overstrength Factors for 15 Selected STTG Bridges.

Bridge ID	Radius of curvature, R m	Width, B m	Span, L_x m	Overstrength Factor $\Omega_{yield\ Line}$	
9-5498	396	7.0	36.6	**1.46**	**1.28**
1	175	9.8	67.1	**0.62**	**0.57**
2	582	7.9	35.1	**1.17**	**1.02**
3	673	11.9	70.1	**0.51**	**0.44**
4-S1	59	8.5	40.2	**1.80**	**1.67**
4-S2		8.5	39.0	1.85	1.71
5-S1	137	9.1	42.7	1.40	1.28
5-S2		9.1	42.7	**1.39**	**1.28**
6-S1	250	11.6	42.7	**1.62**	**1.52**
6-S2		11.6	42.7	**1.62**	**1.52**
7-S1	233	8.5	66.8	**1.45**	**1.37**
7-S2		8.5	57.9	1.69	1.59
8-S1	250	8.5	80.8	1.34	1.27
8-S2		8.5	89.9	**1.25**	**1.18**
9-S1	233	8.5	42.7	**1.56**	**1.44**
9-S2		8.5	46.0	2.34	2.24
9-S3		8.5	38.4	1.68	1.56
10-S1	218	9.1	45.1	1.98	1.88
10-S2		9.1	80.8	1.90	1.84
10-S3		9.1	57.9	**1.67**	**1.59**
11-S1	250	8.5	68.0	1.75	1.69
11-S2		8.5	111.6	1.69	1.65
11-S3		8.5	71.6	**1.64**	**1.59**
12-S1	69	8.5	42.7	1.75	1.63
12-S2		8.5	54.9	2.20	2.10
12-S3		8.5	44.2	**1.71**	**1.60**
13-S1	137	9.1	46.0	1.41	1.32
13-S2		9.1	57.9	1.89	1.80
13-S3		9.1	46.0	**1.40**	**1.30**
14-S1	308	8.5	45.7	**1.63**	**1.52**
14-S2		8.5	57.9	2.07	1.98
14-S3		8.5	45.7	**1.63**	**1.52**
15-S1	247	8.5	61.0	1.70	1.60
15-S2		8.5	89.9	1.86	1.78
15-S3		8.5	61.0	**1.69**	**1.59**

Note: The boldface type value for Ω is the critical (lowest Ω) case for the bridge concerned.

CHAPTER VII

DISCUSSION AND SIGNIFICANCE OF RESULTS WITH RECOMMENDATIONS

7.1. Chapter Summary

The results of the plastic analysis are compared with the results reported by the Finite Element Method (FEM) and the Grillage analysis that were conducted to evaluate the internal redundancy of fracture critical Steel Twin-Tub Girder (STTG) bridges. The three methods serve as an independent check for assessing whether or not an STTG bridge span may be declassified from its fracture critical status. The analysis is conducted for the suite of 15 typical STTG bridges selected from the inventory of the Texas Department of Transportation (TxDOT) in order to help bridge engineers to implement the recommendations and findings of this research in the evaluation regimes of other such bridge spans. The comparison also illustrates how each of the three methods predict the overstrength of the bridge spans based on the underlying assumptions.

7.2. Introduction

The evaluation of fracture critical nature of STTG bridges is proposed to be evaluated by three mutually independent methodologies as part of the TxDOT 0-6937 project, (Hurlebaus et al. 2018). In order to establish reasonable confirmation that the evaluation is sufficiently rigorous, each method is significant since a consistency of results of these independent solutions is essential to validate the decision-making process. The 15 bridges that are considered for this analysis consist of three different kinds of spans with different support conditions that encompass the various possibilities for bridge spans. The results of comparison of all the methods are discussed using load-deflection curves for the FEM and the grillage methods, and the plastic solutions are represented as a band flanked by the upper-bound yield line solution on the top and the lower-

bound strip method solution at the bottom. The implication of the results is discussed in the following sections.

7.3. Comparison of Results of Plastic Methods with FEM and Grillage Analysis

The different kinds of bridges, simply supported single span bridges, the interior spans of three span bridges and the exterior spans of both the two- and three span bridges, are compared using graphical representation. The FEM and Grillage Analysis results are represented in the form of load-displacement curves and the overstrength factor at the defined practical displacement limits are indicated by the diamond markers. The FEM results are represented by a blue curve, while the grillage results are represented in purple. The plastic solution is indicated as a yellow band, with red upper bounded solution and a green lower bounded solution. The three categories of bridge spans have the corresponding overstrength results tabulated in increasing order of their span lengths. In the event of the outer girder undergoing a premature fracture at the critical location, the load will be borne by the moment capacity of transverse yielding of deck slab and by the folded plate mechanism (longitudinal redundancy) existing between the two tub girders. Additional moment capacity will be contributed by the girder at the continuous supports of the two-span and three-span bridges.

7.3.1. Single-Span Simply Supported Bridges

Due to the least redundancy of these bridges, with a degree of indeterminacy of zero, these spans exhibit the least overstrength compared to those multi-span bridges continuous over their supports. Figure 7.1 presents the comparison of overstrength results generated by FEM, grillage analysis and plastic methods for a typical single-span bridge. All methods indicate that sufficient overstrength capacity ($\Omega > 1$) exists even after fracture of the outer girder in case of Bridge 2 with a span length of 35 m.

However, for longer spans, the overstrength capacity is insufficient to sustain the bridge after collapse. Therefore, there must be a limit set for the single-span bridges, beyond which these spans are to remain fracture-critical. The FEM results for the experimentally tested span show that the bridge should remain fracture critical despite the other methods suggesting sufficient overstrength. This disparity may be attributed to the higher accuracy of FEM to capture the three-dimensional behavior.

Moreover, this is a single-lane bridge, which may have been overloaded by the loading assumptions used in these analyses. Table 7.1 summarized the results of all the single-span bridges, listed in an increasing order of the span length. It may be concluded that the single-span bridges must be dealt with caution owing to the lack of sufficient redundancy. If short-span bridges are to be considered for declassification, an advanced FEM analysis must be conducted to check the veracity of the results.

7.3.2. Interior Spans of Bridges Continuous over Both Supports

The interior spans of three-span bridges possess the highest redundancy due to the degree of indeterminacy of 2. Three plastic hinges are formed in this collapse mechanism: two over piers and one at the critical location of maximum positive moment (at midspan, similar to single-span bridges). The moment capacity that contributes to the overstrength capacity of the interior spans of bridges comprises of similar factors as that of their simply-supported counterparts, with the exception of the additional redundancy provided by the transverse hinges and the moment capacity at the supports over the bearing seats.

The results of overstrength capacity computed using FEM, grillage and plastic analyses are compared. It is observed that sufficient capacity ($\Omega > 1$) is assured by all the three methods.

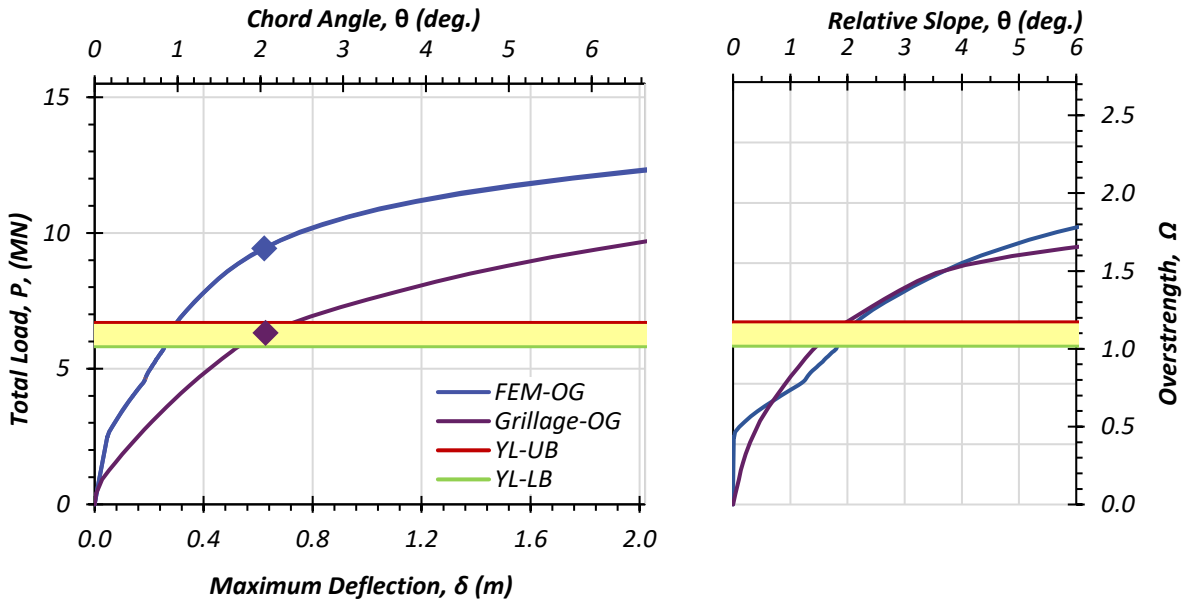

(i) Load displacement *(ii) Deck rotations*

Source: Hurlebaus et al. (2018)

Figure 7.1. Comparison of the Results for Bridge 2, L = 35 m

Table 7.1. Comparison of Overstrength Factors for Simply Supported Single- Spans.

							Yield Line		
ID	**Span**	**R (m)**	**L (m)**	**B (m)**	**S (m)**	**FEM**	**Upper Bound**	**Lower Bound**	**Grillage**
2	1	582.17	35.05	7.92	1.86	1.65	1.17	1.02	1.11
0	1	396.24	36.58	7.01	1.83	0.86	1.46	1.28	1.07
1	1	174.65	67.06	9.75	2.90	0.82	0.62	0.57	0.21
3	1	672.69	70.10	11.89	3.84	0.85	0.51	0.44	0.16

Figure 7.2 presents the comparison results of a typical interior span of a three span bridge, Bridge 9. The lower grillage results may be due to the fact that torsional capacity is not considered for the grillage members, making the analysis computationally lower bound. The FEM analysis is observed to generate results higher than that of the upper bound plastic method. This may be due to the catenary action of the slab that is not accounted for by the plastic theories (Pirayeh Gar et al. 2014). This makes the results of the plastic analysis more conservative.

Table 7.2 presents all the comparison overstrength results of the interior spans for the three methods in a similar fashion of ordering as in the previous section. The shorter of the medium-length interior spans of Bridges 9 and 12 exhibit a sufficient load carrying capacity with a consistently high overstrength ($\Omega > 2$) reported by all three methods. The longer of the medium-length interior spans of Bridges 13 and 14 show a moderate capacity ($1.4<\Omega < 2$). Though the overstrength capacity of the longest interior spans among the bridges under consideration show sufficient design capacity ($\Omega > 1$), it must be noted that the longer spans must be analyzed thoroughly since there is some risk associated with such spans as shown for Bridges 10, 15 and 11. Bridges 11 and 15 show the least overstrength in comparison with the other interior spans. Thus, there is a correlation between the strength and the span length that should be considered for the development of declassification recommendations.

7.3.3. Exterior Spans of Multi-span Continuous Bridges

The end spans of continuous bridges have one support condition and the other free to rotate at the abutment. One degree of indeterminacy exists for this class of bridge spans. Two plastic hinges, one at the critical location of maximum bending moment and the other over interior pier of the bridge. The brittle fracture of the outer girder is assumed to be at 40% of span length measured from the exterior pier as discussed in Section 4.6. The deck slab contributes to a transverse yield

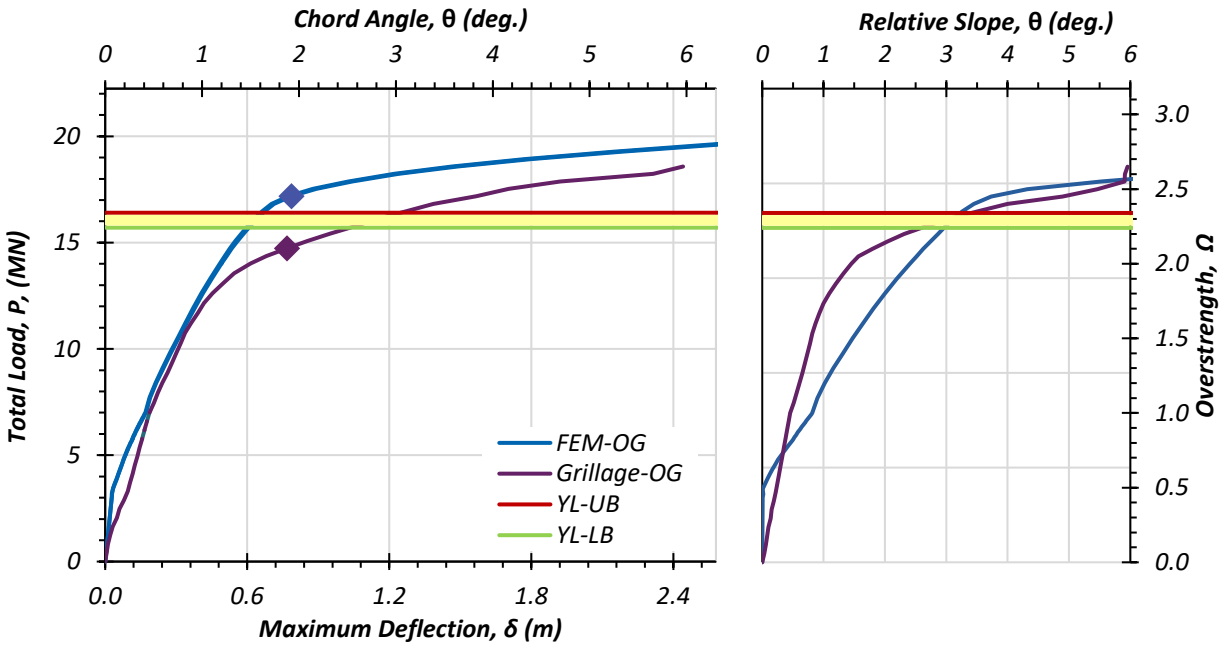

(i) Load displacement *(ii) Deck rotations*

Source: Hurlebaus et al. (2018)

Figure 7.2. Comparison of the Results for Bridge 9, Span 2, L = 46 m

Table 7.2. Comparison of Overstrength Factors for Interior Spans.

							Yield Line		
ID	**Span**	**R (m)**	**L (m)**	**B (m)**	**S (m)**	**FEM**	**Upper Bound**	**Lower Bound**	**Grillage**
9	2	233	46	8.53	2.13	2.45	2.34	2.24	2.1
12	2	69	55	8.53	2.32	1.8	2.2	2.1	1.56
13	2	137	58	9.14	2.83	1.4	1.89	1.8	1.35
14	2	308	58	8.53	1.98	1.8	2.07	1.98	1.35
10	2	218	81	9.14	2.35	1.45	1.9	1.84	1.25
15	2	247	90	8.53	2.44	1.4	1.86	1.78	1.25
11	2	250	112	8.53	2.13	1.2	1.69	1.66	1

moment capacity at the critical location. The girder provides additional redundancy at the interior continuous support. The longitudinal redundancy attributed to the folded plate mechanism is similar to that observed in the single spans and the interior spans.

Figure 7.3 presents a typical exterior span of Bridge 4 with the comparison between the three methods represented graphically. The consistency between FEM and plastic analysis evident from this graph is also reflected in the results of most of the spans in this category. Therefore, the two methods may be shortlisted for further evaluation of the fracture critical nature of these bridge spans. Exterior spans of less than 50 m such as both the exterior spans of Bridges 9, 4, 12, 6 and 14, and the first span of Bridge 10, have a sufficiently high overstrength capacity ($1.5 < \Omega < 2.0$). These results are fairly consistent for all three methods with certain degree of disparity arising due to the difference in the underlying assumptions of these methods. Both spans of Bridges 5 and 13, however, are the outliers of this group of spans since the overstrength ($1.0 \leq \Omega < 1.5$) of these spans is less than the others belonging to this range of span lengths. This reduction in capacity may be attributed to the tighter radii of curvature (137 m) of these two bridges.

Bridges of span length between 50 m to 80 m, such as both the exterior spans of Bridges 7, 15, and 11 and the second span of Bridge 10 are computed to have moderate overstrength ($1.0 \leq \Omega < 1.5$), consistently for most of the spans with all the three methods. The longest of the exterior spans of span length beyond 80 m, such as both exterior spans of Bridge 8 may not be declassified since the overstrength is shown to be insufficient ($\Omega<1$) when the results of all the three methods are studied in conjunction.

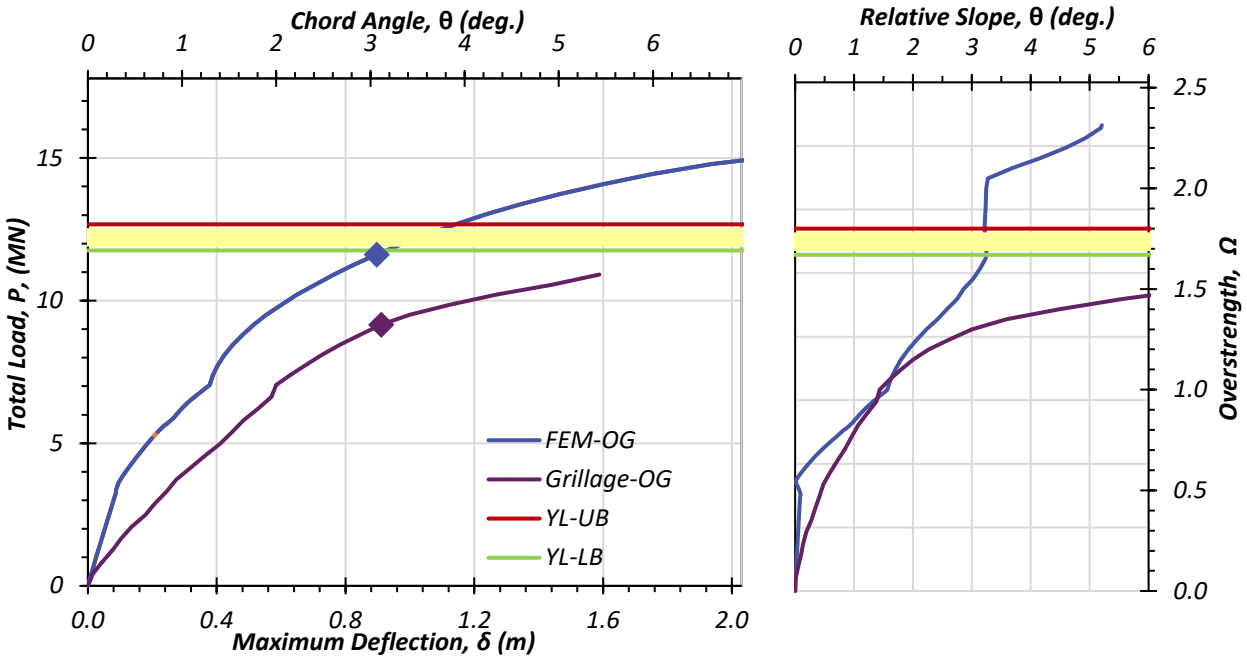

(i) Load displacement *(ii) Deck rotations*

(Hurlebaus et al. 2018)

Figure 7.3 Comparison of the Results for Bridge 4, Span 1, L = 40 m

Table 7.3. Comparison of Overstrength Factors for Exterior Spans.

							Yield Line		
ID	**Span**	**R (m)**	**L (m)**	**B (m)**	**S (m)**	**FEM**	**Upper Bound**	**Lower Bound**	**Grillage**
9	3	233	38	8.53	2.26	1.8	1.68	1.56	1.53
4	2	59	39	8.53	2.32	1.73	1.85	1.71	1.32
4	1	59	40	8.53	2.32	1.65	1.8	1.67	1.3
12	1	69	43	8.53	2.32	1.6	1.75	1.63	1.2
9	1	233	43	8.53	2.26	1.7	1.56	1.44	1.35
6	1	250	43	11.58	2.99	1.8	1.62	1.52	1.43
6	2	250	43	11.58	2.99	1.8	1.62	1.52	1.43
5	1	137	43	9.14	2.96	1.2	1.4	1.28	1.1
5	2	137	43	9.14	2.96	1.2	1.39	1.28	1.1
12	3	69	44	8.53	2.32	1.6	1.71	1.6	1.15
10	1	218	45	9.14	2.35	1.7	1.98	1.88	1.71
13	1	137	46	9.14	2.83	1	1.41	1.32	1.1
13	3	137	46	9.14	2.83	1	1.4	1.3	1.1
14	1	308	46	8.53	1.98	1.65	1.63	1.52	1.25
14	3	308	46	8.53	1.98	1.65	1.63	1.52	1.25
7	2	233	58	8.53	2.26	1.45	1.69	1.59	1.25
10	3	218	58	9.14	2.35	1.45	1.67	1.59	1.25
15	1	247	61	8.53	2.44	1.7	1.7	1.6	1.4
15	3	247	61	8.53	2.44	1.7	1.69	1.59	1.4
7	1	233	67	8.53	2.26	1.2	1.45	1.37	0.94
11	1	250	68	8.53	2.13	1.6	1.75	1.69	1.35
11	3	250	72	8.53	2.13	1.6	1.65	1.59	1.3
8	1	269	81	8.53	2.56	0.99	1.34	1.27	0.83
8	2	269	90	8.53	2.56	0.88	1.25	1.18	0.6

7.4. Significance

Figure 7.4 presents a vivid trend emerging from the results that shows that there exists a relationship between the overstrength capacity of the spans and the corresponding centerline length of the outer girder. For the purpose of developing an overstrength factor that is normalized by the span length, the following relation is derived based on the results of the analysis. The plot shows the results of the analytical overstrength factors of each kind of spans represented as discrete data points and the normalized overstrength is plotted as a black continuous curve using the following expression, while the dashed line shows a lower-bound envelope of the results

$$\omega = \Phi \frac{c(\eta + 1)}{L_x^*} \tag{7.1}$$

in which Φ = a factor if safety, c = a length constant (m, ft); L_x^* = centerline length of the outer girder; and η = number of redundant hinges, where η = 0, 1, and 2 for simply supported, fixed-free, and fixed-fixed end conditions respectively. Based on the mean values of overstrength factor, an overall median value of c = 41 is considered for plotting the curve of ω versus L_x^* to study the trend of the analytical overstrength results in the following graphs in Figure 7.4.

Figure 7.4 (d) shows the cumulative distribution plotted for the ratios of the analytical results (Ω_{UB}) to the overall median ($\Phi = 1$) results (ω) for all the bridge spans considered. The dispersion of the plot is found to be 0.23. Therefore, this statistical analysis confirms that the overstrength of the bridge is greatly influenced by the span length of the bridge and the internal redundancy of the bridges. Thus, one may conclude that it is reasonable to develop the recommendations for the potential reclassification on the basis of the span lengths and the degree of redundancy of each span within a bridge.

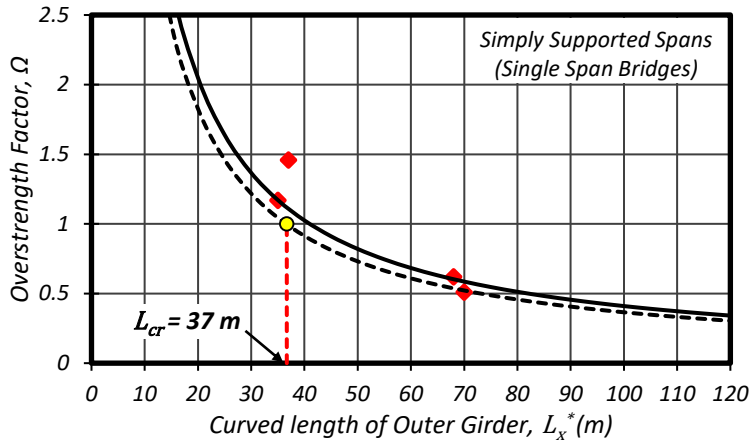

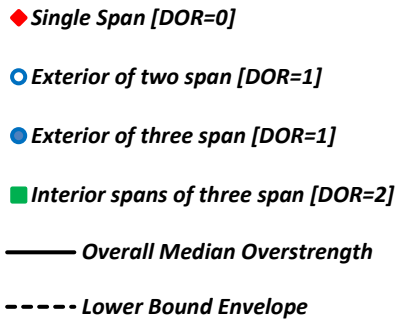

(a) Overstrength Trend for Simply Supported Bridges

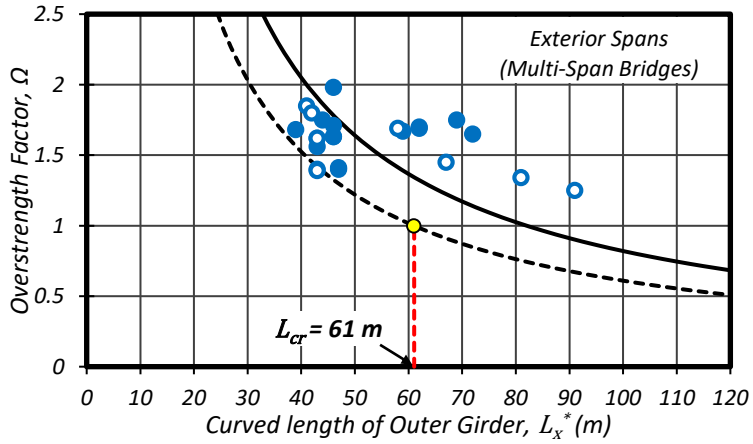

(b) Overstrength Trend for Exterior Spans of Multi-span Bridges

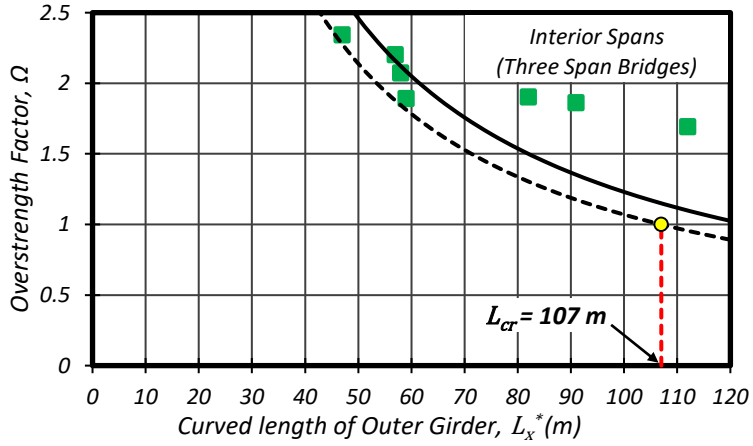

(c) Overstrength Trend for Interior Spans of Three-span Bridges

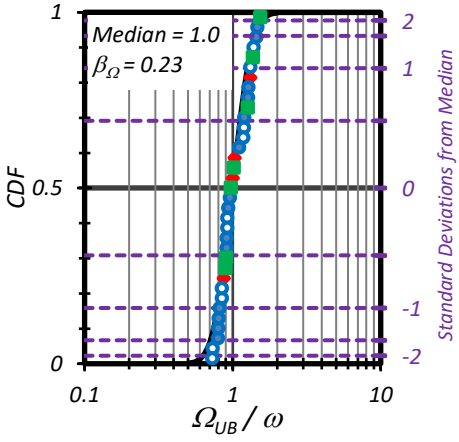

(d) Dispersion of results

Figure 7.4. Relation between Span Length and Overstrength.

7.5. Recommendations

For a final confirmation about the veracity of the reclassification, it is recommended to test using more advanced and computational methods such as Grillage Analysis in SAP2000 and FEM Analysis in software programs. It may be concluded that one method alone is not sufficient to determine the declassification of bridges. However, each method may form a stage in the sequential process of determining the redundancy of STTG bridges. Figure 7.5 presents the analysis schema of redundancy evaluation of STTG bridges using a flow chart representation.

In general, based on the pattern that emerges from the results of the analysis of the overstrength factors, it can be suggested that single-span bridges less than 37 m span length may be subjected to further investigation for potential reclassification. The exterior spans of the two-span and three-span bridges shall continue to possess the *"fracture critical"* status for span lengths greater than 61 m. The interior spans of the three-span bridges of span length longer than 107 m are also recommended to be treated as fracture critical. These recommended critical span lengths are represented as L_{cr} in the plots of Figure 7.4

Generally, it is also observed that as a bridge become wider, its susceptibility to failure and collapse also increases. Additionally, it is observed that the radius of curvature impacts the capacity of the bridge marginally. The tighter the radii, the less stable the bridge may be. The future work in this area may focus on the automation of the plastic analysis into a software that can ensure quicker and thorough optimal study. Sensitivity study may be conducted to check the various parameters involved in the research that influence the outcomes of the overstrength factor.

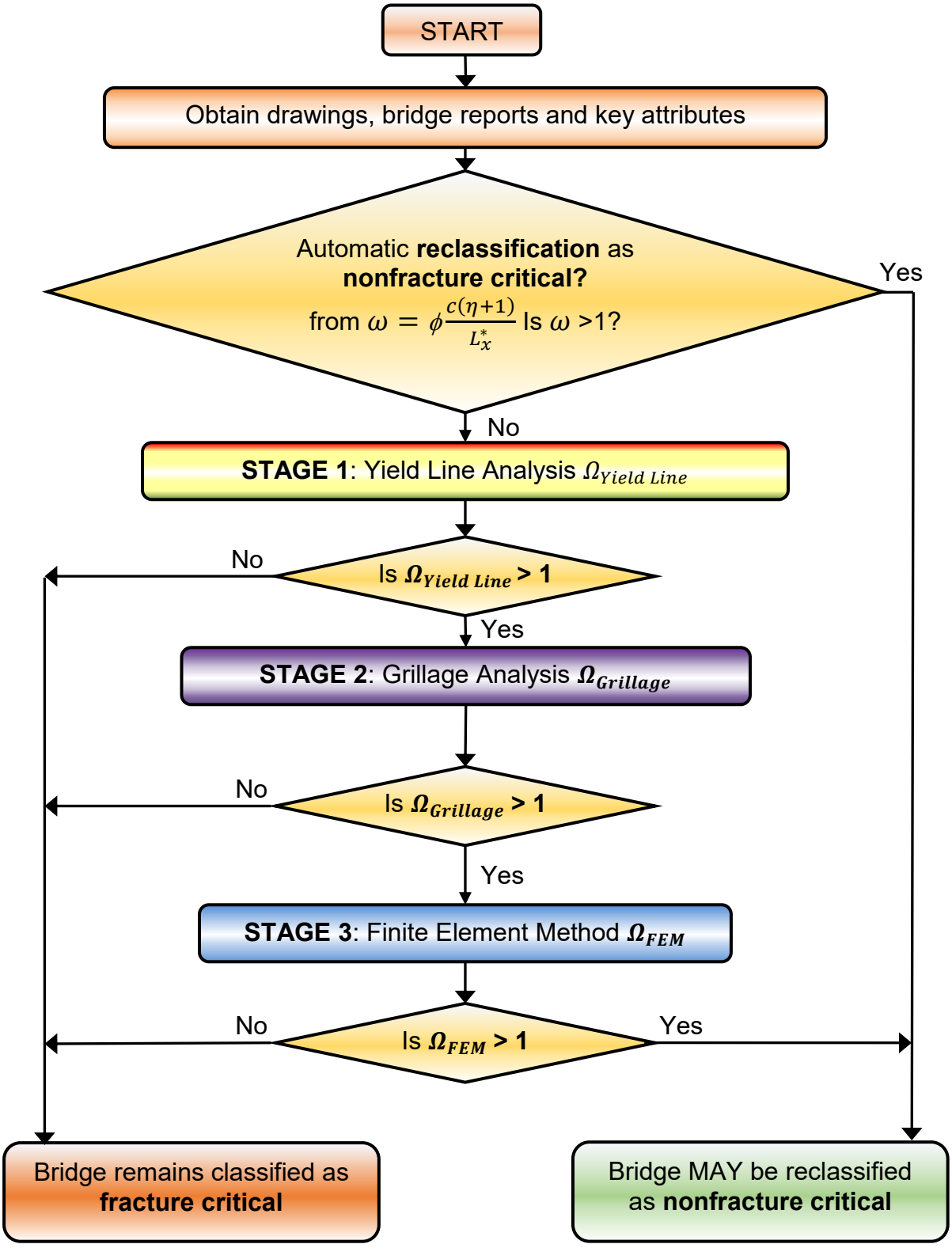

Source: (Hurlebaus et al. 2018)

Figure 7.5. Flowchart for Analysis Procedure of STTG Bridges.

CHAPTER VII

SUMMARY AND CONCLUSIONS

8.1. Summary

The limit analyses methods were evaluated in detail by reviewing the previous work conducted for the evaluation of failure analysis. The methods were assessed and developed for the application of these analytical techniques to compute the reserve capacity of the fracture critical Steel Twin-Tub Girder (STTG) bridges. The assessment of this class of bridges was initiated by implementing the yield line theory to solve an experimentally conducted collapse. The experimentally tested bridge of the TxDOT 9-5498 project was analyzed by simulating the test loading. The experimental sand loading was used to postulate the critical yield line mechanism after a series of rigorous minimization analyses using several possible admissible mechanisms were conducted. The result obtained from the critical mechanism was validated by the experimental results and this accurate collapse analysis using yield line theory confirmed that plastic methods may serve as a viable solution to analyze the longer span bridges effectively. Earlier studies had not truly captured the collapse behavior of the longer span bridges accurately. This analysis was modified to account for all the components of the composite STTG bridge section such as the deck slab, the outer girder with the web and bottom flange fractured and the shear studs connecting the deck slab to the girders.

The validation of the theoretical yield line analysis with the experimental results was followed by the second phase of the research that was the analysis of 15 STTG bridges under standard traffic loading (HL-93) for the purpose of evaluation of their fracture critical status. The critical mechanism was postulated for the given loading to model the combined flexural and torsional bending of the deck slab. The minimization analysis was conducted to determine the

critical mechanism and an equivalent strip method solution was generated by neglecting torsion. The two solutions of upper bound (yield line method) and lower bound (strip method) were developed to obtain a range of overstrength capacity for each span. The analysis guidelines were drafted to sequentially explain the procedure of carrying out the analysis technique thus derived. These guidelines were developed for one span of each kind to encompass all the various cases of spans that are included among the 15 selected bridges. The procedure was then implemented to the remaining spans and the results of each bridge were discussed and the concluding remarks were mentioned based on the observation of the results.

8.2. Conclusions

1. This thesis has shown that plastic analysis is an expeditious way to ascertain the reserve capacity of Twin-Tub girder bridges when one of the girders has prematurely fractured.
2. The modification of the conventional yield line theory to account for the combined beam-slab action of the STTG girder bridge captures the flexural capacity of both the deck slabs and the girders.
3. The extra capacity imparted by the internal work done due to the tensile failure of the shear studs can also be modeled and mathematically incorporated as an equivalent internal work done by the studs in resisting the pull-out of studs at failure.
4. The true redundancy of the experimental STTG bridge that was not accounted for in the yield line analysis reported in the TxDOT 0-6937 project has been effectively reflected in the results obtained from the postulated mechanism that combines the structural components of the bridge such as the fractured girder, the deck slab and the shear studs that were pulled out.

5. The critical mechanism postulated to predict the capacity of the test bridge with the simulated sand load achieved validation from the experimental result of the load capacity of the said bridge. The collapse load calculated using the yield line analysis was 1570 kN, while the experiment conducted during TxDOT Research Project 9-5498 gave a load of 1592 kN. The yield line result is 1.40% lower than the reported collapse load. The analysis modified the yield line theory to account for the stud failure.
6. Moreover, the failure load analysis using the yield line theory modeled the sand load as wheel load (point load) in Barnard et al. (2010) instead of the uniformly distributed load. This equivalence of the two different types of loading is to be discouraged since the crack patterns essential to the yield line solution vary with the manner in which the loads are being applied. It is also evident that the results of the proposed mechanism, developed by modelling the sand loading to closely simulate the actual test conditions, are accurate since the veracity of the results are validated using the experimental results with an error of less than 2%. This underestimation is attributed to the catenary action and the strain hardening effects of the slab structure.
7. The mechanism developed for the sand loading is not the most optimal solution for the HL-93 loading. This was observed because the sand load was uniformly distributed while the HL-93 loading is a combination of concentrated load and continuous load. This impacts the geometry of the collapse mechanism, and consequently the internal and external work done by these loads. The point loading resulted in a more fanned mechanism typical for such loading in slabs. Therefore, a new mechanism is to be postulated.
8. The presence of the remaining part of the fractured girder affects the kinematics of the beam forcing a folded plate mechanism to take a zig-zag formation that is shown in this

thesis. This additional torsional effect, in combination with the flexural effects, are incorporated in a mechanism postulated for the HL-93 loading. The postulated mechanism is generalized to obtain a solution that can be used to analyze the STTG bridges with differing boundary conditions. The solution is further modified to account for the width and curvature of the bridge that influence the extent of the external work done by the second lane of HL-93 loading.

9. It can be observed that there are several spans that are proven to show sufficient redundancy (indicated by overstrength factor greater than unity) that can initiate a process of reclassification of such bridges. Recommendations are made for a this reclassification process based on a comparative study of the plastic methods with the other computational methods such as FEM and grillage analysis.

REFERENCES

AASHTO (2017). "AASHTO LRFD Bridge Design Specifications." American Association of State Highway and Transportation Officials (AASHTO), Washington, DC.

ABAQUS (2014). "Dassault Systemes ABAQUS, S. A. Version 6.14." *Providence, RI: Dassault Systèmes*.

ACI-318 (2017). "Building code requirements for structural concrete (ACI 318-17) and commentary." ACI Committee, American Concrete Institute, and International Organization for Standardization.

Armer, G. S. T. (1968). "Strip Method-a New Approach to Design of Slabs.", Concrete Vol. 2, No. 9, 358-363.

Bach, C., Graf, O., and GRCB (1911-1925). "Experimental Testing." *Stuttgart Materials Testing Establishment*

Barker, R. M., and Puckett, J. A. (1987). *Design of highway bridges based on AASHTO LRFD bridge design specifications*.

Barnard, T., Hovell, C. G., Sutton, J. P., Mouras, J. M., Neuman, B. J., Samaras, V. A., Kim, J., Williamson, E. B., and Frank, K. H. (2010). "Modeling the Response of Fracture Critical Steel Box-Girder Bridges." *Report No. FHWA/TX-10/9-5498*, Center for Transportation Research at the Univ. of Texas at Austin, Austin, TX.

Cardenas, A. E., and Sozen, M. A. (1973). "Flexural yield capacity of slabs.", Journal Proceedings. Vol. 70. No. 2., 124-126.

Crawford, R. E. (1964). "Limit design of reinforced concrete slabs." *Journal of the Engineering Mechanics Division*, 90(5), 321-342.

DCCR (1962). "The Analysis of Slabs by Yield-Line Theory." Dutch Committee for Concrete Research Report No. 26A Translation No.135 Cement and Concrete Association, London, 36.

DCCR (1963). "Experimental Investigations of the Plastic Behavior of Slabs." *Translation No. 136, Cement and Concrete Association, London*, Dutch Committee for Concrete Research, Report No. 26B, TNO Institute for Building Materials and Structures, 35.

Drucker, D., Prager, W., and Greenberg, H. (1952). "Extended limit design theorems for continuous media." *Quarterly of applied mathematics*, 9(4), 381-389.

ECC (1962). *The Application of the Yield-Line Theory to Calculations of the Flexural Strength of Slab and Flat-slab Floors*, European Concrete Committee, Translated by C. V. Amerongen, Cement and Concrete Association.

ECC (1972). "Slabs and Plane Structures." Recommendations of the European Concrete Committee Volume 3.

Gvozdev, A. (1938). "The determination of the value of the collapse load for statically indeterminate systems undergoing plastic deformation." *Akademia Nauk SSSR, Moscow/Leningrad*, 19, 38.

Haque, M. E. (1997). "Uniform Bridge element identification system for database management for roadway bridges." *Journal of Bridge Engineering*, 2(4), 183-188.

Herald-Dispatch (December 15, 1967). "Silver Bridge Collapse " *The Herald-Dispatch*, Huntington, WV 25701 (http://herald-dispatch.com).

Hillerborg, A. (1956). "Equilibrium theory for reinforced concrete slabs." *Betong*, 41(4), 171-182.

Hillerborg, A. (1960). "A plastic theory for the design of reinforced concrete slabs." *Prel. Publications, 6th Congr. mt. Ass. Bri. Struct. Eng., Stockholm*.

Hillerborg, A. (1964). "Strip method for slabs on columns, L-shaped plates, etc. Translated from Swedish by FA Blakey." CSIRO, Division of Building Research, Melbourne.

Hogarty, M. A. (July 17, 1983). "Mianus River Bridge collapse." *The New Haven Register*, New Haven(https://www.nhregister.com).

Hognestad, E. (1953). "Yield-line theory for the ultimate flexural strength of reinforced concrete slabs.", Journal Proceedings. Vol. 49. No. 3, 637-656.

Horne, M. R. (1971). " Plastic Theory of Structures." *M.I.T. Press, Cambridge, Massachusetts*.

Hurlebaus, S., Mander, J. B., Terzioglu, T., Boger, N. C., and Fatima, A. (2018). "ANALYSIS GUIDELINES AND EXAMPLES FOR FRACTURE CRITICAL STEEL TWIN TUB GIRDER BRIDGES, FHWA/TX-18/0-6937-P1."

Hurlebaus, S., Mander, J. B., Terzioglu, T., Boger, N. C., and Fatima, A. (2018). "FRACTURE CRITICAL STEEL TWIN TUB GIRDER BRIDGES: TECHNICAL REPORT." *Technical Report Documentation Page 1. Report No. FHWA/TX-18/0-6937-R1*.

Ingerslev, A. (1923). "The strength of rectangular slabs.", Struct. Eng 1.1, 3-14.

Jain, S. C., and Kennedy, J. B. (1974). "Yield criterion for reinforced concrete slabs.", Journal of the Structural Division 100.3, 631-644.

Jiang, D. (2015). "Experiments, Analysis and Design Models for Slab on Prestressed Concrete Girder Bridge Structures." Doctoral dissertation, Texas A&M University, College Station, TX.

Johansen, K. W. (1962). *Yield-line theory*, Cement and Concrete Association.

Johansen, K. W. (1972). *Yield-line formulae for slabs*, CRC Press.

Jones, L. (1965). "The use of nodal forces in yield-line analysis." *Magazine of Concrete Research Special Publication*, 63-74.

Jones, L. L. (1962). *Ultimate load analysis of reinforced and prestressed concrete structures*, Chatto & Windus.

Kemp, K. (1965). "The Evaluation of Nodal and Edge Forces in Yield-Line Theory." *Magazine of Concrete Research Special Publication*, 3-12.

Kemp, K., Morley, C., Wielsen, M., Wood, R., and Jones, L. (1965). "'Recent developments in yield line theory." *The evaluation of nodal and edge forces in the yield-line theory*.

Kemp, K. O. (1962). "A Lower Bound Solution to the Collapse of an Orthotropically Reinforced Slab on Simple Supports." Vol. 14 No. 41, 79-84.

Kennedy, G., and Goodchild, C. (2004). "Practical yield line design." *Concrete Centre, Surrey, UK*.

Lenkei, P. (1967). "Discussion of Ref. 5.10." Proc. ACI (64), 786-789.

Lenschow, R., and Sozen, M. A. (1967). "A yield criterion for reinforced concrete slabs.", Journal Proceedings. Vol. 64. No. 5, 266-273.

Lindsay, R. (2004). "Experiments on the Seismic Performance of Hollow-Core Floor Systems in Precast Concrete Buildings." University of Canterbury, New Zealand.

Lindsay, R., Mander, J. B., and Bull, D. K. (2004). "Experiments on the seismic performance of hollow-core floor systems in precast concrete buildings." *Master of Engineering Thesis*.

Lwin, M. (2012). "Clarification of Requirements for Fracture Critical Members." *FHWA Memorandum HIBT*, 10.

Mander, T. J., Mander, J. B., and Head, M. H. (2010). "Modified yield line theory for full-depth precast concrete bridge deck overhang panels." *Journal of Bridge Engineering*, 16(1), 12-20.

Meyboom, J. (2002). *Limit analysis of reinforced concrete slabs*, vdf Hochschulverlag AG.

Middleton, C. (1997). "Concrete bridge assessment: an alternative approach." *Structural engineer*, 75(23/24).

Middleton, C. (2008). "Generalised collapse analysis of concrete bridges." *Magazine of Concrete Research*, 60(8), 575.

Milošević, B., Mijalković, M., Petrović, Ž., and Hadžimujović, M. (2010). "The application of the limit analysis theorem and the adaptation theorem for determining the failure load of continuous beams." *Scientific Tehnical Review*, 60(3-4), 82-92.

Morley, C. T. (1965). "Equilibrium Methods for Least Upper Bounds of Rigid-Plastic Plates." *Magazine of Concrete Research Special Publication*, Recent Development in Yield-Line Theory(Cement and Concrete Association), 13-24.

Morley, C. T. (1988). "Nodal forces in slabs and the equilibrium method." *Buttersworths, London*, 195-220.

Mouras, J. M., Sutton, J. P., Frank, K. H., and Williamson, E. B. (2008). "The tensile capacity of welded shear studs." *Report No. FHWA/TX-09/9-5498-2*, Center for Transportation Research at the Univ. of Texas at Austin, Austin, TX.

Neal, B. (1977). "THE PLASTIC METHODS OF STRUCTURAL ANALYSIS-THIRD (SI) EDITION."

Neuman, B. J. (2009). "Evaluating the redundancy of steel bridges: Full-scale destructive testing of a fracture critical twin box-girder steel bridge." Master of Science in Engineering, University of Texas at Austin, Austin, TX.

Nielsen, M. P. (1965). "A New Nodal-Force Theory." *Magazine of Concrete Research Special Publication*, Recent Development in Yield-Line Theory, Cement Concrete Association, London, 25-30.

Nielsen, M. P., and Hoang, L. C. (2016). *Limit analysis and concrete plasticity*, CRC press.

NTSB (1970). "Collapse of US 35 Highway Bridge Point Pleasant, West Virginia December 15, 1967." National Transportation Safety Board.

NTSB (1984). "Collapse of a Suspended Span of Inter- state Route 95 Highway Bridge over the Mianus River, Greenwich, Connecticut June 28, 1983.", National Transportation Safety Board (NTSB).

Park, R. (1968). "Limit Design for Reinforced Concrete Slabs." University of Canterbury, New Zealand.

Park, R., and Gamble, W. L. (2000). *Reinforced concrete slabs.* , John Wiley & Sons.

Park, R. L., Park, R., and Paulay, T. (1975). "Reinforced concrete structures.", John Wiley & Sons.

PB (December 2003). "A review of bridge assessment failures on the motorway and trunk road network." Parsons Brinckerhoff.

Pirayeh Gar, S., Mander, J. B., Head, M., and Hurlebaus, S. (2014). "FRP Slab Capacity Using Yield Line Theory." *Journal of Composites for Construction*, 18(6).

Prager, W., and Hodge, P. G. (1951). "Theory of perfectly plastic solids."

Quintas, V. ı. n. (2003). "Two main methods for yield line analysis of slabs." *Journal of Engineering Mechanics*, 129(2), 223-231.

Sawczuk, A., and Jaeger, T. (1963). "Grenztrag fähigkeits theorie der platten ", Springer-Verlag, Berlin.

Schmalz, J. (June 24, 1984). "Year After Bridge Collapse: Questions and Pain Still Linger." New York Times, CN11.

Shukla, S. N. (1973). "Handbook for design of slabs by yield-line and strip methods.", Structural Engineering Research Centre, Roorkee, India, 180.

Sutton, J. P. (2007). "Evaluating the redundancy of steel bridges: Effect of a bridge haunch on the strength and behavior of shear studs under tensile loading." MS Thesis. The University of Texas at Austin, Austin, TX.

Taylor, R., Maher, D., and Hayes, B. (1966). "Effect of the arrangement of reinforcement on the behaviour of reinforced concrete slabs." *Magazine of concrete research*, 18(55), 85-94.

Thoft-Christensen, P., Jensen, F., Middleton, C., and Blackmore, A. (1997). "Revised rules for concrete bridges." *Safety of bridges*, 175-188.

Wood, R. (1965). "New techniques in nodal-force theory for slabs." *Recent developments in yield-line theory*, 31-62.

Wood, R., and Jones, L. (1967). "Yield line analysis of slabs." *Chatto & Windus and Thames & Hudson, London*.

Wood, R. H. (1961). "Plastic and elastic design of slabs and plates.", Thames and Hudson, London, 344.